DIFFERENTIAL CAPACITY OF STAINLESS STEEL IN POTASSIUM CHLORIDE SOLUTIONS DURING POTENTIOSTATIC AND GALVANOSTATIC POLARIZATION

By

M. ELAINE CURLEY-FIORINO

A DISSERTATION PRESENTED TO THE GRADUATE COUNCIL
OF THE UNIVERSITY OF FLORIDA
IN PARTIAL FULFILLMENT OF THE REQUIREMENTS
FOR THE DEGREE OF DOCTOR OF PHILOSOPHY

UNIVERSITY OF FLORIDA

1975

The author dedicates this dissertation to her husband, John A. Fiorino.

ACKNOWLEDGEMENTS

The author would like to express her gratitude to the members of her committee; Dr. E. D. Verink, Jr., Dr. J. D. Winefordner, Dr. W. S. Brey, Dr. R. Bates, and especially to her research director, Dr. G. M. Schmid for the interest and assistance given to her in the course of this investigation and in the preparation of this manuscript.

She would also like to thank Mr. R. Dugan and Mr. A. Grant and their associates for their help in the technical aspects of this work.

Steel samples were provided by the United States Steel Corporation.

The author is also grateful for the financial assistance received from the University of Florida in the form of Graduate School Fellowships.

Finally, the author would like to thank Dr. and Mrs. James L. Fortuna and Mr. and Mrs. Willis Bodine for their friendship and encouragement during her graduate career.

TABLE OF CONTENTS

LIST OF TABLES

LIST OF FIGURES

Abstract of Dissertation Presented to the Graduate Council of the University of Florida in Partial Fulfillment of the Requirements for the Degree of Doctor of Philosophy

DIFFERENTIAL CAPACITY OF STAINLESS STEEL IN POTASSIUM CHLORIDE SOLUTIONS DURING POTENTIOSTATIC AND GALVANOSTATIC POLARIZATION

By

M. ELAINE CURLEY-FIORINO

June, 1975

Chairman: Gerhard M. Schmid
Major Department: Chemistry

Potentiostatic and galvanostatic polarization of AISI 304 stainless steel was performed in deaerated solutions of 0.0 through 1.0 M potassium chloride at pH 2.4. Sodium sulfate was added to an ionic strength of one. Cylindrical electrodes were mechanically polished and prepolarized at -0.700 V for twenty minutes. The differential capacity of the metal-solution interface was determined as a function of potential using the single pulse technique.

All potentials are given versus the saturated calomel electrode. Current densities and differential capacities are referred to the electrode geometric area.

During potentiostatic polarization, an active-passive transition is observed for all solutions. The rest potential (-0.48 V) and primary passivation potential

(-0.42 V) are independent of solution composition. The critical current density increases with the total anion concentration. The capacity peak occurring slightly negative to the primary passivation potential is attributed to specific adsorption of the anions involved in the dissolution-passivation mechanism. The potential at which the electrode becomes totally passive shifts positive with increasing chloride ion concentration and is dependent on kinetic rather than thermodynamic factors.

Transpassive dissolution initiates between 0.57 and 0.64 V and exhibits Tafel behavior. Both the current density maximum (10^{-4} A cm^{-2}) and the corresponding potential (0.95 V) associated with the onset of secondary passivity are independent of solution composition. The capacity peak observed in this region is attributed to adsorption of the passivating species.

In solutions of $\geqslant 0.3$ M potassium chloride, an increase in current density caused by pitting starts at potentials normally in the passive region. The pitting potential depends on the relative amounts of chloride and sulfate ions present. No capacity peak is observed prior to pitting breakdown.

The capacity, between the potential of total passivity and the capacity minimum occurring at 0.60 V, is approximately independent of the stability of the passive state. This independence results from the domination of the interfacial capacitance by that of the passive film, obscuring

any changes in the film-solution capacity which may occur. The sudden decrease in capacity observed at 0.30 V is attributed to a change in the dielectric constant of the film. Between 0.3 and 0.6 V, film growth follows an inverse logarithmic law.

The potential-time behavior of samples subjected to galvanostatic polarization depends on both current density and solution composition. Systems not susceptible to pitting reach and maintain a positive steady state potential. In systems subject to pitting, the maximum potential attained is unstable and a shift in potential to more active values occurs.

In 0.3 M potassium chloride intermediate arrests produced by a given current density as well as the maximum potential achieved prior to breakdown correspond to potential arrests in the non-pitting systems. In 0.5 M potassium chloride pitting breakdown occurs from a potential maximum which is considerably below that observed in 0.3 M but the behavior at more negative potentials is similar.

It is assumed, therefore, that the initial effect of the anodic current on the metal surface at a given potential is the same in all cases and that pitting succeeds through the perturbation of these initial surface conditions by chloride ion.

Tafel behavior is associated with the arrests at -0.4, 0.8, 0.85, and 1.12 V. Active dissolution at -0.4 V exhibits a slope of 0.060 V decade^{-1} and is thought to proceed by the Heusler mechanism. Arrests at 0.8, 0.85 and 1.12 V correspond to transpassive dissolution, secondary passivity, and oxygen evolution, respectively. Capacity peaks are associated with the latter two effects and with the arrest at -0.4 V but not with pitting breakdown.

CHAPTER I

INTRODUCTION

A metal is in the passive state when it is inert in an environment in which, on the basis of thermodynamics, it should corrode readily. An ennoblement of the potential of the metal-environment interface accompanies the onset of passivation. Passivity has been recognized since 1836, when Faraday[1] observed the stability of iron metal immersed in concentrated nitric acid. However, the nature of the surface species leading to the onset and maintenance of the passive state is still not well understood. The two major theories advanced to explain the phenomenon are the bulk oxide theory and the adsorption theory.

The oxide film theory proposes that a bulk oxide is formed directly on the metal surface from the products of the metal dissolution reaction.[2,3,4] This oxide then acts as a physical barrier between the metal surface and the aggressive environment.

The adsorption theory of passivity attributes passivation of the metal surface to the adsorption of an "oxygen" species in less than or equal to monolayer quantities.[5,6] Two variations of the adsorption theory

have been described. In the chemical variation proposed by Uhlig,[7,8] adsorbed oxygen atoms are believed to satisfy the surface valences of all atoms on the metal surface. The correlation of the theoretical and experimental concentrations of components of transition metal alloys needed to bring about a sharp increase in the ease with which the alloys are made passive lends support to this hypothesis. The electrochemical variation ascribes the retardation of the metal dissolution reaction to a change in the double layer structure caused by the dipolar character of chemisorbed oxygen.[9] Orientation of the dipole with its positive end towards the solution increases the activation energy necessary for the metal dissolution reaction.

Hackerman[10] has proposed a theory intermediate to the above two. Here, the adsorption of oxygen atoms on the metal results in a metastable state lending temporary protection to the surface. Following electron transfer from the metal to adsorbed oxygen atoms, an amorphous bulk oxide is formed by cation migration through the adsorbed array. It is this bulk oxide which provides long-term protection. This theory, originally postulated for metals in oxygen-containing solutions, has also been proposed to explain the passivation mechanism of iron-chromium alloys in deaerated acidic sodium sulfate solutions.[11] A similar mechanism has been proposed by Frankenthal[12] for the passivation of an iron-24 chromium

alloy. Electron diffraction studies of the surface of stainless steels exposed to oxidizing acids or the atmosphere for short times at intermediate temperatures (25 to 60°C) have shown that the passive film formed is non-crystalline.[13] Transmission microscopy studies of films formed on an iron-24 chromium alloy during potentiostatic polarization in 0.5 M sulfuric acid show that they are also amorphous.[14]

The corrosion resistance of austenitic stainless steels in diverse environments is a result of the high degree of passive state stability conferred by the presence of chromium in amounts $\geq$ 12 percent.[15, 16] However, in specific media, especially in halide solutions, this corrosion resistance is lost, as evidenced by the onset of intense local attack, i. e., pitting. The mechanism by which pits nucleate and propagate in the presence of chloride ion has been investigated in great detail. Excellent reviews are given by Kolotyrkin[17] and Szklarska-Smialowska.[18]

The pitting phenomenon has been characterized by three parameters: the pitting potential, negative to which no pits can nucleate; the critical chloride ion concentration, the minimum concentration needed to initiate pitting in a given system; and the induction time, the time, at a given potential, which passes prior to breakdown. Thus, studies have been carried out

to examine the effect of metal composition,[19, 20, 21, 22, 23] defect density of a metal surface,[24, 25] grain size,[26] solution composition,[27, 28, 29, 22] sulfide inclusions,[30, 31, 32] and temperature[28] on the pitting potential and/or the location and number of pit sites. The critical chloride ion concentration has been shown to depend strongly on the concentration of inhibiting anions (e.g., sulfate, hydroxyl and nitrate ions) in the solution[33, 34, 35, 28] as well as on alloy composition.[36] The induction time has been found to decrease with increasing chloride ion concentration,[37, 38, 39, 40] potential of passivation,[39, 40] and temperature.[38]

The influence of an induction time is seen both in potentiostatic and galvanostatic polarization measurements. Previous works on austenitic stainless steels in chloride-containing solutions have shown that the application of a constant anodic current to an initially active electrode shifts the potential positive to a maximum value.[41] Despite the continued application of the current, the potential then decreases rapidly to a value normally in the passive region. The length of time to potential breakdown is a function of the current density and the chloride ion concentration. Examination of the metal surface shows that pitting has occurred.

The steady state potential achieved after breakdown has been called the protection potential of the system under study.[42] At potentials between the protection and pitting potentials previously nucleated pits can continue to grow but no new pits may form. At potentials negative to the protection potential, all existing pits become inactive.[35]

Anodic potentiostatic polarization to values more positive than the pitting potential also causes pit formation. A change in potential to values just positive to the pitting potential results in a decrease in current density with time from the initially high value associated with double layer charging.[40] This current decrease represents the readjustment of the electrode-solution interface to maintain the passive condition. After a time interval which depends on solution composition and potential, the current decrease is replaced by current oscillations signifying the pitting-induced breakdown of passivity. As the potential is made still more positive, the time for which passivity is maintained decreases until an induction period is no longer apparent.[43]

Mechanisms proposed to explain the dependence of pitting parameters on experimental variables are a function of the assumed nature of the passivating film. On the basis of a bulk oxide, Hoar[3] has described a mechanical breakdown process in which the mutual repulsion

of anions adsorbed on the oxide surface leads to the formation of cracks. A relationship between critical breakdown stress and surface tension as influenced by anion specific adsorption has been derived by Sato.[44] Hoar and Jacob[45] have also suggested that a metal cation is dissolved from the oxide through the formation of a metal-chloride complex containing 2.5 to 4.5 chloride ions. Cation migration through the film then allows continuation of the process. If the passive film is assumed to be an adsorbed "oxygen" species, then its replacement by chloride ions will lead to activation of the metal when a critical surface concentration of chloride ion is attained.[28, 17]

The presence of an induction time associated with pitting breakdown suggests that a time consuming change in surface structure is occurring. If the specific adsorption of chloride ion is involved in this change, then its incorporation into the electrical double layer should be reflected in the differential capacity-potential behavior of the interface.

The electrical double layer, in its ability to store charge, acts as a capacitor. The magnitude of the capacity associated with it is a complex function of potential and is therefore defined as a differential capacity, $\partial q/\partial E$. In the absence of specific adsorption, only water molecules populate the compact double layer,

the region between the metal and the Outer Helmholtz Plane. The capacity of the interface can then be represented by two capacitors in series; that of the region between the metal and the Outer Helmholtz Plane (OHP); and that of the region between the OHP and the bulk of the solution (the diffuse double layer). In dilute solutions ($\leqslant 0.001$ M), the capacity of the latter is small and dominates the interfacial capacity. In concentrated solutions, all of the diffuse double layer charge is located close to the OHP. The interface then behaves like a single parallel plate condenser, i.e., its capacity is approximately independent of potential.

When specifically adsorbed ions populate the IHP in a concentrated solution (> 0.001 M), the interface again functions as two capacitors in series. Bockris and Reddy,[46] in their treatment of the effect of contact adsorption on the total capacity of the metal-solution interface, derive the equation

$$1/C = 1/K_{M\text{-}OHP} - \left(\frac{1}{K_{M\text{-}OHP}} - \frac{1}{K_{M\text{-}IHP}}\right)\left(\frac{\partial q_{CA}}{\partial q_M}\right) \quad (1)$$

where C is the total measured differential capacity and $K_{M\text{-}OHP}$ and $K_{M\text{-}IHP}$ are the integral capacities associated with the metal to Outer Helmholtz Plane and metal to Inner Helmholtz Plane regions, respectively. The function, $\partial q_{CA}/\partial q_M$, represents the change in the amount of specifically adsorbed ion, q_{CA}, with the charge on the metal, q_M. Thus, as the charge on the metal becomes more

positive with increasing potential, an increase in the degree of specific adsorption with metal charge ($\partial^2 q_{CA}/\partial q_M^2 > 0$) should occur, producing an increase in the measured differential capacity of the interface. As growth continues, however, the buildup of lateral repulsion forces tends to decrease the degree to which specific adsorption occurs at a given metal charge. This inflection in the q_{CA}-q_M relationship results in a peak in the differential capacity-potential curve ($\partial^2 q_{CA}/\partial q_M^2 = 0$). Differential capacity measurements have been successfully applied to the determination of the specific adsorption of sulfate, perchlorate and chloride ions on iron.[47, 48, 49, 50]

The presence of a positive charge on the metal surface implies polarization at potentials positive to its zero point of charge. Studies of binary alloys suggest that the zero point of charge of an alloy should approach that of its component with the most negative zero point of charge if it is present in sufficient concentration.[51] The zero points of charge for nickel, chromium and iron have been determined in acidic sulfate solutions.[52] The corresponding values are -0.57, -0.69 and -0.62 V, respectively. It is expected then, that the zero point of charge of active stainless steel should be close to that of chromium, i.e. -0.69 V.

In order to explain the potential dependence of the activating effect of chloride ion in terms of specific adsorption to a critical surface concentration on the passive electrode, the zero point of charge of the passive surface must lie in the passive region. For passive iron, the zero point of charge occurs at -0.125 V in 0.01 M sodium hydroxide.[52] This positive shift in value from that observed on active iron can be attributed to an increase in work function resulting from the presence of an adsorbed "oxygen" species or an oxide film. The extension of this phenomenon to stainless steel seems logical.

The primary purpose of the experiments conducted in this study was the determination of the effect of chloride ion on the capacity-potential behavior of stainless steel observed during potentiostatic and galvanostatic polarization in solutions initiating pitting. In order to explain the potential arrests observed during constant current polarization, the potentiostatic studies were extended to cover the potential range from active dissolution to oxygen evolution. Corresponding capacity values were determined and the current-potential and capacity-potential data correlated.

The relationship between the rate of an electrochemical reaction and the potential difference across the interface at which it occurs is discussed in detail by Bockris and

Reddy.[46] When electron transfer is rate-determining, i.e., the system is under activation control, the current-potential relation is given by the general form of the Butler-Volmer equation,

$$i = i_o \exp \frac{\vec{\alpha} F}{RT}\eta - i_o \exp\left(-\frac{\overleftarrow{\alpha} F}{RT}\right)\eta \qquad (2)$$

where i_o is the exchange current density, the α's are the transfer coefficients, and η is the overvoltage. All other terms have their usual meaning. The first term on the right hand side of equation 2 is the current density resulting from the oxidation (anodic) reaction. The second term pertains to the reduction (cathodic) reaction.

At the equilibrium potential of the rate-determining reaction, the overvoltage, which represents the potential difference across the interface in excess of the equilibrium potential difference ($E - E_o$), is zero. The net current density observed (i) will therefore also be zero since at equilibrium the rates of the anodic and cathodic reactions will be equal. The transfer coefficients determine what fraction of the potential difference across the interface is operative in changing the energy barrier for the oxidation and reduction reactions.

As the potential difference across the interface is made more positive ($\eta > 0$), the contribution of the anodic current density to the total current density will increase. At a sufficiently positive overvoltage ($\sim$0.120 V for a one-electron transfer reaction), the

influence of the cathodic current density becomes negligible. The current-potential relationship is then given by

$$i = i_o \exp \frac{\vec{\alpha} F}{RT} \eta \qquad (3)$$

which can be put in logarithmic form and rearranged to give

$$\eta = \frac{2.3\ RT}{\vec{\alpha} F} \log i - \frac{2.3\ RT}{\vec{\alpha} F} \log i_o \qquad (4)$$

A plot of overvoltage versus log i is therefore linear. Such plots are known as Tafel lines. The slope of the line contains the transfer coefficient which is a complex function of the total number of electrons transferred during the reaction as well as the mechanism by which the reaction proceeds. From the slope of the line and its intercept, the exchange current density for the reaction can be calculated.

In systems in which a faradaic current can flow, i.e., charge can cross the metal-solution interface, the electrical behavior of the interface can be represented by a resistor in series with a capacitor and resistor in parallel. The series resistor represents the resistance of the solution to current flow. The capacity is the differential double layer capacity. The parallel resistor represents the polarization resistance of the faradaic reaction, decreasing as the rate constant of the reaction increases. In cases of low polarization resistance, the determination of the differential capacity is difficult since the polarization resistance can act as a leakage

path for the signal measuring the capacity. Faradaic current also interferes indirectly by causing a change in the true electrode surface area as well as in the solution composition.

The use of the classical alternating current technique in which the interface forms one arm of an impedance bridge to determine the double layer capacity on a solid electrode is precluded because of the dependence of the capacity value measured on signal frequency.[53] Most of the direct interference can be eliminated, however, by the use of the single pulse method of differential capacity measurement developed by Riney, Schmid and Hackerman.[54] Analysis of the linear segment of the potential transient resulting from a single current pulse allows calculation of the capacity at the point from which the pulse initiates since

$$C = i(dt/dE)_{t=0} \qquad (5)$$

where i is the pulse magnitude and dt/dE is the slope of the potential-time transient evaluated at t = 0.

CHAPTER II

EXPERIMENTAL

Experimental Design

The material investigated was stainless steel, AISI 304, provided by the United States Steel Corporation. Its composition was given as 0.03 C, 0.027 P, 1.10 Mn, 0.022 S, 0.43 Si, 9.26 Ni, 18.6 Cr, 0.39 Mo, and 0.04 N (weight percent). Bar stock was machined to cylinders with a diameter of 6 mm and a height of 9 mm (Figure 1). The cylinders were tapped, threaded, and mechanically polished at 2400 rpm with 400 followed by 600 grit emery paper. They were then degreased with spectral grade benzene in an ultrasonic cleaner, rinsed with triply distilled water, and stored in a closed polyethylene container until needed.

Primary studies were carried out in solutions containing 0.0, 1.17×10^{-2}, 9.97×10^{-2}, 0.301, 0.508, and 1.0 M potassium chloride. Solution pH was measured with a Beckman pH meter and adjusted to 2.4 with concentrated sulfuric acid. Sodium sulfate was added as required to maintain an ionic strength of one (0.318, 0.313, 0.284, 0.232, 0.147, and 0.00 M, respectively). Secondary experiments involved solutions of pH 2.4 containing 0.102, 0.123 and 1.0 M potassium chloride with no sodium sulfate additions as well as 0.3 M potassium chloride at pH 1.52

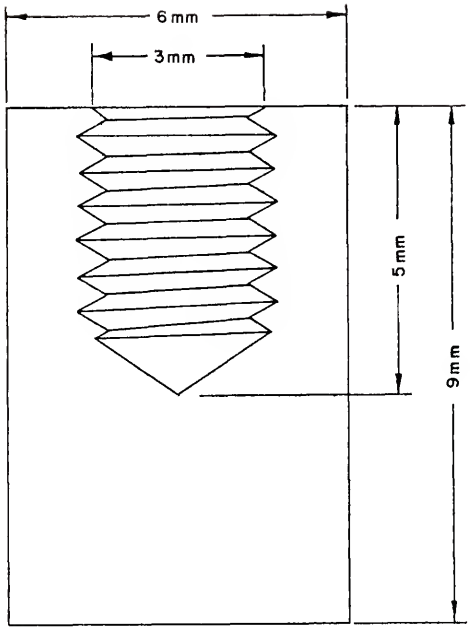

Figure 1. Stainless steel electrode.

and 6.22. All chemicals used in solution preparation were reagent grade. Recrystallization of potassium chloride from triply distilled water had no effect on experimental results. The water employed was distilled from alkaline potassium permanganate and then from a two-stage Heraeus quartz still and collected in a two-liter Pyrex volumetric flask. Its maximum conductivity, determined with a General Radio Impedance Bridge, was $2 \times 10^{-6} \Omega^{-1} cm^{-1}$.

Platinum electrodes, generally used in pre-electrolysis to remove electroactive impurities from the solution, have been shown to dissolve when polarized anodically in both sulfate and chloride containing solutions.[55] Because of the possibility of contaminating both the solution and the stainless steel surface with platinum, a pre-electrolysis step was therefore omitted.

The electrochemical cell was made of Pyrex and was of conventional design (Figure 2). A Luggin capillary connected the saturated calomel reference electrode (SCE) to the cell via two solution-lubricated mercury-seal stopcocks and a potassium chloride salt bridge. A 1 cm^2 platinum flag auxiliary electrode was mounted on the cell with a standard taper joint. For use in constant current polarization and capacitance measurements, a platinum gauze basket, approximately 100 cm^2 in area (Engelhard Industries), was mounted concentric to the test electrode. The cell cap incorporated a 24/40 standard taper joint for mounting the test electrode.

Figure 2. Electrochemical cell.

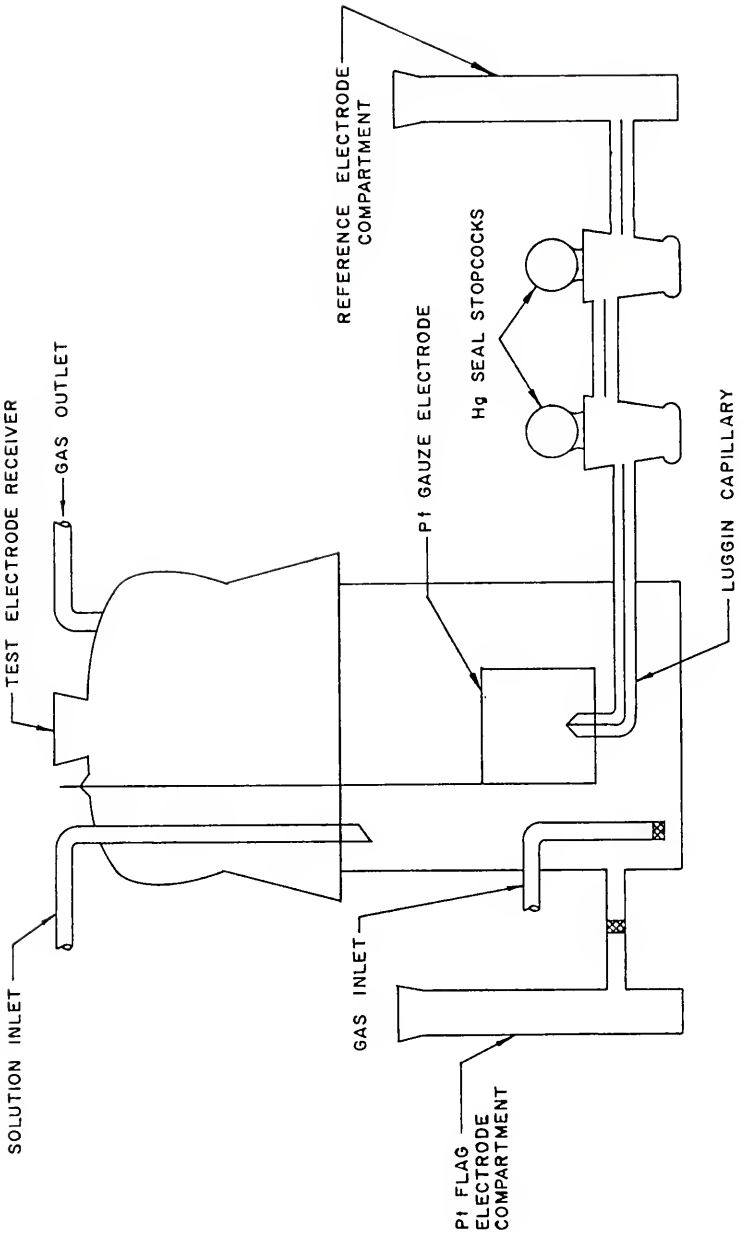
REFERENCE ELECTRODE COMPARTMENT
Hg SEAL STOPCOCKS
Pt GAUZE ELECTRODE
LUGGIN CAPILLARY
TEST ELECTRODE RECEIVER
GAS OUTLET
SOLUTION INLET
GAS INLET
Pt FLAG ELECTRODE COMPARTMENT

The electrode holder (Figure 3) was made from a Kel-F rod machined to approximately 1 cm in diameter in which a 3 mm center hole was drilled. The rod was then heated and a threaded stainless steel rod inserted so that thread protruded on both ends. The Kel-F rod was shrunk in an ice bath to facilitate its insertion into a 1 cm ID glass stirrer bearing sleeve which had a 24/40 standard taper joint attached. The sample was then affixed to the protruding steel rod. The electrode area exposed to solution was approximately 2 cm^2. The sample-sample holder seal could be tightened by turning a finger nut at the top of the assembly. Teflon washers were placed between both the sample and holder and the nut and holder to reinforce the seal. Spot checks of the shielded top surface of the test electrode showed no evidence of corrosion indicating the absence of leakage.

Experimental Technique

Solutions were deaerated with helium (99.99 percent) for a minimum of eight hours prior to use. Prepurification and water saturation of the gas was accomplished by passing it through a 12 cm column of Linde 5 Å molecular sieve pellets into a gas wash bottle containing triply distilled water. The gas then flowed into a two-liter reservoir containing the solution and continued through a dispersion

Figure 3. Kel-F electrode holder.

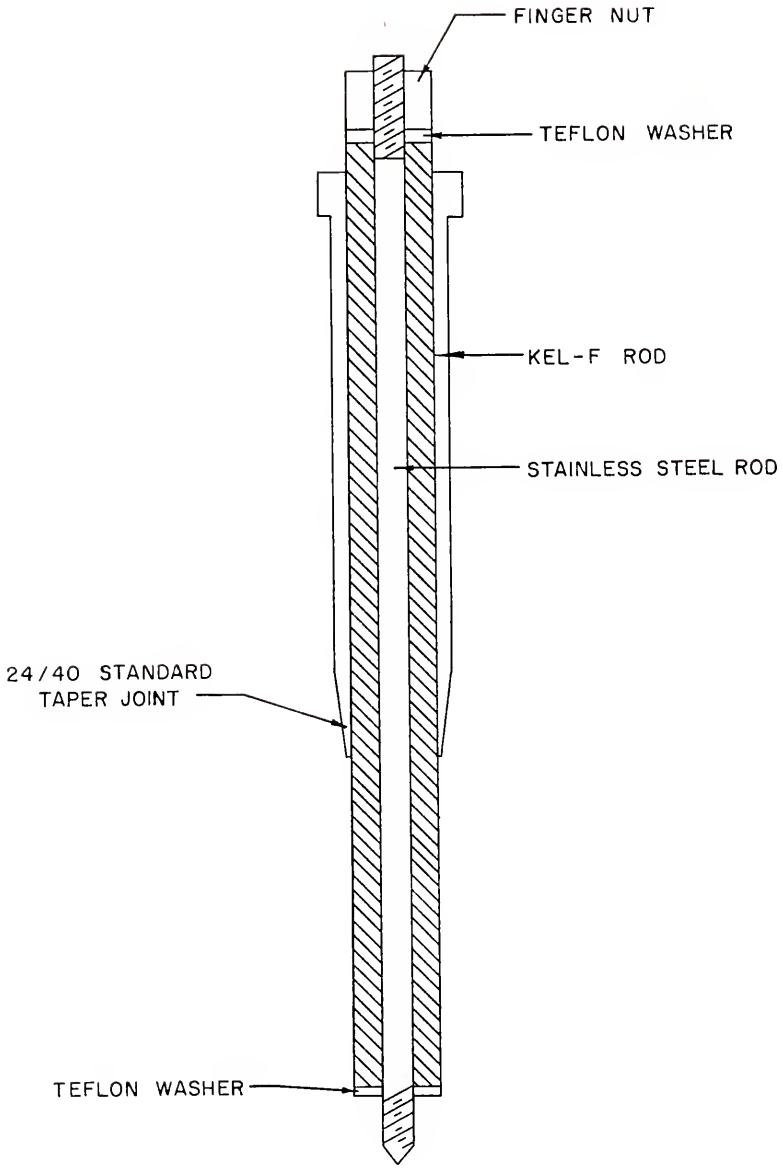
FINGER NUT
TEFLON WASHER
KEL-F ROD
STAINLESS STEEL ROD
24/40 STANDARD
TAPER JOINT
TEFLON WASHER

tube into the electrochemical cell. The cell gas outlet terminated in a gas wash bottle to prevent contamination of the cell contents with ambient air.

Immediately before each experiment, the cell was washed with hot chromo-sulfuric acid cleaning solution and rinsed with triply distilled water. Gas pressure was then diverted to fill the cell with deaerated solution from the reservoir. The stainless steel sample was secured on the Kel-F holder, rinsed with triply distilled water and the solution to be studied, and immersed in solution. All samples were pretreated at -0.700 V for twenty minutes to reduce air-formed surface films. Solution stirring was accomplished with a magnetic stirring bar and the helium flow continued throughout the experiment. All solutions were at room temperature and all potentials are reported relative to the saturated calomel electrode. Current density and differential capacity were calculated using electrode geometric areas. The test electrode was grounded during all experiments.

Potentiostatic polarization

The block diagram of the system employed in potentiostatic experiments is shown in Figure 4. Polarization was accomplished with a slightly modified Harrar[56] potentiostat. (Two each of obsolete transistors 2N333A and HA7534 were replaced with the equivalent circuit elements 2N3568, 2N5869, and 2N3644,2N5867.)

Figure 4. Block diagram of the potentiostatic polarization circuit.

A. Test electrode
B. Reference electrode
C. Platinum flag electrode
D. Platinum gauze electrode

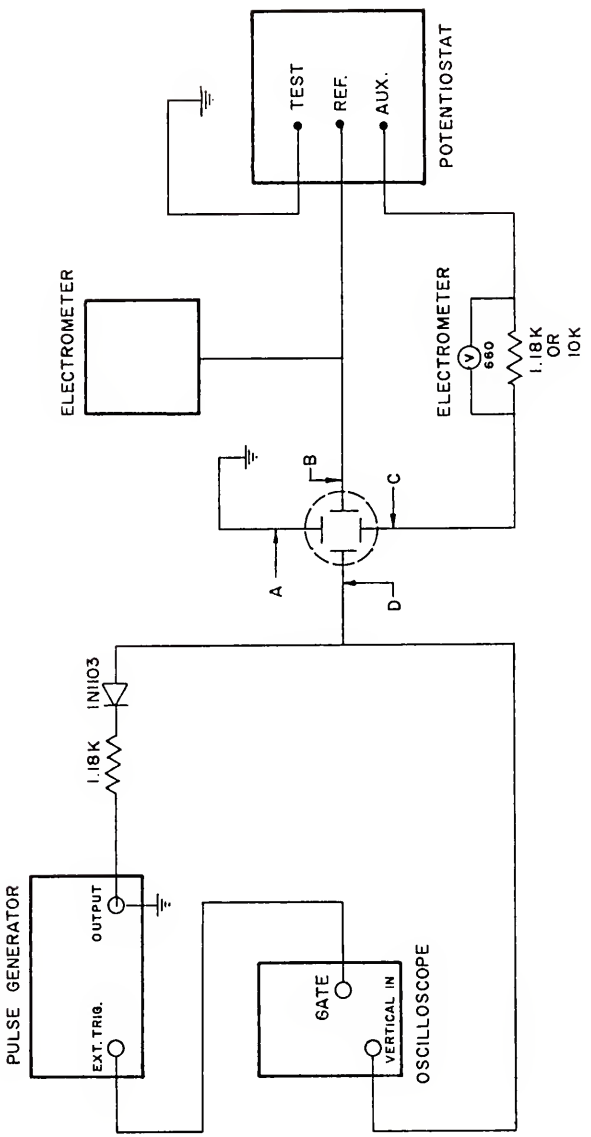
POTENTIOSTAT
TEST
REF.
AUX.
ELECTROMETER
ELECTROMETER
660
1.18K
OR
10K
B
C
A
D
1N1103
1.18K
PULSE GENERATOR
OUTPUT
EXT. TRIG.
GATE
VERTICAL IN
OSCILLOSCOPE

After prepolarization at -0.700 V the potential of the test electrode was shifted anodic in step-wise increments. The magnitude of the imposed step depended on the potential range under investigation and the electrochemical reaction(s) associated with it. In regions where changes in potential caused significant changes in current density, steps of 20 to 30 mV were generally employed. In regions of approximately constant current, 50 mV steps were used. A Keithley 610B electrometer was used to monitor the applied potential. After an arbitrary time interval of 10 minutes, the current flowing in the auxiliary-test electrode circuit was determined from the potential drop across a 1.18 kΩ or a 10 kΩ wire-wound precision resistor (1 percent) shunting the input of a Keithley 660 electrometer ($10^{14}\Omega$ input impedance).

The differential capacity of the stainless steel-solution interface was determined as a function of potential using the single pulse method.[54] A voltage pulse from the gate of a Tektronix 549 storage oscilloscope was used to trigger a Tektronix 114 Pulse Generator. The 100 μsec square wave current pulse produced was applied to the platinum basket-test electrode circuit. The resulting potential-time transient was recorded on the oscilloscope operated in the storage mode at a sensitivity of 2 or 5 mV cm^{-1} and 2 or 5 μsec cm^{-1}. Differential capacity values were calculated from the linear segment of the transient slope during the initial 10 μsec of the pulse. Since the transient is

linear between 4 and 10 μsec, the slope determined between these two points is equivalent to that of the tangent drawn to the curve at t = 4 μsec. Measuring times of 4 μsec correspond to an alternating current frequency of approximately 1.2×10^5 Hz. Since a frequency of 10^5 Hz is required to eliminate faradaic interference completely,[57] very little interference is expected.

Prior to each experiment, the pulse magnitude was calibrated using standard capacitors and resistors. The current density of the pulse could be calculated from the known value of capacity in the calibration circuit, the measured slope of the transient, and the electrode geometric area. Pulse magnitude was approximately 5 mA cm^{-2} and was independent of capacity between 1 and 10 μfarads.

Galvanostatic polarization

After potentiostatic prepolarization the system was switched to galvanostatic control using a two-position toggle switch. A block diagram of the circuit used during galvanostatic polarization experiments is given in Figure 5. A constant current was supplied to the platinum basket-test electrode circuit by a Hewlett Packard 881A power supply operated in the constant voltage mode in series with a bank of resistors (4.7 to 47.8 kΩ). The positive terminal of the power supply was grounded to establish the test electrode as the anode. The current magnitude was determined from the voltage drop developed

Figure 5. Block diagram of the galvanostatic polarization circuit.

A. Test electrode
B. Reference electrode
C. Platinum flag electrode
D. Platinum gauze electrode

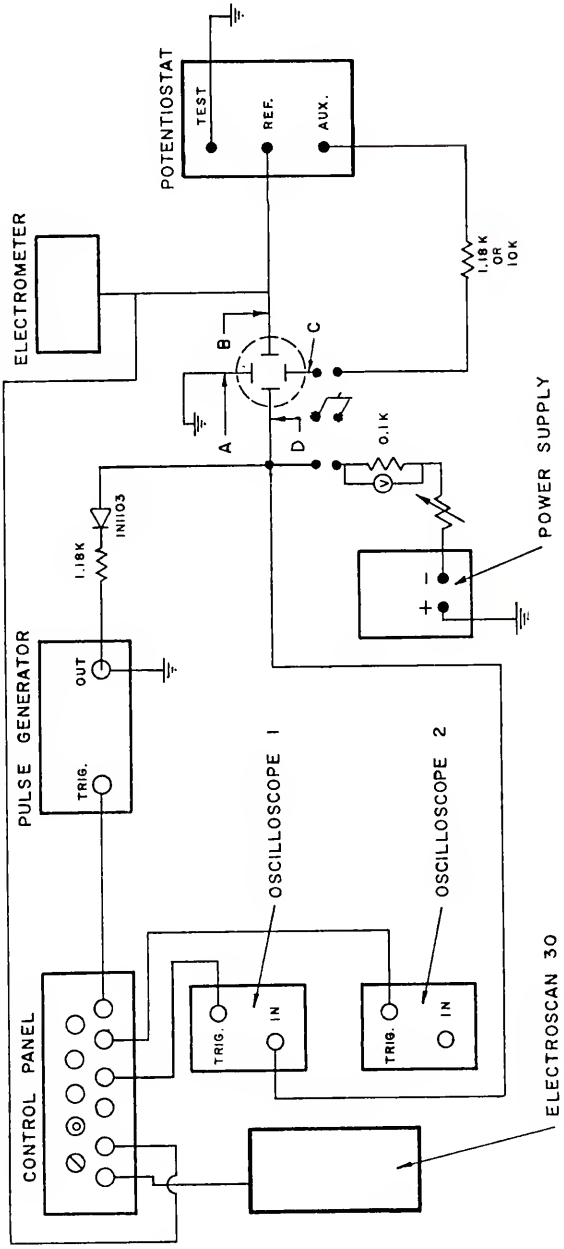
POTENTIOSTAT
TEST
REF.
AUX.
ELECTROMETER
1.18K OR 10K
B
C
A
D
0.1K
POWER SUPPLY
1.18K
IN1103
PULSE GENERATOR
OUT
TRIG.
OSCILLOSCOPE 1
OSCILLOSCOPE 2
CONTROL PANEL
TRIG.
IN
TRIG.
IN
ELECTROSCAN 30

across a 100Ω precision resistor (1 percent) using a Keithley 660 electrometer and was adjusted by varying the series resistance and the voltage output of the power supply. Applied current densities ranged from 0.99×10^{-4} to 2.0×10^{-3} A cm^{-2}. The resulting potential-time curve was displayed on the recorder of a Beckman Electroscan 30. Potential values were monitored with a Keithley 610B electrometer.

A study of differential capacity as a function of potential was also carried out during constant current polarization. As described above, a square wave current pulse was delivered from the pulse generator to the platinum basket-test electrode circuit. The resulting potential-time trace was displayed on the storage oscilloscope and the capacity calculated from the initial slope of the transient and the predetermined pulse magnitude.

The development of the theory of the single pulse method assumes that a perturbation current is applied to a system under constant current polarization at a steady-state potential so that the current before and after the pulse remains the same. Since, during potentiostatic polarization of austenitic stainless steel, either a steady state current or a very slow decrease in current with time is observed, the method should be directly applicable. For galvanostatic polarization the constant current condition

is satisfied but a continuous change in potential with time occurs.[7] However, for small measuring times ($\leqslant$ 10 μsec), the change in potential will be negligible.

Because of the rapid change in potential with time during constant current polarization, difficulties were encountered in the correlation of capacity values and the potentials at which they were determined. A system was therefore developed which facilitated the sequential storage of pulse-produced transients and supplied a marker signal to the Electroscan recorder whenever the pulse generator was triggered (Figure 6).

Two oscilloscopes were used sequentially. Depression of PG 1 or PG 2 on the control panel (Figure 7) first changed the DC level of the input of the oscilloscope in use by 10 mV. This provided automatic downward displacement of the successively produced potential-time transients. A two-step generator was associated with PG 1, an eight-step generator with PG 2. In most cases, the oscilloscope sensitivity needed for precise determination of the transient slope (2 or 5 mV cm^{-1}) precluded the use of automatic stepping, and vertical displacement was accomplished manually instead.

Figure 6. Block diagram of the circuit employed in capacity-potential data correlation.

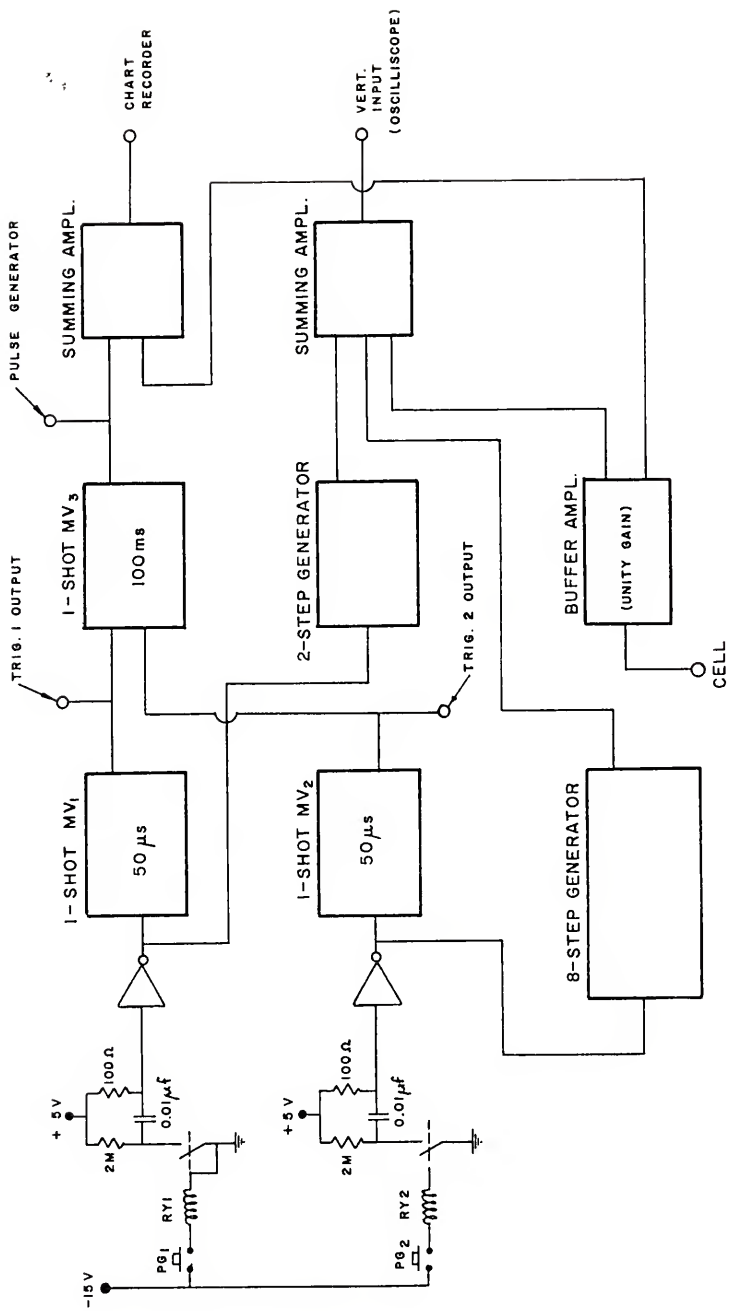
CHART RECORDER
VERT. INPUT (OSCILLISCOPE)
SUMMING AMPL.
SUMMING AMPL.
PULSE GENERATOR
1-SHOT MV3
100 ms
2-STEP GENERATOR
BUFFER AMPL.
(UNITY GAIN)
CELL
TRIG. 1 OUTPUT
TRIG. 2 OUTPUT
1-SHOT MV1
50 μs
1-SHOT MV2
50 μs
8-STEP GENERATOR
+5 V
100 Ω
0.01 μf
2M
+5 V
100 Ω
0.01 μf
2M
RY1
RY2
PG1
PG2
-15 V

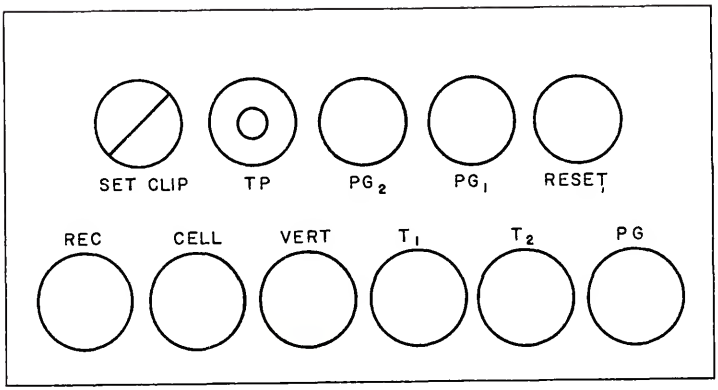

Figure 7. Control panel.

Then, after a 50 μsec delay, the horizontal sweep of the oscilloscope was triggered. Simultaneously, 15 V, 100 msec pulse was supplied to the external trigger of the pulse generator to produce the current pulse needed to determine the capacity. At the same time a 50 mV, 100 msec pulse was superimposed on the galvanostatic potential-time response signal from the cell to the recorder.

Since the potential values recorded during constant current polarization reached 1.4 V, while the marker pulse superimposed on this signal was only 50 mV, the cell signal was passed through a buffered amplifier and could be clipped at a preset value. The recorder sensitivity could therefore be adjusted to display the pulse marker while the entire potential-time curve remained on chart.

CHAPTER III

RESULTS

Current-Potential Behavior During Potentiostatic Polarization

The response of the stainless steel samples to potentiostatic polarization is given schematically in Figure 8. The region ABC represents the transition from the active to the passive state characteristic of this material in the solutions employed. An adjoining region of approximately constant current is then usually observed (CC'D). The increase in current on further polarization is caused by loss of passive state stability as the result of pitting (DE) or of transpassivity (FG). The potential and current density notations on the schematic are defined below. They are presented in the text in approximately the same order in which they arise during polarization.

Possible interrelationships between experimentally determined current densities, potentials, and/or solution composition variables were examined. The various data were plotted. If a plot appeared to be linear, then a linear regression analysis was performed. Only curves with correlation coefficients (r^2) of $\geqslant 0.90$ were reported as linear.

Figure 8. Schematic potentiostatic current-potential behavior.

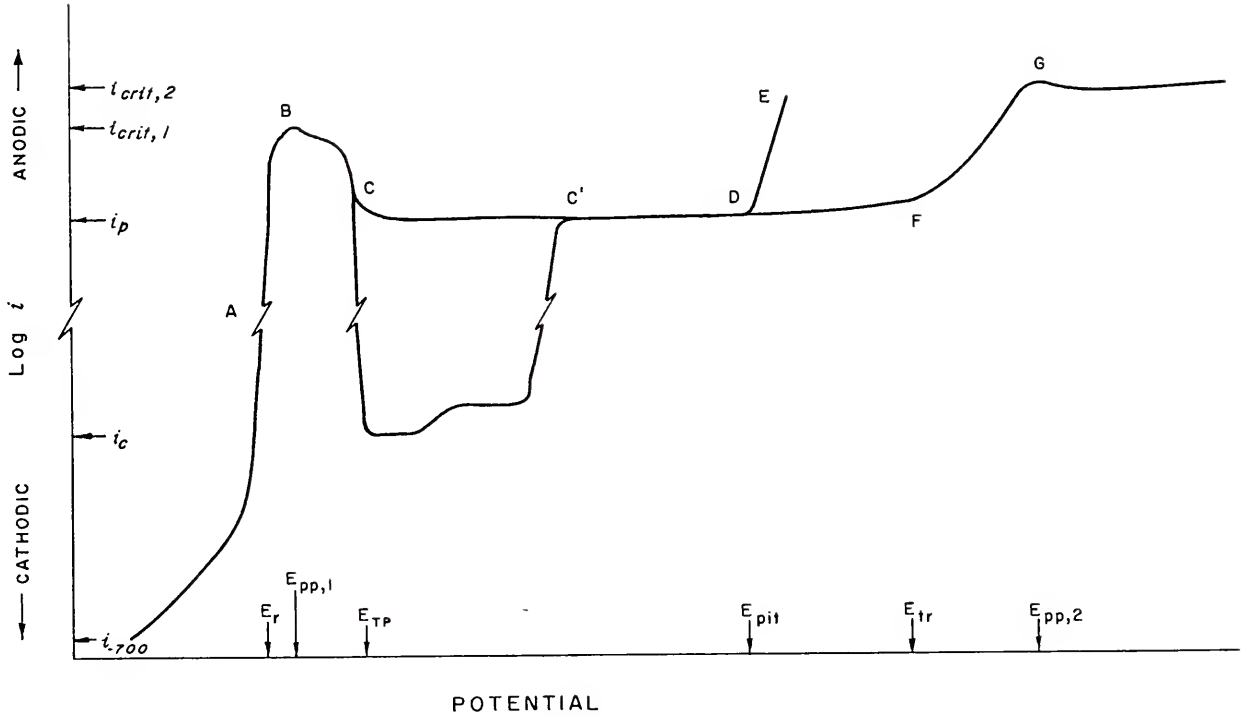
ANODIC
CATHODIC
Log i
$i_{crit,2}$
$i_{crit,1}$
i_p
i_c
i_{-700}
A
B
C
C'
D
E
F
G
E_r
$E_{pp,1}$
E_{TP}
E_{pit}
E_{tr}
$E_{pp,2}$
POTENTIAL

Primary solutions

Characteristic potentials and current densities determined from the potentiostatic polarization curves obtained in primary solutions are presented in Tables 1 - 4. The solution composition parameters investigated are listed in Table 5. The logarithms of these functions have also been considered. Relationships with correlation coefficients $\geqslant 0.90$ are reported in Table 6.

After the twenty-minute prepolarization period at -0.700 V, net currents are cathodic with values between 2.1×10^{-3} and 5.3×10^{-3} A cm^{-2}. No correlation between the hydrogen evolution current and solution composition at constant pH and constant potential is apparent (Table 1). As the potential is shifted anodic, the measured current decreases and becomes zero at the rest potential, E_r. The rest potential is defined as that potential at which the absolute values of the internal anodic and cathodic currents become equal, resulting in a net external current flow of zero. Values of the rest potential determined here are -0.450 to -0.510 V. The maximum average deviation for data obtained for a given solution composition is 16 mV for 0.0 M potassium chloride (Table 2). For all other compositions it is substantially less ($\leqslant 7$ mV).

Polarization at potentials positive to E_r results in a net anodic current which increases with potential to a maximum, signifying the onset of passivation. This maximum current density and its corresponding potential are the

Table 1

Potentiostatic current-potential behavior in primary solutions (average curves).

$[Cl^-]$ x 10^1	$[SO_4^{2-}]$ x 10^1	pH	i_{-700} (A cm^{-2}) x 10^3	E_r (V,SCE)	$E_{pp,1}$ (V,SCE)	$i_{crit,1}$ (A cm^{-2}) x 10^5	i_p (A cm^{-2}) x 10^7	E_{TP} (V,SCE)	E_{pit}(V,SCE) inc	gr
0	3.34	2.40	-2.20	-0.453	-0.420	2.26	12.90	-0.285	-	-
0.117	3.29	2.40	-3.10	-0.475	-0.425	2.73	5.25	-0.255	-	-
0.997	3.00	2.40	-3.50	-0.480	-0.432	3.13	6.40	-0.242	-	-
3.01	2.48	2.35	-2.23	-0.470	-0.420	3.43	7.85	-0.230	+0.395	+0.360
5.08	1.63	2.42	-2.06	-0.510	-0.400	8.49	-	-0.205	0.00	-0.012
10.0	0.16	2.40	-5.31	-0.460	-0.400	6.73	-	-0.160	-0.090	-0.155

Table 2

Potentiostatic current-potential behavior in primary solutions (individual experiments).

$[Cl^-]_l$ x 10^1	$[SO_4^=]_l$ x 10^1	pH	i_{-700} (A cm^{-2}) x 10^3	E_r (V,SCE)	$E_{pp,l}$ (V,SCE)	$i_{crit,l}$ (A cm^{-2}) x 10^5	i_p (A cm^{-2}) x 10^7	E_{TP} (V,SCE)	E_{pit}(V,SCE) inc	gr
0	3.34	2.40	-2.3	-0.420	-0.400	1.31	10.7	-0.278	-	-
			-	-0.460	-0.430	2.65	21.5	-0.287	-	-
			-2.1	-0.460	-0.410	1.90	65.9	-0.287	-	-
0.117	3.29	2.40	-2.7	-0.473	-0.410	3.4	5.32	-0.255		
			-3.5	-0.473	-0.420	2.3	5.18	-0.265		
0.997	3.00	2.40	-3.8	-0.480	-0.430	3.3	7.19	-0.237		
			-3.2	-0.475	-0.430	2.9	5.01	-0.250		
3.01	2.48	2.35	-1.8	-0.475	-0.420	3.55	7.23	-0.230	0.420	0.365
			-2.7	-0.480	-0.415	3.39	8.48	-0.226	0.370	0.360
5.08	1.63	2.42	-2.4	-0.508	-0.400	8.3	-	-0.200	0.00	-0.020
			-1.9	-0.520	-0.400	7.6	-	-0.200	0.00	-0.047
			-1.9	-0.520	-0.400	9.5	-	-0.210	0.00	-0.020
10.0	0.160	2.40	-4.9	-0.460	-0.400	7.3	-	-0.197	-0.10	-0.145
			-5.8	-0.460	-0.400	6.2	-	-0.197	-0.05	-0.175

Table 3

Cathodic loop in primary solutions.

$[Cl^-]$ x 10^1	$[SO_4^{2-}]$ x 10^1	pH	i_{-700} ($A\ cm^{-2}$) x 10^3	C_{-700} ($\mu f\ cm^{-2}$)	C_1 ($\mu f\ cm^{-2}$)	Negative loop (V,SCE)	i_c ($A\ cm^{-2}$) x 10^7	i_{-200} ($A\ cm^{-2}$) x 10^7
0	3.34	2.40	-2.31	130	66	-	-	13.4
			-	28	80	-	-	27.3
			-2.10	78	183	-0.30 to 0.00	-13.6	-9.13
0.117	3.29	2.40	-2.67	55	110	-	-	4.54
			-3.54	66	177	-0.250	-2.27	3.10
0.997	3.00	2.40	-3.83	73	124	-	-	10.4
			-3.18	52	81	-0.27 to -0.20	-3.89	-0.09
3.01	2.48	2.35	-1.8	43	71	-	-	9.66
			-2.67	43	68	-	-	11.5
5.08	1.63	2.42	-2.45	21	46	-	-	5.97
			-1.89	21	54	-	-	8.15
			-1.85	23	65	-	-	10.6
10.0	0.160	2.40	-4.86	39	126	-0.20 to -0.15	-4.25	-4.25
			-5.77	46	88	-	-	3.42

Table 4

Transpassive behavior in primary solutions.

$[Cl^-]$ x 10^{-1}	$[SO_4^{2-}]$ x 10^{-1}	pH	b_a V decade^{-1}	E_{tr} (V,SCE)	$E_{pp,2}$ (V,SCE)	$i_{crit,2}$ (A cm^{-2}) x 10^4	$\Delta i_{..}$ (A cm^{-2}) x 10^6
0.0	3.34	2.40	0.114	0.671	0.950	1.12	21
0.117	3.29	2.40	0.114	0.641	0.950	1.02	14
0.997	3.00	2.40	0.150	0.575	0.950	1.03	17

Table 5

Solution composition parameters investigated in primary solutions.

Cl^a	SO_4/Cl	$Cl/(Cl + SO_4)$	$Cl/(Cl + 2\ SO_4)$	$Cl/(Cl + \frac{1}{2}\ SO_4)$	$pH + \log(Cl + SO_4)$
0.0	-	0	0	0	1.92
1.17×10^{-2}	28.1	0.034	0.017	0.066	1.93
9.97×10^{-2}	3.00	0.249	0.142	0.400	2.00
0.301	0.82	0.548	0.377	0.707	2.09
0.508	0.32	0.755	0.609	0.861	2.25
1.00	0.016	0.984	0.968	0.982	2.40

[a] Cl and SO_4 represent the analytical concentration of chloride and sulfate, respectively. The brackets and charge designations have been omitted for clarity.

Table 6

Interrelationships in potentiostatic experiments in primary solutions.

Independent variable	Dependent variable	Slope	Correlation coefficient	Data points
pH + log(SO_4 + Cl)[a]	log i_{crit}	1.10	(0.83)	6
Cl	E_{TP}	0.108 V $mole^{-1}$	0.93	6
Cl/(Cl + SO_4)	E_{TP}	0.103 V	0.92	6
Cl/(Cl + 2 SO_4)	E_{TP}	0.110 V	0.94	6
pH + log (SO_4 + Cl)	E_{TP}	0.218 V $decade^{-1}$	0.94	6
log(SO_4/Cl)	E_{TP}	a. 2 segments		
		-0.016 V $decade^{-1}$	0.98	3
		-0.039 V $decade^{-1}$	0.99	3
		b. 1 segment		
		-0.030 V $decade^{-1}$	0.94	5
Cl	i_p	8.68 x 10^{-7} A cm^{-2} $mole^{-1}$	0.97	3
Cl/(Cl + SO_4)	i_p	5.03 x 10^{-7} A cm^{-2}	1.00	3
Cl/(Cl + 2 SO_4)	i_p	7.09 x 10^{-7} A cm^{-2}	0.99	3
Cl/(Cl + ½ SO_4)	i_p	4.05 x 10^{-7} A cm^{-2}	0.99	3
log (SO_4/Cl)	log i_p	-0.11	0.99	3
pH + log (SO_4 + Cl)	log i_p	1.05	0.99	3

Table 6 continued

Independent variable	Dependent variable	Slope	Correlation coefficient	Data points
log Cl	$E_{pit(gr)}$	-0.96 V decade^{-1}	0.91	3
SO_4/Cl	$E_{pit(gr)}$	0.65 V	0.99	3
$Cl/(Cl + SO_4)$	$E_{pit(gr)}$	-1.17 V	0.92	3
$\log\{Cl/(Cl + SO_4)\}$	$E_{pit(gr)}$	-2.09 V decade^{-1}	0.97	3
$\log\{Cl/(Cl + 2\ SO_4)\}$	$E_{pit(gr)}$	-1.26 V decade^{-1}	0.94	3
$Cl/(Cl + \frac{1}{2}\ SO_4)$	$E_{pit(gr)}$	-1.90 V	0.97	3
$\log\{Cl/(Cl + \frac{1}{2}\ SO_4)\}$	$E_{pit(gr)}$	-3.73 decade^{-1}	0.97	3
$pH + \log\{SO_4 + Cl)\}$	$E_{pit(gr)}$	-1.67 V decade^{-1}	0.95	3
SO_4/Cl	$E_{pit(inc)}$	0.62 V	0.96	3
$\log\{Cl/(Cl + SO_4)\}$	$E_{pit(inc)}$	-1.98 V decade^{-1}	0.92	3
$\log\{Cl/(Cl + \frac{1}{2}\ SO_4)\}$	$E_{pit(inc)}$	-3.54 V decade^{-1}	0.93	3

Table 6 continued

Independent variable	Dependent variable	Slope	Correlation coefficient	Data points
$Cl/(Cl + \frac{1}{2} SO_4)$	$E_{pit(inc)}$	-1.80 V	0.92	3
$pH + \log(SO_4 + Cl)$	$E_{pit(inc)}$	-1.57 V decade^{-1}	0.95	3

[a] Cl and SO_4 represent the analytical concentration of chloride and sulfate, respectively. The brackets and charge designations have been omitted for clarity.

critical current density (i_{crit}) and the primary passivation potential ($E_{pp,1}$), respectively. All values of i_{crit} measured here are between 1.3×10^{-5} and 9.50×10^{-5} A cm^{-2}. Although, in some cases, the lowest value of critical current density observed at a given chloride ion concentration approximates the highest seen in the next lower chloride ion concentration, there is a definite trend in the average values toward a reproducible maximum at 0.508 M potassium chloride (Table 2).

The only relationship for which linearity is suggested is that between the logarithm of critical current density and the solution composition function, pH + log ($[SO_4^{2-}]$ + $[Cl^-]$), where $[SO_4^{2-}]$ and $[Cl^-]$ are the analytical concentrations of sulfate and chloride, respectively. A slope of 1.10 is measured (Figure 9). No linearity is found between the logarithm of i_{crit} and E_r, contrary to the work of Wilde.[58] However, the most negative rest potential and highest critical current density values occur in the same system.

From its value at the maximum the current density then decreases to a low value ($\sim 10^{-6}$ A cm^{-2}) characteristic of the passive region, i_p, and is approximately independent of potential. In some cases, prior to the attainment of the passive current value, a negative current loop is observed (Ci_cC'). Experimentally determined characteristics of the loop are presented in Table 3 and an experimental

Figure 9. Variation of the logarithm of the critical current density with the concentration function, pH + log ($[SO_4^{2-}]$ + $[Cl^-]$).

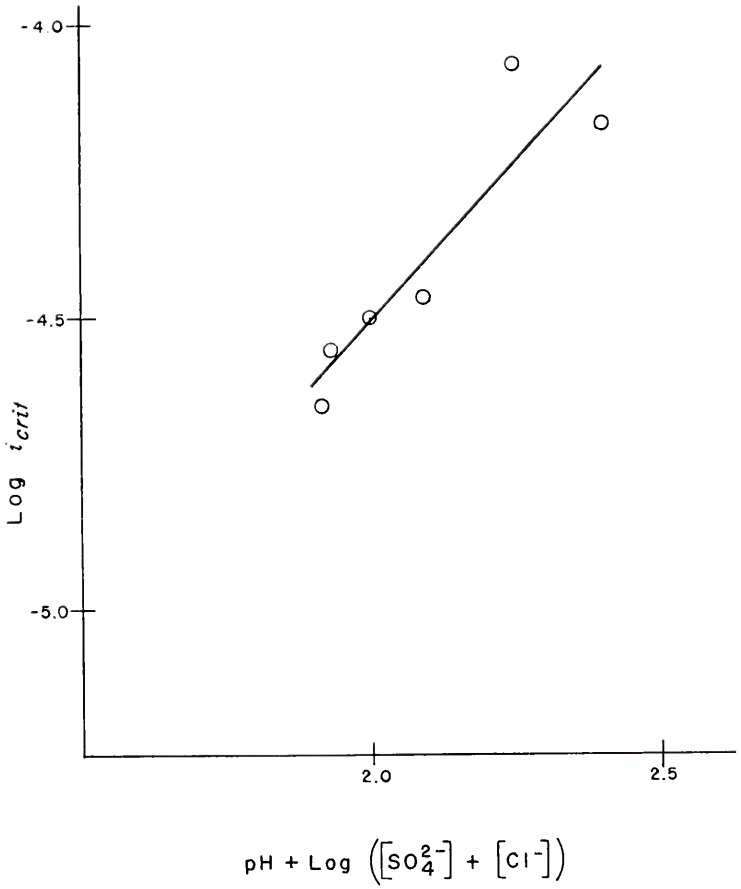
-4.0
-4.5
-5.0
Log i_{crit}
2.0
2.5
pH + Log $\left(\left[SO_4^{2-}\right] + \left[Cl^-\right]\right)$

curve containing a cathodic loop is presented in Figure 10. The potential range in which it occurs, -0.30 to 0.0 V, is independent of solution composition. The maximum cathodic current density associated with the loop, i_c (1.36×10^{-6} A cm^{-2}), is largest in solutions with no chloride ion (0.334 M sulfate). Solutions containing chloride ion show significantly lower current values (2.3×10^{-7} to 4.2×10^{-7} A cm^{-2}) which increase slightly with increasing chloride ion concentration.

To minimize the effect of the negative current loop, the magnitude of i_p is evaluated at 0.3 V except in 0.508 and 1.0 M potassium chloride where pitting occurs below this potential. The dependence of the passive current density on solution composition is qualitatively similar to that of the cathodic loop current. The addition of 1.17×10^{-2} M chloride ion causes a substantial lowering of i_p from the value observed in 0.334 M sulfate (5.25×10^{-7} versus 1.29×10^{-6} A cm^{-2}, respectively) (Table 1). A further increase in chloride content is accompanied by a slight increase in passive current density. In this region of increasing current, several linear relationships between i_p and solution composition are observed (Table 6). Because of the narrow range covered by the three values of the passive current density available (5.25×10^{-7} through 7.85×10^{-7} A cm^{-2}), the validity of these relationships is questionable.

Figure 10. Potentiostatic polarization curve showing cathodic loop obtained in 0.334 M sodium sulfate at pH 2.40.

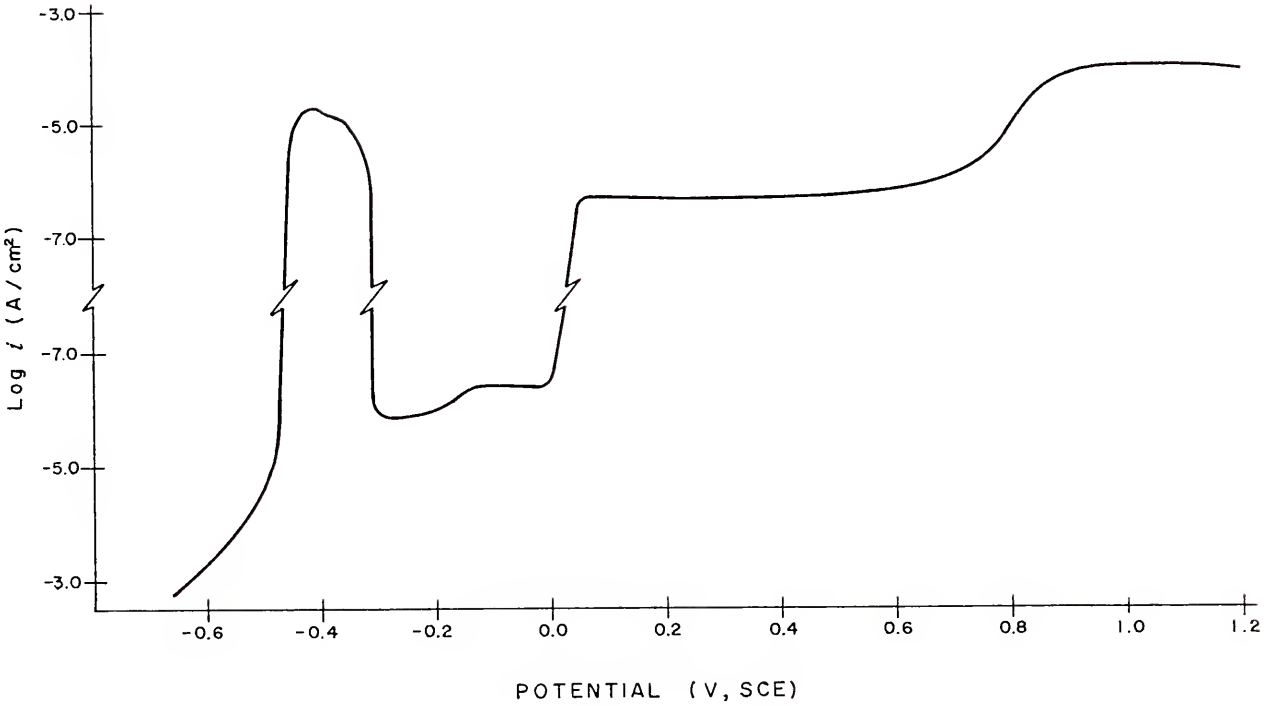
-3.0
-5.0
-7.0
-7.0
-5.0
-3.0
Log i (A / cm²)
-0.6
-0.4
-0.2
0.0
0.2
0.4
0.6
0.8
1.0
1.2
POTENTIAL (V, SCE)

The classical evaluation of the potential of total passivity, E_{TP}, involves the determination of the point at which the current increases from its value in the passive region into the anodic loop of the active-passive transition during a cathodic potential scan.[59, 60] In the present work the potential of total passivity is defined as the intersection of the line defined by the decrease in anodic current from the maximum (anodic potential scan) with the value of the passive current at 0.30 V. This method gives more reproducible results because of the random cathodic loop observed here.

Values of E_{TP} observed undergo a positive shift (from -0.285 to -0.160 V) as the chloride ion concentration of the solution is increased (Table 1). Examination of the interrelation of E_{TP} and solution parameters suggests several possibilities (Figures 11-15):

Relationship	Slope	r^2
1. $\partial E_{TP}/\partial [Cl^-]$	0.108 V mole^{-1}l	0.93
2. $\partial E_{TP}/\partial \{[Cl^-]/([SO_4^{2-}] + [Cl^-])\}$	0.103 V	0.92
3. $\partial E_{TP}/\partial \{[Cl^-]/(_2[SO_4^{2-}] + [Cl^-])\}$	0.110 V	0.94
4. $\partial E_{TP}/\partial \{pH + \log([SO_4^{2-}] + [Cl^-])\}$	0.218 V decade^{-1}	0.94
5. $\partial E_{TP}/\partial \{\log([SO_4^{2-}]/[Cl^-])\}$		

a. two segments with slopes -0.016 and -0.039 V decade^{-1} and correlation coefficients of 0.98 and 0.99, respectively or

Figure 11. Variation of the potential of total passivity with chloride ion concentration.

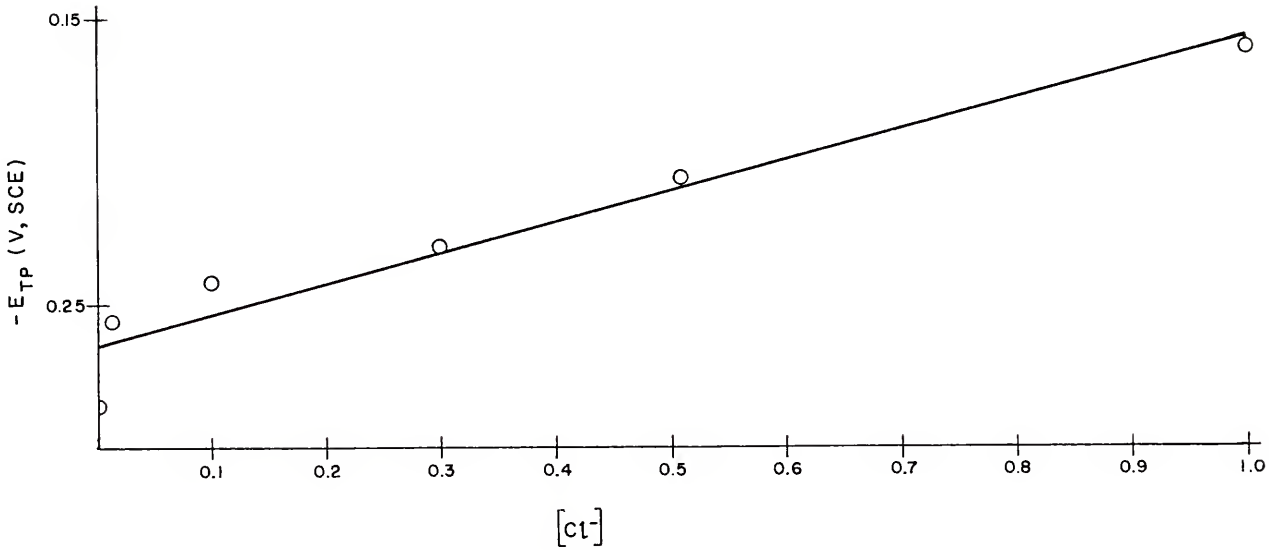
0.15
0.25
$-E_{TP}$ (V, SCE)
0.1
0.2
0.3
0.4
0.5
0.6
0.7
0.8
0.9
1.0
$[Cl^-]$

Figure 12. Variation of the potential of total passivity with the concentration function, $[Cl^-] / ([SO_4^{2-}] + [Cl^-])$.

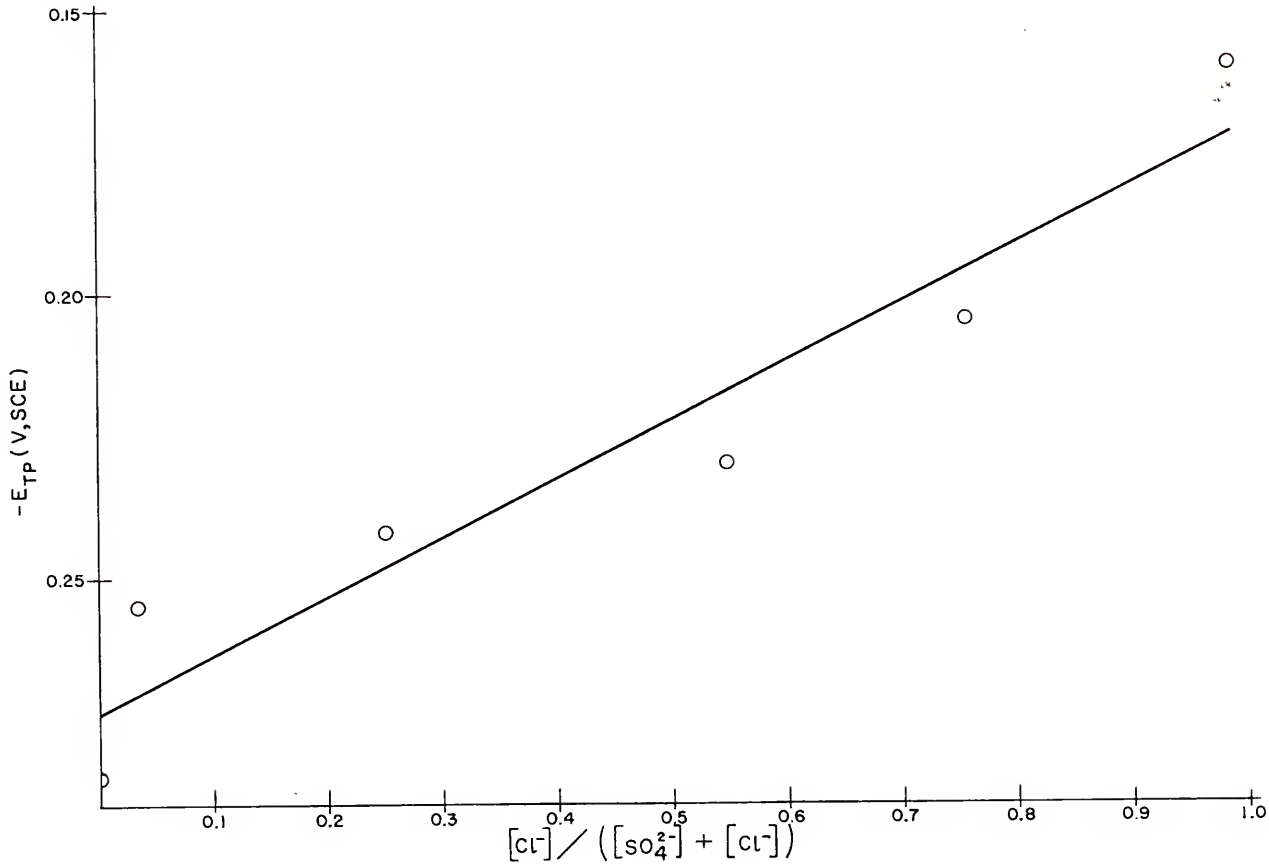
0.15
0.20
0.25
$-E_{TP}$ (V, SCE)
0.1
0.2
0.3
0.4
0.5
0.6
0.7
0.8
0.9
1.0
$[Cl^-] / ([SO_4^{2-}] + [Cl^-])$

Figure 13. Variation of the potential of total passivity with the concentration function, $[Cl^-] / (2 [SO_4^{2-}] + [Cl^-])$.

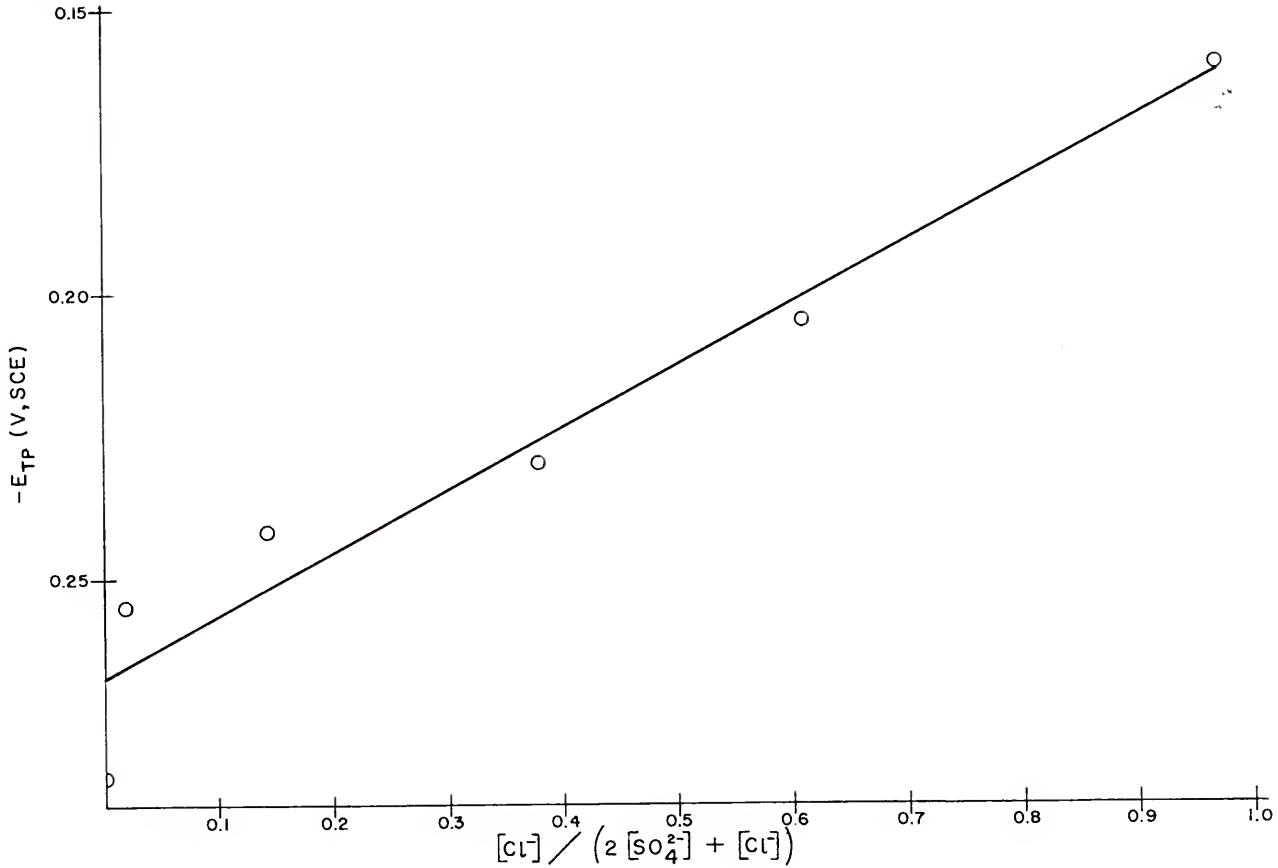
0.15
0.20
0.25
$-E_{TP}$ (V, SCE)
0.1
0.2
0.3
0.4
0.5
0.6
0.7
0.8
0.9
1.0
$[Cl^-] / (2[SO_4^{2-}] + [Cl^-])$

Figure 14. Variation of the potential of total passivity with the concentration function, pH + log ($[SO_4^{2-}]$ + $[Cl^-]$).

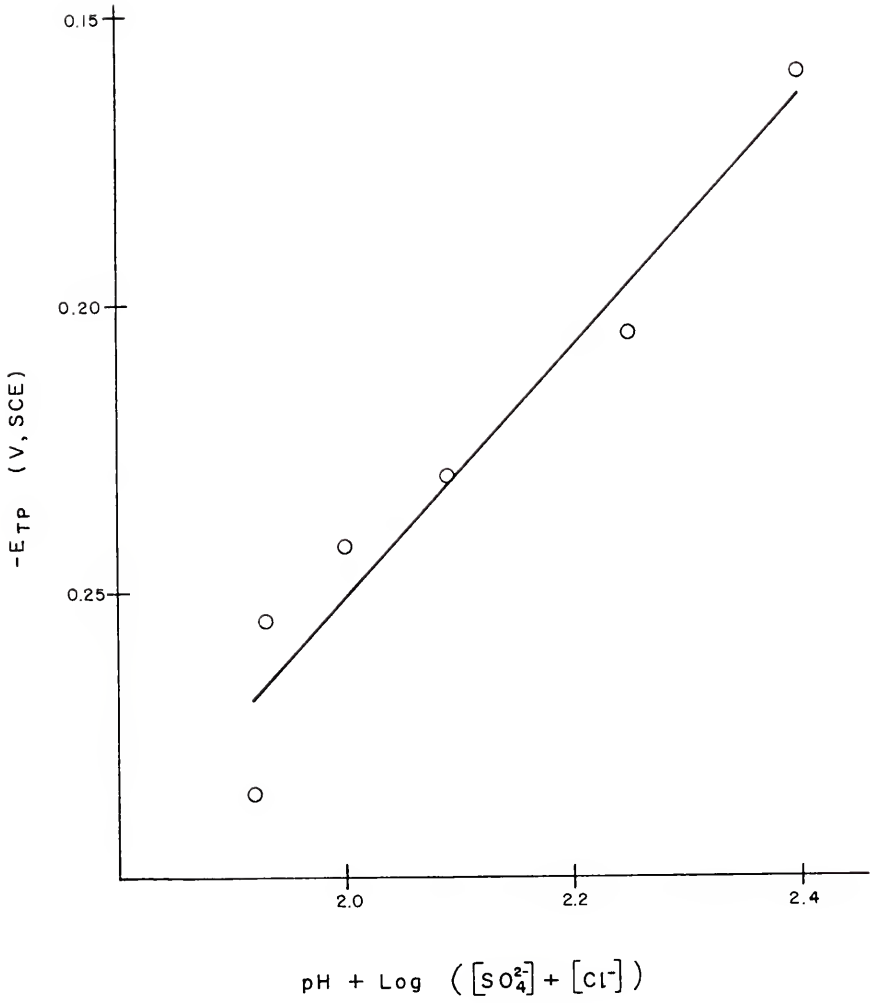
0.15
0.20
0.25
$-E_{TP}$ (V, SCE)
2.0
2.2
2.4
pH + Log $([SO_4^{2-}] + [Cl^-])$

Figure 15. Variation of the potential of total passivity with the concentration function, log ($[SO_4^{2-}] / [Cl^-]$).

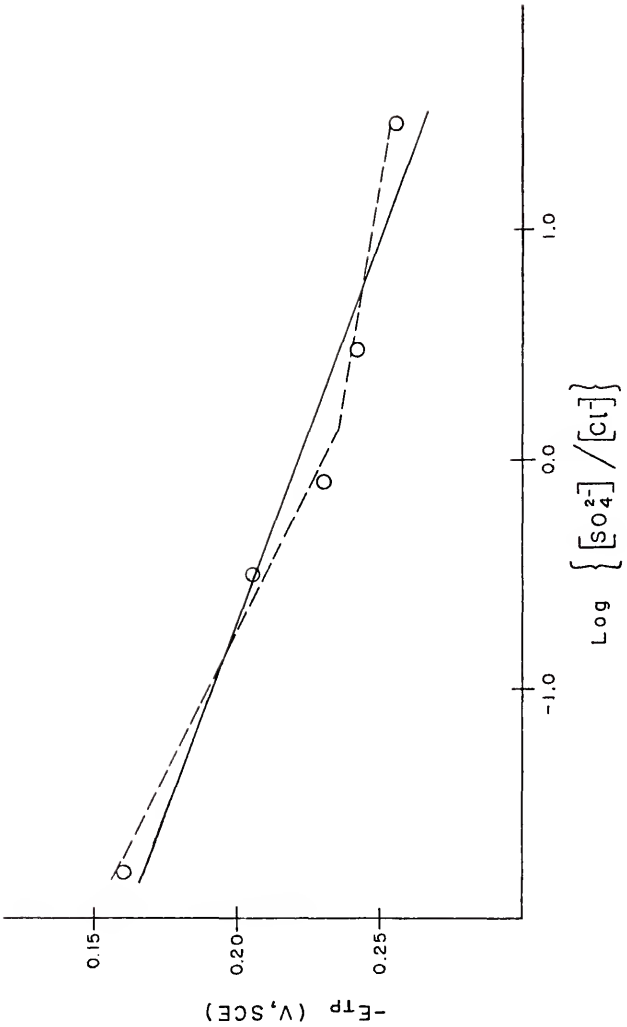
-E_TP (V, SCE)
0.15
0.20
0.25
-1.0
0.0
1.0
Log {[SO4 2-] /[Cl-]}

b. one segment with slope -0.030 V decade^{-1} and correlation coefficient 0.94.

The latter plot lends itself to two interpretations. It may be considered to have two linear segments whose point of intersection occurs at E_{TP} = -0.230 V and 0.301 M potassium chloride which is the smallest chloride ion concentration investigated in which pitting occurs. However, evaluation of data in terms of one single line is also feasible. Differentiation between the two possibilities is difficult because only five data points are available.

In solutions whose sulfate to chloride ion concentration ratio is greater than one ($\geqslant$ 0.3 M chloride), a continuing shift to more anodic potentials results in the breakdown of the passive state with the onset of pitting. An experimentally determined polarization curve showing the influence of pitting is given in Figure 16. Two values are recorded for the potential at which pitting initiates, E_{pit}. $E_{pit(inc)}$ is the most negative potential at which any increase in current density with time is observed within the ten minute waiting period. At potentials slightly positive to $E_{pit(inc)}$ (0 to $\sim$ 150 mV), an initial decrease in current followed by current spikes is usually observed. At more positive potentials an immediate increase in current density occurs. $E_{pit(gr)}$ is the potential obtained by extrapolation of the increasing pitting current density-potential curve back to the point at which it intersects the value of the passive current at 0.30 V.

Figure 16. Potentiostatic polarization curve showing the influence of pitting obtained in 0.301 M potassium chloride at pH 2.35.

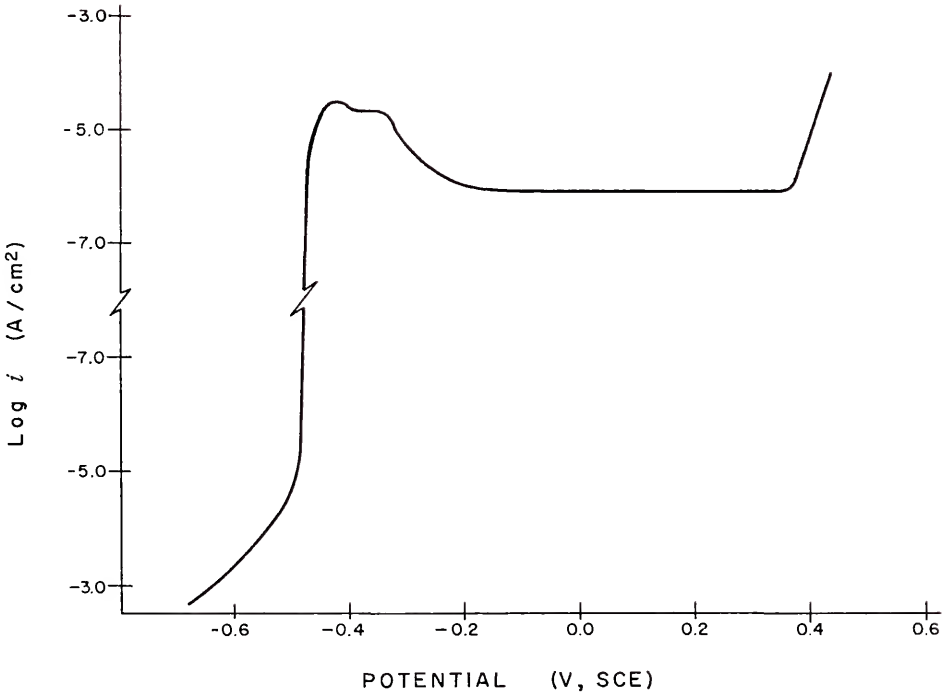
-3.0
-5.0
-7.0
-7.0
-5.0
-3.0
Log i (A / cm²)
-0.6
-0.4
-0.2
0.0
0.2
0.4
0.6
POTENTIAL (V, SCE)

Both values of E_{pit} are arbitrary because of the imposed time limitation for current measurement and the heavy fluctuations in current of up to an order of magnitude observed in this potential range, respectively. Thus, the induction period for pitting may be greater than ten minutes at potentials more negative than $E_{pit(inc)}$ and the current magnitude, after ten minutes at a given potential, is a random function of time as a result of the fluctuations present. The graphically determined value of the pitting potential, $E_{pit(gr)}$, is always the more negative. A three-fold increase in chloride ion concentration shifts $E_{pit(inc)}$ from 0.395 to -0.090 V and $E_{pit(gr)}$ from 0.360 to -0.155 V.

Several linear relationships are observed between E_{pit} and the solution composition parameters examined. Their corresponding slopes, intercepts, and correlation coefficients are reported in Table 6. Because only three data points are available, it is difficult to judge which of these relationships, if any, are valid. It does appear, however, that the potential at which pitting initiates shifts toward more active values as the chloride ion concentration of the solution is increased.

In systems not subject to pitting attack (< 0.3 M potassium chloride), loss of passive state stability occurs with the onset of transpassive dissolution (Table 4). The disolution reaction in this region involves oxidation of

chromium(III) in the passive film to chromium(VI) and exhibits Tafel behavior over 1 to 1.5 decades of current. An anodic Tafel slope of 0.114 V decade^{-1} is observed in 0.0 M and 1.17 x 10^{-2} M potassium chloride, while a value of 0.150 V decade^{-1} is found for 9.97 x 10^{-2} M potassium chloride. The potential at which transpassivity initiates, E_{tr}, is taken as the intersection of the computed Tafel line with the passive current density at 0.30 V. E_{tr} shifts negative from 0.671 to 0.575 V with increasing chloride ion concentration.

Continued anodic polarization produces a slight current maximum as a result of secondary passivity. Neither the current magnitude at the maximum, $i_{crit,2}$ (1 x 10^{-4} A cm^{-2}), nor its associated potential, $E_{pp,2}$ (0.95 V), is affected by solution composition at constant pH. The current then decreases to a minimum prior to oxygen evolution. The degree of stability of secondary passivity is represented by the difference in the magnitude of the maximum and minimum current values, Δ i. Present results indicate that the stability decreases slightly on addition of chloride ion to solutions originally 0.334 M in sulfate ion at pH 2.4. Current differences, Δ i, of 14 to 17 μA cm^{-2} and 21 μA cm^{-2} are observed for 1.17 x 10^{-2} to 9.97 x 10^{-2} M potassium chloride and 0.0 M potassium chloride (0.334 M sulfate), respectively.

Secondary solutions

A brief survey of the effect of chloride ion concentration in the absence of sulfate ion on the polarization curve was carried out at pH 2.4 (hydrochloric acid) in solutions containing 0.102, 0.123 and 1.0 M potassium chloride. Characteristic potentials and current densities obtained from the polarization curves are presented in Tables 7 and 8. Linear relationships with correlation coefficients $\geqslant 0.90$ are reported in Table 9 with the corresponding slopes.

Cathodic current magnitudes at -0.700 V are significantly lower than those in sulfate containing solutions, varying from 1.25×10^{-3} to 7.06×10^{-4} A cm^{-2} in the chloride range 0.102 to 1.0 M. An increase in concentration from 0.102 to 0.123 M causes only a slight shift in rest potential (-0.470 to -0.480 V) while the rest potential for 1.0 M potassium chloride occurs at -0.505 V, a negative shift of 45 mV. The primary passivation potential is not a function of chloride concentration. In the absence of sulfate ion i_{crit} changes linearly with chloride ion concentration (Figure 17) and with the rest potential (Figure 18). The corresponding slopes are 3.11×10^{-5} A cm^{-2} $mole^{-1}$ l ($r^2 = 0.98$) and -15.7 decades V^{-1} ($r^2 = 1.0$), respectively. A linear relationship is also observed between the logarithm of the critical current density and the concentration function, pH + log ($[SO_4^{2-}]$ + $[Cl^-]$) (Figure 19). The corresponding line has a slope of 0.48

Table 7

Potentiostatic current-potential behavior in secondary solutions (average curves).

$[Cl^-]$ x 10^1	$[SO_4^{2-}]$ x 10^1	pH	i_{-700} (A cm^{-2}) x 10^4	E_r (V,SCE)	$E_{pp,1}$ (V,SCE)	$i_{crit,1}$ (A cm^{-2}) x 10^5	i_p (A cm^{-2}) x 10^7	E_{TP} (V,SCE)	E_{pit}(V,SCE) inc	gr
Polarization in the absence of sulfate ion										
1.02	0	2.40	-12.5	-0.470	-0.420	1.18	-	-0.287	0.140	0.070
1.23	0	2.35	-12.5	-0.480	-0.400	1.69	-	-0.273	-0.025	-0.120
10.0	0	2.42	-7.06	-0.505	-0.420	4.17	-	-0.250	-0.100	-0.132
Polarization at varied pH										
3.01	0.233	1.52	-203.0	-0.420	-0.370	4.65	-0.681	-0.205	0.425	0.397
3.01	0.248	2.35	-22.30	-0.470	-0.430	3.43	7.85	-0.230	0.395	0.360
3.01	0	6.22	-0.0013	-0.760	-0.500	0.147	-	-	-	-

Table 8

Potentiostatic current-potential behavior in secondary solutions (individual experiments).

$[Cl^-]$ x 10^1	$[SO_4^{2-}]$ x 10^1	pH	i_{-700} (A cm^{-2}) x 10^4	E_r (V,SCE)	$E_{pp,1}$ (V,SCE)	$i_{crit,1}$ (A cm^{-2}) x 10^5	i_p (A cm^{-2}) x 10^7	E_{TP} (V,SCE)	E_{pit}(V,SCE) inc	gr
Polarization in the absence of sulfate ion										
1.02	0	2.40	-12.3	-0.460	-0.420	0.881	-	-0.287	-	0.075
			-12.6	-0.480	-0.420	1.49	-	-0.282	-	0.120
1.23	0	2.35	-15.3	-0.480	-0.400	1.7	-	-0.285	-0.05	-0.107
			-9.61	-0.480	-0.400	1.68	-	-0.270	0.00	-0.120
10.0	0	2.42	-5.71	-0.500	-0.420	4.69	-	-0.250	-0.10	-0.155
			-8.42	-0.500	-0.420	3.70	-	-0.235	-0.10	-0.120
Polarization at varied pH										
3.01	2.33	1.52	-189.0	-0.400	-0.350	4.1	7.61	-0.240	0.450	0.335
			-196.0	-0.440	-0.370	5.8	7.49	-0.230	0.400	0.400
			-224.0	-0.400	-0.370	5.25	2.80	-0.155	0.400	0.460
3.01	2.48	2.35	-18.0	-0.475	-0.420	3.55	7.23	-0.230	0.420	0.365
			-27.0	-0.480	-0.415	3.39	8.48	-0.226	0.370	0.360
3.06	0	6.22	-0.0013	-0.760	-0.500	0.147	-	-	-	-

Figure 17. Variation of the critical current density with chloride ion concentration.

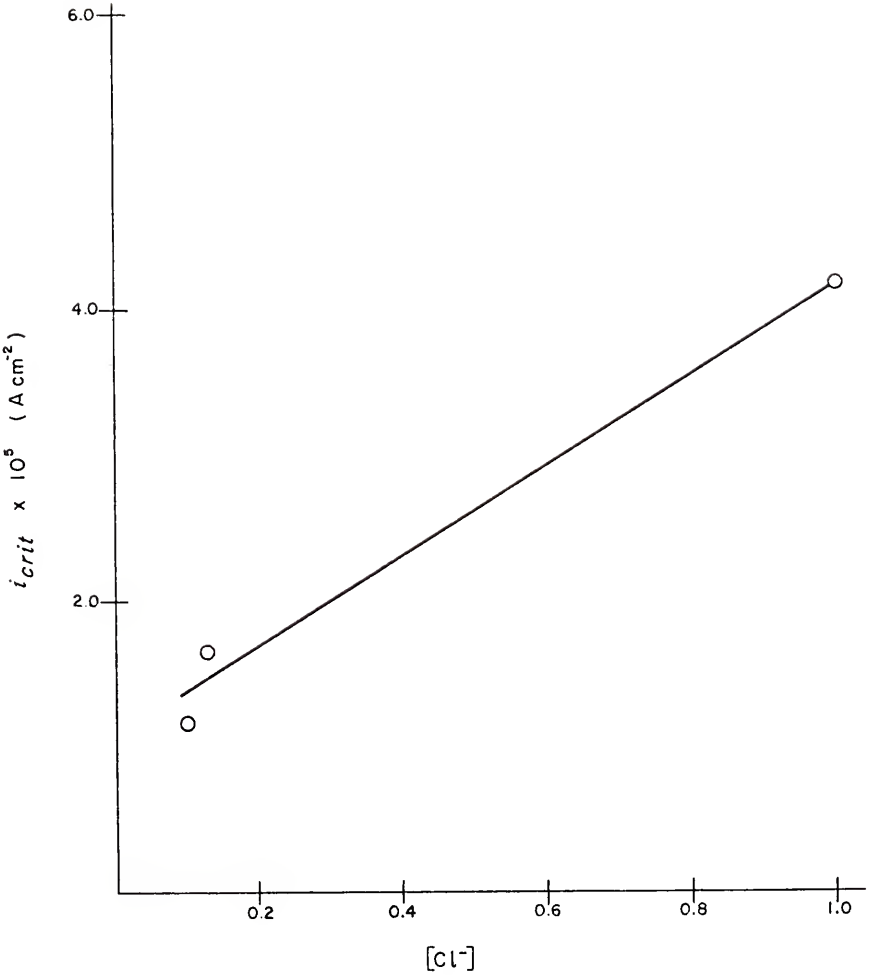
6.0
4.0
2.0
i_{crit} x 10^5 (A cm^{-2})
0.2
0.4
0.6
0.8
1.0
[Cl⁻]

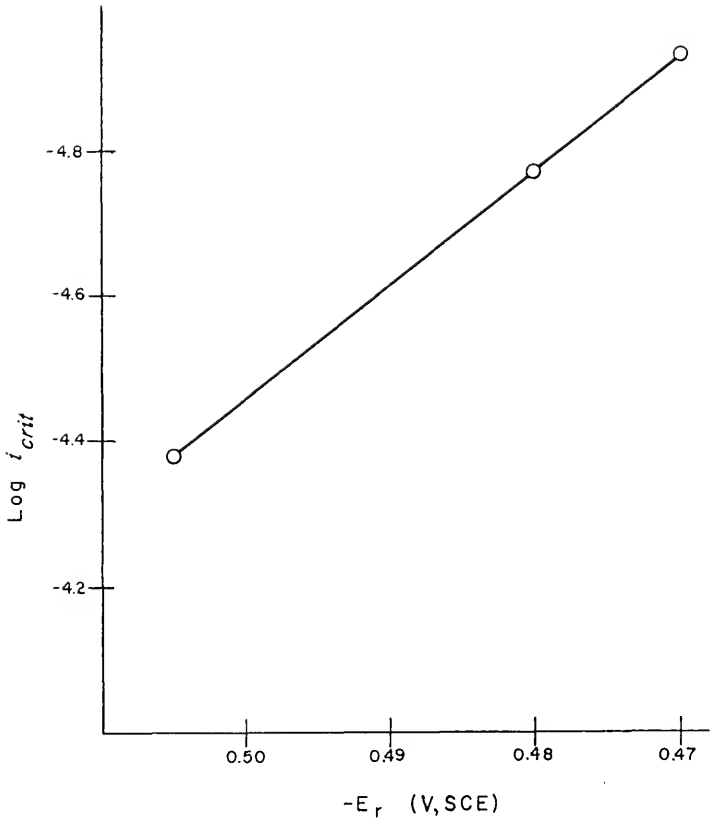
-4.8
-4.6
-4.4
-4.2
Log i_{crit}
0.50
0.49
0.48
0.47
$-E_r$ (V, SCE)

Figure 19. Variation of the logarithm of the critical current density with the concentration function, pH + log ($[SO_4^{2-}]$ + $[Cl^-]$).

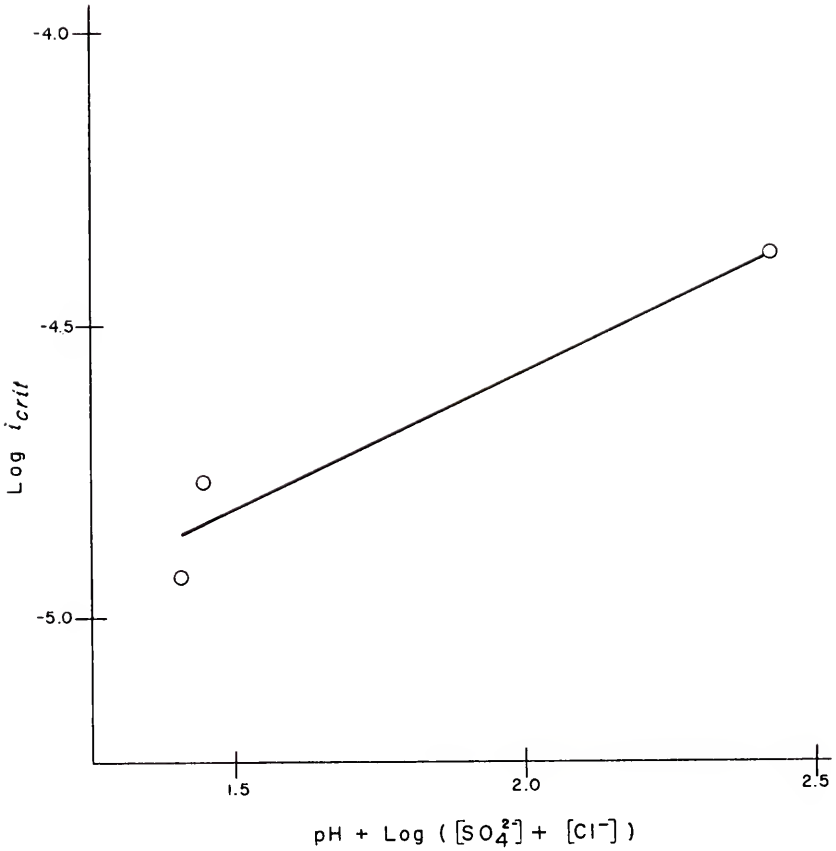
-4.0
-4.5
-5.0
Log i_{crit}
1.5
2.0
2.5
pH + Log ($[SO_4^{2-}]$ + $[Cl^-]$)

Figure 20. Variation of the potential of total passivity with rest potential.

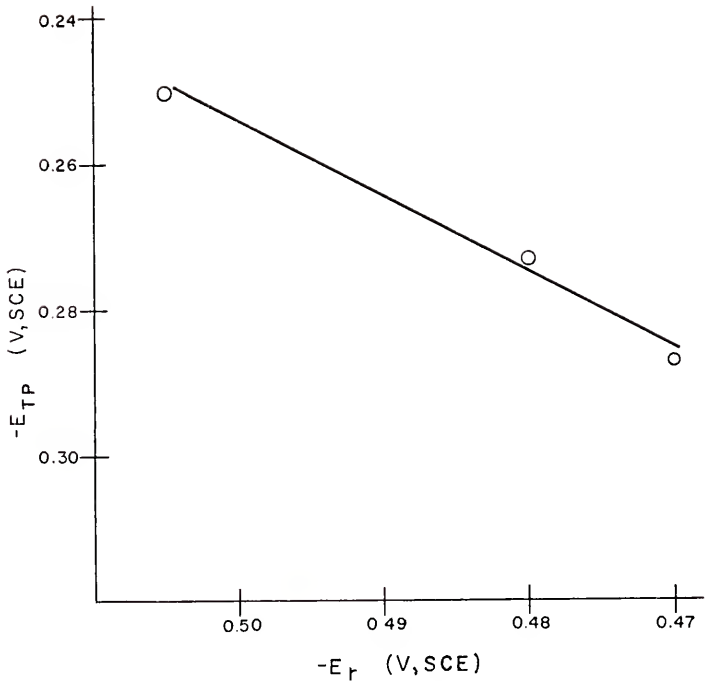
0.24
0.26
0.28
0.30
-E_TP (V,SCE)
0.50
0.49
0.48
0.47
-E_r (V,SCE)

Figure 21. Variation of the logarithm of the critical current density with the potential of total passivity.

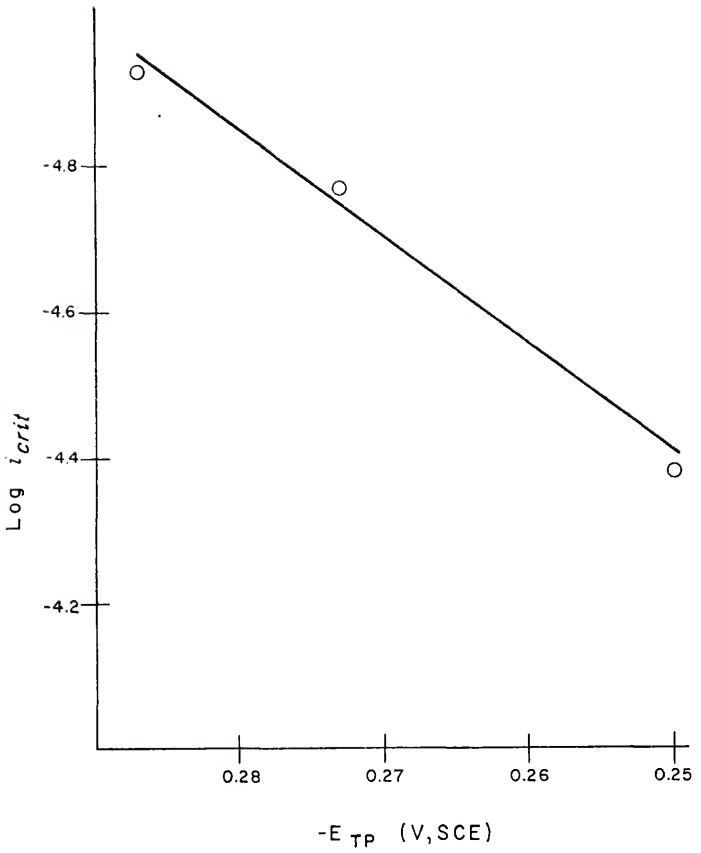
-4.8
-4.6
-4.4
-4.2
Log i_{crit}
0.28
0.27
0.26
0.25
-E TP (V, SCE)

and a correlation coefficient of 0.93. No cathodic current loop is observed in these solutions.

Little change in the potential of total passivity is observed in going from 0.102 to 0.123 M potassium chloride when data from individual runs are examined. Values are -0.287 V and -0.282 V for the former and -0.285 V and -0.270 V for the latter. However, average values show a definite positive trend with increasing chloride ion concentration in agreement with the value of -0.250 V found in 1.0 M potassium chloride.

A one-to-one correlation between E_{TP} and E_r is suggested (Figure 20). The corresponding slope is -1.03. The log of i_{crit} increases as E_{TP} becomes more positive at the rate of 15.1 decades V^{-1} (Figure 21).

In the absence of sulfate ion, pitting occurs at all chloride ion concentrations investigated. A negative shift in the pitting potential occurs with increasing chloride ion concentration but no statistically valid variation in this relationship is apparent.

The effect of pH on polarization curve parameters was also examined in 0.3 M potassium chloride at pH 1.52, 2.35 and 6.22 (Table 7,8). In the former two cases, sodium sulfate additions of 0.233 M and 0.248 M, respectively, maintained the ionic strength at one. No sulfate was added to the latter and polarization in this system was

terminated after passivation occurred. Possible linear relationships are presented in Table 9.

Net currents at -0.700 V are cathodic and decrease with decreasing hydronium ion activity. Values of 2.03×10^{-2}, 2.23×10^{-3} and 1.34×10^{-7} A cm^{-2} are recorded for pH 1.52, 2.35, and 6.22, respectively. A linear relationship is observed between both the rest potential and pH (-0.073 V pH^{-1}) (Figure 22) and the primary passivation potential and pH (-0.025 V pH^{-1}) (Figure 23). The slope of the straight line resulting from a plot of log i_{crit} vs pH is -0.328 (Figure 24). A linear relationship is also observed between the logarithm of the critical current density and the concentration function, pH + log ($[SO_4^{2-}]$ + $[Cl^-]$) (Figure 25). A slope of -0.35 and a correlation coefficient of 0.99 are associated with the line.

No cathodic loop is found in the pH 2.35 solutions but one does occur between -0.15 and 0.0 V in two of three experiments at pH 1.52 (Table 10). The maximum associated cathodic current density is 4.5×10^{-7} A cm^{-2}.

The increase in pH from 1.52 to 2.35 shifts the potential of total passivity to more active values (-0.205 to -0.230 V) and changes the current density at 0.300 V from cathodic to anodic values. An active shift in pitting potential also occurs.

Table 9

Interrelationships in potentiostatic experiments in secondary solutions.

Independent Variable	Dependent Variable	Slope	Correlation Coefficient	Data Points
$[Cl^-]$	i crit	3.11×10^{-5} A cm^{-2} $moles^{-1}$ l	0.98	3
E_r	log i crit	15.7 decades V^{-1}	1.0	3
E_r	E_{TP}	-1.03	0.99	3
E_{TP}	log i crit	15.1 decades V^{-1}	0.99	3
pH + log ($[SO_4^{2-}]$ + $[Cl^-]$)	log i crit	0.48	0.93	3
pH	E_r	-0.073 V pH^{-1}	1.0	3
pH	E_{pp}	-0.025 V pH^{-1}	0.91	3
pH	log i crit	-0.328	0.99	3
pH + log ($[SO_4^{2-}]$ + $[Cl^-]$)	log i crit	-0.35	0.99	3

Figure 22. Variation of the primary passivation potential with pH.

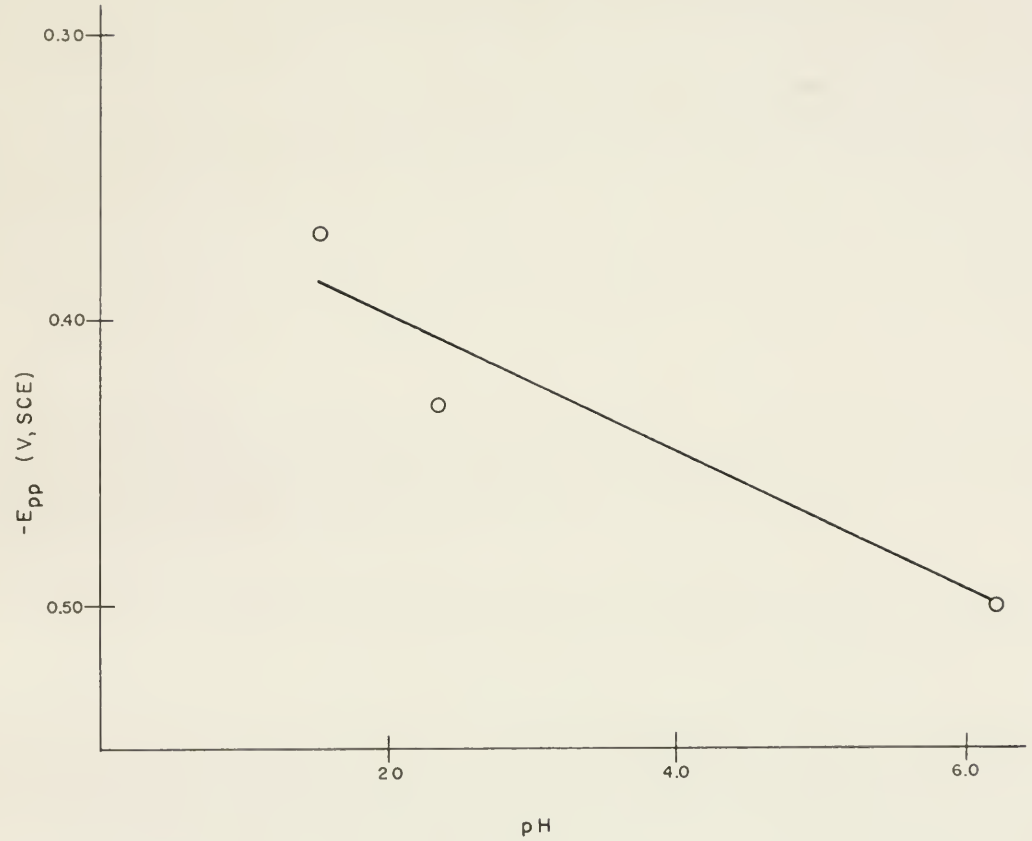
0.30
0.40
0.50
-Epp (V, SCE)
2.0
4.0
6.0
pH

Figure 23. Variation of the rest potential with pH.

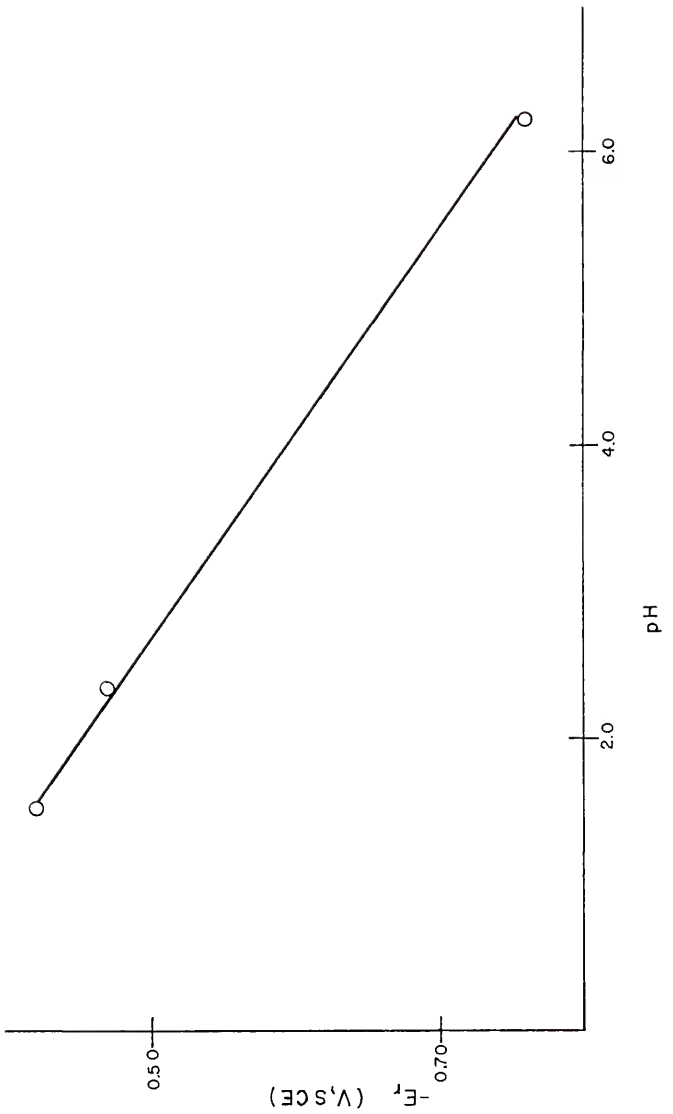
-E_r (V,s CE)
0.50
0.70
2.0
4.0
6.0
pH

Figure 24. Variation of the logarithm of the critical current density with pH.

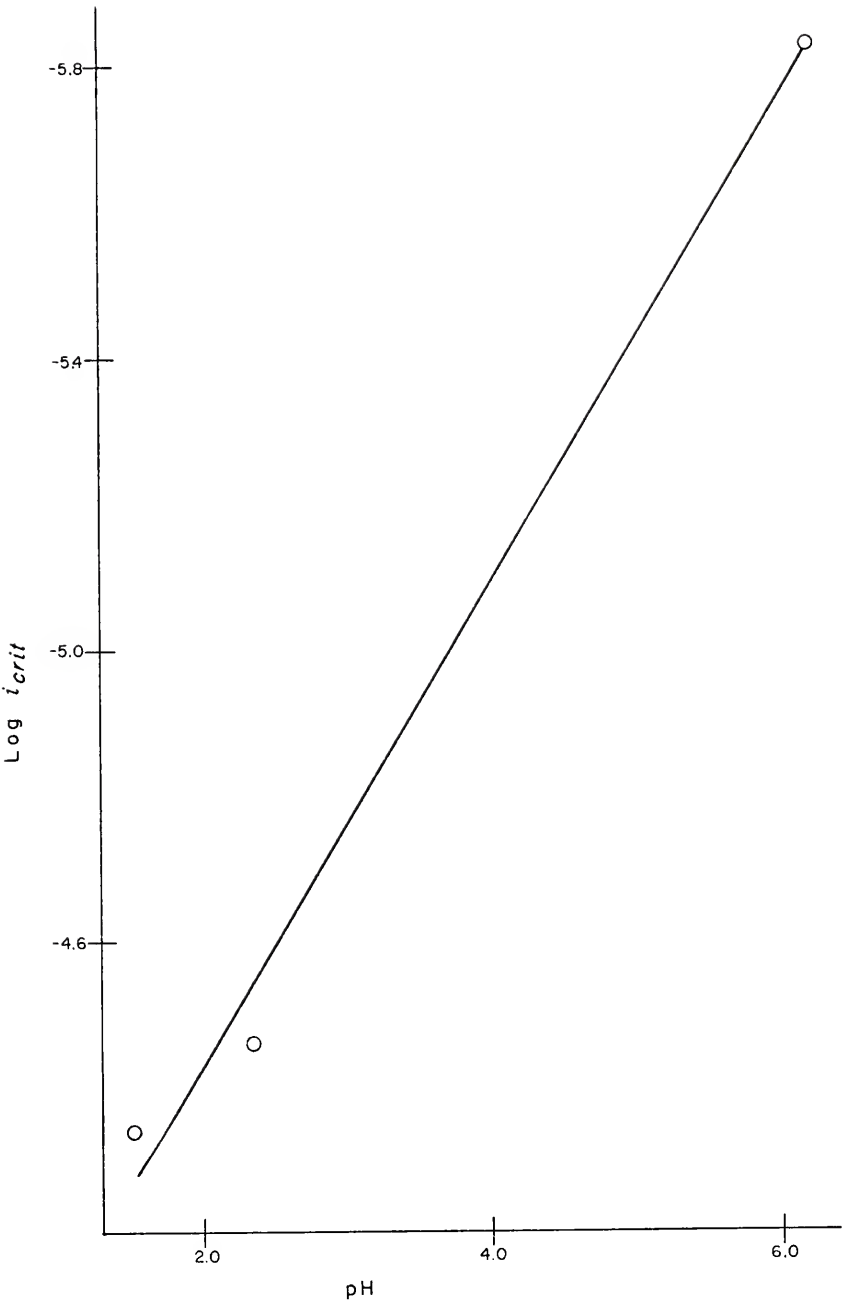
-5.8
-5.4
-5.0
-4.6
Log i_{crit}
2.0
4.0
6.0
pH

Figure 25. Variation of the logarithm of the critical current density with the concentration function, pH + log ($[SO_4^{2-}]$ + $[Cl^-]$) .

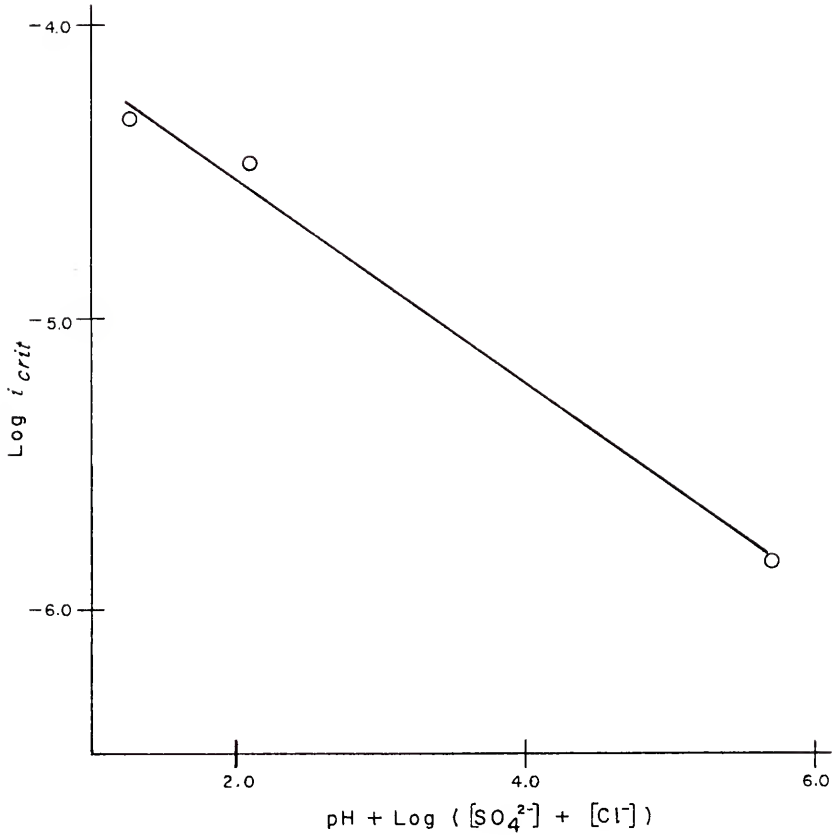
-4.0
-5.0
-6.0
Log i_{crit}
2.0
4.0
6.0
pH + Log ($[SO_4^{2-}]$ + $[Cl^-]$)

Capacity-Potential Behavior During Potentiostatic Polarization

The capacity-potential behavior determined from the average curve for a given solution composition is used as the basis for data analysis. A schematic representation of the dependence of capacity on potential in the absence of hydrogen interference (see below) is given in Figure 26. In only a few cases are the characteristic potentials determined from the average curve not representative of values found on individual runs (Tables 11-14).

Primary solutions

After prepolarization at -0.700 V for twenty minutes, capacity values of 40 to 60 μf cm^{-2} are typically observed. The one exception is 0.5 M potassium chloride (22 μf cm^{-2}).

A definite increase in capacity with increasing potential occurs in the region of active dissolution of the metal surface. In systems relatively free from interference (see below), a single capacity peak (C_1) is then described at a potential (E_1) which is usually 0 to 40 mV more negative than the corresponding primary passivation potential. The capacity maximum ranges from 62 to 73 μf cm^{-2} and is independent of solution composition.

In some cases, however, capacity peak values of greater than 100 μf cm^{-2} are observed in this region. They appear to be associated with the presence of the cathodic loop described above or with anodic current densities ($\sim 5 \times 10^{-7}$ A cm^{-2}) between -0.3 and 0.0 V which are lower than the

Figure 26. Potentiostatic capacity-potential behavior in the absence of hydrogen interference.

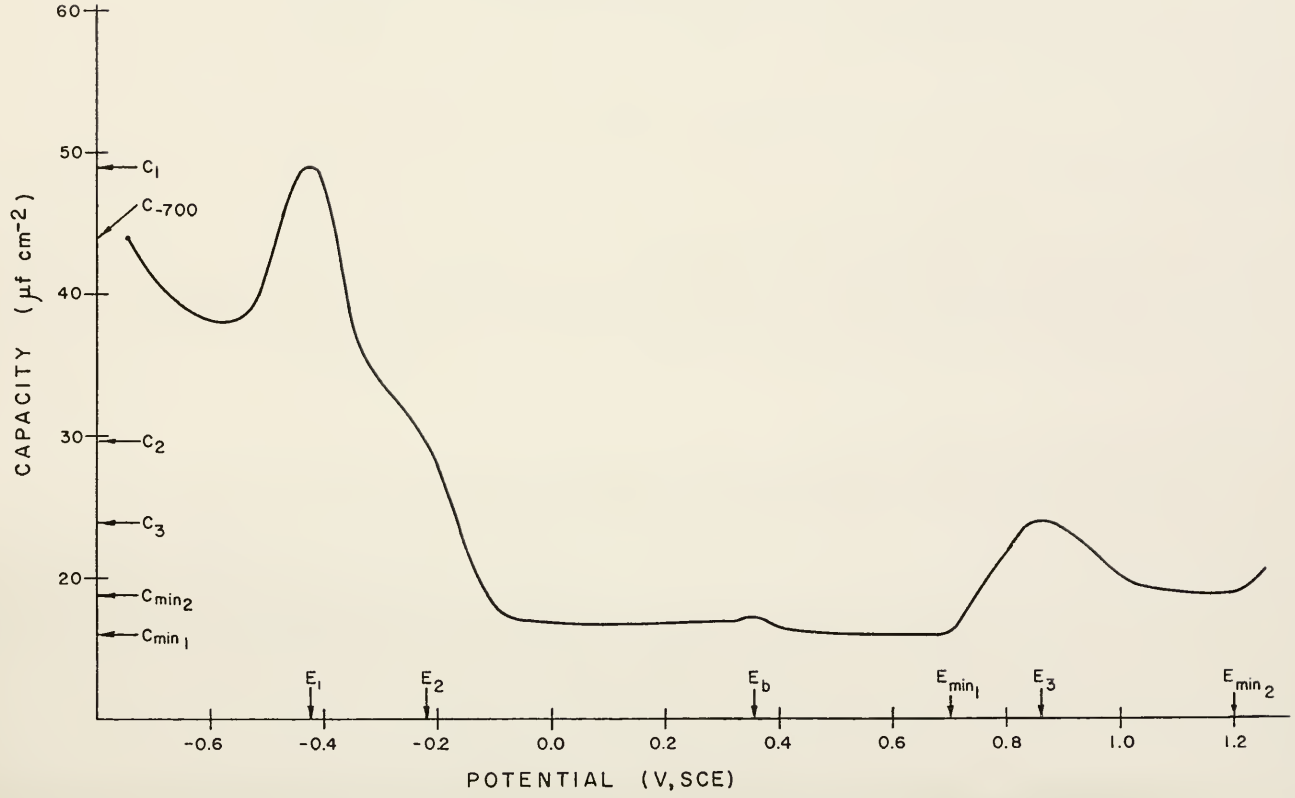
60
50
40
30
20
CAPACITY (μf cm-2)
C1
C-700
C2
C3
Cmin2
Cmin1
E1
E2
Eb
Emin1
E3
Emin2
-0.6
-0.4
-0.2
0.0
0.2
0.4
0.6
0.8
1.0
1.2
POTENTIAL (V, SCE)

Table 10

Cathodic loop in secondary solutions.

$[Cl^-]$ x 10^1	$[SO_4^{2-}]$ x 10^1	pH	i_{700} (A cm^{-2}) x 10^3	C_{-700} ($\mu f\ cm^{-2}$)	C_l ($\mu f\ cm^{-2}$)	Negative loop (V,SCE)	i_c (A cm^{-2}) x 10^7	i_{-200} (A cm^{-2}) x 10^7
1.02	0	2.40	-1.23	-	50	-	-	9.04
			-1.22	28	140	-	-	22.5
			-1.26	20	54	-	-	5.92
1.23	0	2.35	-1.54	28	56	-	-	13.2
			-0.96	31	56	-	-	16.3
10.0	0	2.42	-0.571	22	55	-	- -	6.24
			-0.842	31	59	-	-	4.75
3.01	2.33	1.52	-18.5	-	125	-0.15 to -0.10	-3.14	0.680
			-19.6	83	124	-	-	2.36
			-22.4	83	166	-0.15 to -0.00	-5.7	8.16
3.01	2.48	2.35	-1.8	43	71	-	-	9.66
			-2.67	43	68	-	-	11.5

Table 11

Potentiostatic capacity-potential behavior in primary solutions (average curves).

$[Cl^-]_1$ x 10^1	$[SO_4^{2-}]$ x 10^1	pH	C_{-700} (μf cm^{-2})	E_1 (V,SCE)	C_1 (μf cm^{-2})	E_2 (V,SCE)	C_2 (μf cm^{-2})	E_b (V,SCE)	C_b (μf cm^{-2})	$E_{min,1}$ (V,SCE)	$C_{min,1}$ (μf cm^{-2})	E_3 (V,SCE)	C_3 (μf cm^{-2}
3.34	0.0	2.40	40	-0.420	116[a] 73[b]	-0.235	53	0.31	21	0.600	13	0.90	27
3.29	0.117	2.40	61	-0.420	124[a]	-0.215	74	0.28	22	0.650	15	0.85	50
3.00	0.997	2.40	63	-0.430	93[a]	-0.270	48	0.30	18	0.650	14	0.85	29
2.48	0.301	2.35	44	-0.400	69	-0.220	28	0.30	20	-	-	-	
1.63	5.08	2.42	22	-0.400	60	-0.200	22	-	-	-	-	-	
10.0	0.96	2.40	42	-0.450	117[a]	-0.300	32	-	-	-	-	-	

a negative loop influence

b average of curves with no negative loop interference

Table 12

Potentiostatic capacity-potential behavior in primary solution (individual experiments).

$[Cl^-]$ x 10^1	$[SO_4^{2-}]$ x 10^1	pH	C_{-700} ($\mu f\ cm^{-2}$)	E_1 (V,SCE)	C_1 ($\mu f\ cm^{-2}$)	E_2 (V,SCE)	C_2 ($\mu f\ cm^{-2}$)	E_b (V,SCE)	C_b ($\mu f\ cm^{-2}$)	$E_{min,1}$ (V,SCE)	$C_{min,1}$ ($\mu f\ cm^{-2}$)	E_3 (V,SCE)	C_3 ($\mu f\ cm^{-2}$)
0	3.34	2.4	13	-0.420	66	-0.210	39	-	-	0.600	11	0.900	25
			28	-0.420	80	-0.250	56	-	-	0.500	11	0.87	25
			78	-0.360[a]	160	-0.215	64	0.32	28	0.650	15	0.89	39
0.117	3.29	2.4	56	-0.355[a]	111	-0.200	67	0.37	23	0.600	14	0.90	50
			67	-0.430[a]	199	-0.230	81	0.30	21	0.600	15	0.85	53
0.997	3.00	2.4	73	-0.430	124	-0.180	48	0.35	19	0.650	15	0.89	29
			52	-0.420[a]	80	-0.270	52	0.28	19	0.550	13	0.85	29
3.01	2.48	2.35	44	-0.400	69	-0.215[c]	34	0.30	20	-	-	-	-
			44	-0.425	66	-0.200[c]	38	0.35	21	-	-	-	-
5.08	1.63	2.42	21	-0.430	46	-0.150[c]	17	-	-	-	-	-	-
			21	-0.400	66	-0.200[c]	22	-	-	-	-	-	-
			33	-0.420	75	-0.200[c]	24	-	-	-	-	-	-
10.0	0.16	2.40	39	-0.415[a]	126	-0.240[c]	29	-	-	-	-	-	-
			47	-0.440[a]	89	-0.270[c]	29	-	-	-	-	-	-

a negative loop interference
b capacity break rather than peak

Table 13

Potentiostatic capacity-potential behavior in secondary solutions (average curves).

$[Cl^-]$ x 10^1	$[SO_4^{2-}]$ x 10^1	pH	C_{-700} ($\mu f\ cm^{-2}$)	E_1 (V,SCE)	C_1 ($\mu f\ cm^{-2}$)	E_2 (V,SCE)	C_2 ($\mu f\ cm^{-2}$)	E_b (V,SCE)	C_b ($\mu f\ cm^{-2}$)
Polarization in the absence of sulfate ion									
1.02	0	2.40	-	-0.435	51	-0.250[b]	26	(-0.15)	18
1.23	0	2.35	29	-0.450	49	-	-	-	-
10.0	0	2.42	27	-0.450	57	-	-	-	-
Polarization with varied pH									
3.01	2.33	1.52	83	-0.420	124[a]	-0.310	62	-	-
3.01	2.48	2.35	44	-0.400	69	-0.220	28	0.30	0.20

[a] negative loop interference

[b] capacity break rather than peak

Table 14

Potentiostatic capacity-potential behavior in secondary solutions (individual experiments).

$[Cl^-]$ x 10^1	$[SO_4^{2-}]$ x 10^1	pH	C_{-700} ($\mu f\ cm^{-2}$)	E_1 (V,SCE)	C_1 ($\mu f\ cm^{-2}$)	V_2 (V,SCE)	C_2 ($\mu f\ cm^{-2}$)	E_b (V,SCE)	C_b ($\mu f\ cm^{-2}$)
			Polarization in the absence of sulfate ion						
1.02	0	2.40	21	-0.440	50	-0.315	26	-0.14	18
			-	-0.450	53	-0.270	26	-	-
1.23	0	2.35	26	-0.420	47	-	-	-	-
			31	-0.450	56	-	-	-	-
10.0	0	2.42	23	-0.450	54	-	-	-	-
			30	-0.460	59	-	-	-	-
			Polarization with varied pH						
3.01	2.33	1.52	-	-0.420	125[a]	-0.300	63	0.40	15
			83	-0.440	124	-0.300	64	-	-
			83	-0.430	166[a]	-0.290	63	0.35	18
3.01	2.48	2.35	44	-0.400	69	-0.215	34	0.30	20
			44	-0.425	66	-0.200	38	0.35	21

[a] negative loop interference

usual values of i_p ($\sim 10^{-6}$ A cm^{-2}) found in this potential region. An assessment of the fine structure of the general capacity-potential behavior here is hindered by scatter. Although scatter is present in all systems studied, the effect is much more pronounced in regions where the capacity is large. Resolution of the data into two peaks, one in the vicinity of the primary passivation potential, the other slightly positive to it, seems possible, but is not unequivocal. In the vicinity of the potential of total passivity, either a capacity peak or a sudden decrease in capacity is observed for all systems (E_2, C_2).

Further anodic polarization results in a smooth decrease in capacity to 20 to 25 μf cm^{-2} for 0.0 M through 0.3 M potassium chloride solutions and 13 to 15 μf cm^{-2} for 0.5 and 1.0 M potassium chloride. The capacity in the passive region then continues to decrease slowly until a potential of 0.28 to 0.31 V (E_b) is attained (in 0.0 through 0.3 M potassium chloride)or until measurements are terminated at potentials positive to the pitting potential (in 0.5 and 1.0 M potassium chloride).

Polarization beyond E_b causes a small drop off in capacity followed by a slow decrease to a minimum value of 11 to 15 μf cm^{-2} ($C_{min,1}$) at 0.6 to 0.65 V ($E_{min,1}$). Plots of 1/C vs E in the potential region from E_b to $E_{min,1}$ are linear (Table 15). Slopes of 0.06, 0.09, 0.06, and 0.04 $V^{-1}cm^2\mu f^{-1}$ are observed for 0.0, 1.17 x 10^{-2}, 9.97 x 10^{-2},

Table 15

Capacity-potential behavior in the potential range of linearity of 1/C versus E.

$[Cl^-]$ x 10^1	$[SO_4^{2-}]$ x 10^1	pH	E range (V,SCE)	Intercept (μf^{-1} cm^2)	Slope (cm^2 μf^{-1} V^{-1})	Correlation Coefficient
			Average curves			
0	3.34	2.40	0.25 to 0.60	0.039	0.06	0.90
0.117	3.29	2.40	0.30 to 0.55	0.021	0.09	0.87
0.997	3.00	2.40	0.30 to 0.65	0.039	0.06	0.90
3.01	2.48	2.35	0.25 to 0.44	0.036	0.04	0.87
3.01	2.33	1.52	0.35 to 0.42	0.025	0.12	0.97
			Individual experiments			
1.02	0	2.40	-0.05 to 0.20	0.058	0.08	0.62
3.01	2.33	1.52	0.35 to 0.42	0.022	0.10	0.88

and 0.3 M potassium chloride, respectively. The corresponding intercepts and correlation coefficients obtained by linear regression analysis are also presented in Table 15.

The increase in current observed in the transpassive region is accompanied by an increase in capacity to a maximum (C_3) of 27 to 53 μf cm^{-2} at a potential of 0.85 to 0.90 V (E_3). The capacity then decreases to a minimum of 19 to 22 μf cm^{-2} ($C_{min,2}$) at 1.20 V ($E_{min,2}$) and increases sharply at still more positive potentials.

Secondary solutions

The change in capacity with potential for solutions of varying chloride ion concentration in the absence of sulfate ion and those at pH 1.52 (0.3 M potassium chloride, 0.233 M sulfate) corresponds closely to that described above over the entire investigated potential range (Tables 13 and 14). However, a capacity peak is associated with the potential of total passivity only for the 0.102 M potassium, chloride, pH 2.4 system.

Pitting occurs in all instances here. The capacity values observed prior to and in the pitting region are similar to those seen in the same potential regions in nonaggressive solutions (11 to 20 μf cm^{-2}) where the surface remains passive. Polarization, continued for one experiment at pH 1.52, shows a capacity minimum at 0.6 V followed by an increase in capacity in the transpassive region. No capacity increase is associated with the increase of current caused by the onset of pitting.

Galvanostatic Polarization

Potential-time behavior

After potentiostatic prepolarization at -0.700 V, control was switched to the galvanostatic circuit. The potential-time response resulting from the application of anodic current densities from 1 x 10^{-4} to 2 x 10^{-3} A cm^{-2} was observed. Only primary solutions (constant ionic strength, pH 2.4) were investigated. Chloride ion concentrations were varied from 0.0 to 0.518 M.

A schematic representation of the current-induced potential transient is given in Figure 27. The arrests observed and the stability of the maximum potential achieved for a given system are a function of the current density and solution composition employed. Chronopotentiometric techniques of curve analysis are used to determine plateau length (t) and associated potential values ($E_{t/4}$), although the theory is not directly applicable to systems with forced convection.[61,62] Results have been tabulated (Tables 16-19). In some cases, current polarization was repeated using the same electrode and solution. Even though prepolarization at -0.700 V was carried out before each use, the potential value of the first arrest, E_1, was found to shift anodic with continued use while the arrest length became shorter. Little effect on the potential of the more noble arrests was observed but plateau lengths became irreproducible. Data analysis is therefore based,

Figure 27. Schematic representation of the galvanostatic potential-time curve in the presence (1) and absence (2) of pitting breakdown.

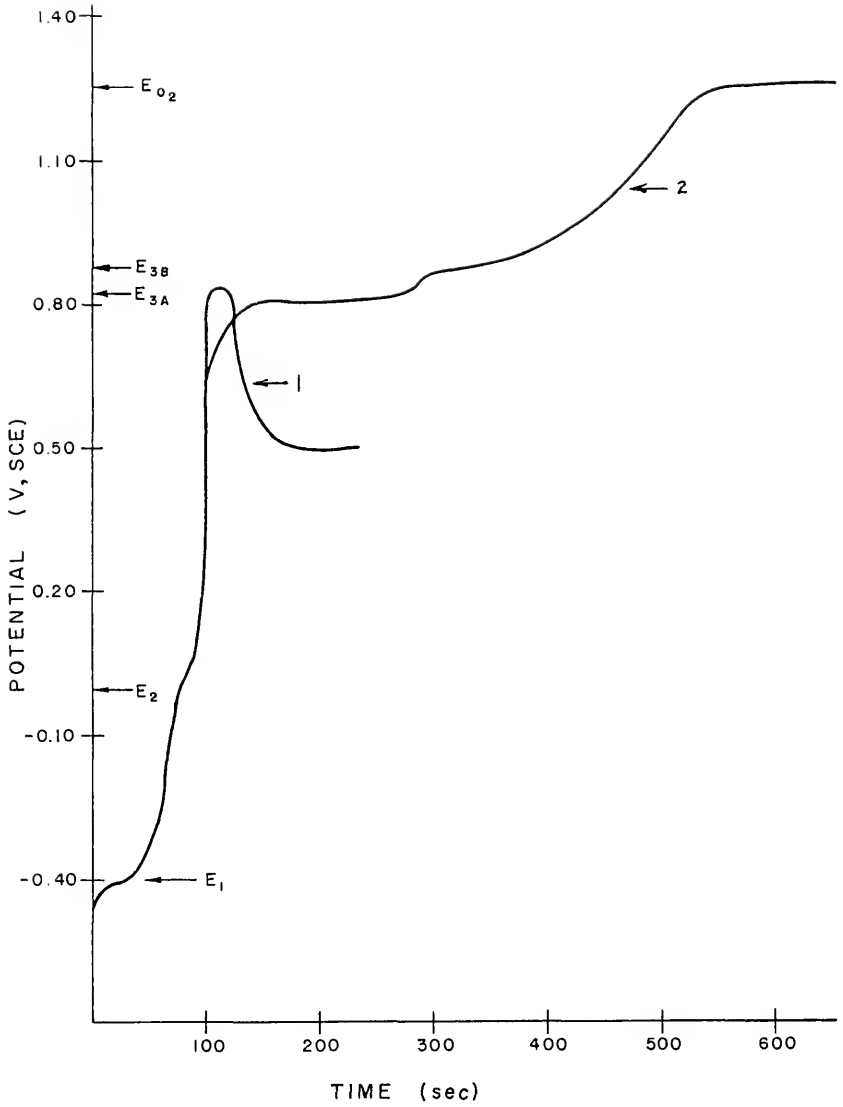
1.40
1.10
0.80
0.50
0.20
-0.10
-0.40
E_{O_2}
E_{3B}
E_{3A}
E_2
E_1
1
2
POTENTIAL (V, SCE)
100
200
300
400
500
600
TIME (sec)

Table 16

Galvanostatic potential-time behavior (0.0 M potassium chloride).

i ($A\ cm^{-2}$) x 10^4	E_1 (V,SCE)	t_1(sec)	E_2 (V,SCE)	t_2(sec)	E_{3A} (V,SCE)	t_{3A}(sec)	E_{3B} (V,SCE)	t_{3B}(sec)	E_{O_2} (V,SCE)	t_{O_2}(sec)
0.983	-0.421	222	-0.095	21	0.804	264	0.849	steady-state	-	-
0.993	-0.421	314	-0.077	18	0.800	255	0.883	steady-state	-	-
0.992	-0.435	1282	-0.110	30	0.798	420	0.840	steady-state	-	-
1.943	-0.401	243	-0.040	8	0.810		0.875	-	0.936	steady-state
1.919	-0.363	65	-0.080	10	0.827	107	0.886	-	1.125	steady-state
1.945	-0.405	161	-0.150	12	0.830	104	0.880	-	1.145	steady-state
3.772	-0.395	77	-0.045	5	0.830	130	0.890	214	1.26	steady-state
3.765	-0.400	77	0.015	3	0.825	65	0.895	-	1.24	steady-state
9.95	-0.365	19	-0.04	1	-	-	0.903	37	1.36	steady-state
16.5	-0.358	7.5	0.200	1	-	-	0.920	6.5	1.40	steady-state

Table 17

Galvanostatic potential-time behavior (0.100 M potassium chloride).

i (A cm^{-2}) x 10^4	E_1 (V,SCE)	$t_{1(sec)}$	E_2 (V,SCE)	$t_{2(sec)}$	E_{3A} (V,SCE)	$t_{3A(sec)}$	E_{3B} (V,SCE)	$t_{3B(sec)}$	E_{O_2} (V,SCE)	$t_{O_{2(sec)}}$
0.993	-0.439	1759	-0.110	44	0.783	steady-state	-	-	-	-
1.93	-0.420	292	-0.125	16	0.810	180	0.868	steady-state	-	-
3.723	-0.415	104	-0.010	4	0.852	66	0.902	150	1.25	steady-state
10.0	-0.374	34	0.10	1	-	-	0.900	64	1.37	steady-state
20.0	-0.388	12	0.155	1	-	-	0.952	9	1.41	steady-state

Table 18

Galvanostatic potential-time behavior (0.303 M potassium chloride).

i ($A\ cm^{-2}$) $\times 10^4$	E_1 (V,SCE)	t_1(sec)	E_2 (V,SCE)	t_2(sec)	E_{3A} (V,SCE)	t_{3A}(sec)	E_{3B} (V,SCE)	t_{3B}(sec)	E_{O_2} (V,SCE)	t_{O_2}(sec)
1.93	-0.423	338	-0.130	18	0.765	5.5	-	-	-	-
3.77	-0.419	77	0.09	1	0.871	7	-	-	-	-
3.75	-0.410	87	0.09	1	0.891	6	-	-	-	-
3.76	-0.417	65	0.011	1	0.881	8	-	-	-	-
3.73	-0.413	115	0.12	1	0.859	15	-	-	-	-
3.84	-0.418	83	0.06	1	0.858	4	-	-	-	-
3.85	-0.415	81	0.08	1	0.880	12	-	-	-	-
3.82	-0.422	94	0.081	1	0.857	4	-	-	-	-
3.77	-0.417	89	0.08	1	0.880	4	-	-	-	-
10.14	-0.363	25		1	-		0.925	12	1.30	2.5
10.00	-0.385	25		1	-		0.937	8	-	-
10.21	-0.385	19		1	0.895	8.7	1.04	2	-	-
10.10	-0.374	17		1	-	-	0.939	9	1.34	5
10.00	-0.411	25		1	0.877	-	0.936	3	-	-
19.74	-0.360	5		1	-	-	0.905	5	1.380	4
19.84	-0.360	5		1	-	-	0.921	4	1.390	16

Table 19

Galvanostatic potential-time behavior (0.518 M potassium chloride).

i ($A\ cm^{-2}$) $\times 10^4$	E_1 (V,SCE)	t_1(sec)	E_2 (V,SCE)	t_2(sec)	E_{max} (V,SCE)	t_{max}(sec)
0.997	-0.425	1511	-0.125	37	0.447	5
1.93	-0.427	304	-0.075	12	0.471	1.6
3.89	-0.421	72	-0.140	7	0.508	1.4
9.95	-0.409	29	-0.08	3	0.683	0.7
20.20	-0.412	12	0.21	1	0.798	0.5

in most cases, on the potential transient resulting from the first current application. Open circuit behavior and galvanostatic polarization from open circuit are also investigated.

All systems studied exhibit an initial potential arrest near -0.4 V. The reaction occurring is assumed to be dissolution of iron from the alloy as iron(II). For a given solution the current-arrest potential relationship shows Tafel behavior (Table 20). A slope of 0.06 V decade^{-1} is found for chloride ion concentrations of 0.0 through 0.303 M. Exchange current densities, calculated from the slopes and intercepts of the Tafel lines (see Introduction), range from 2.27 x 10^{-6} to 1.11 x 10^{-3} A cm^{-2} (Table 20). In 0.518 M potassium chloride a change in Tafel slope to 0.014 V decade^{-1} occurs.

The variation in E_1 with solution composition for a given current density is a function of the current density applied. Solutions containing chloride ion (0.100 through 0.518 M) at low current densities ($\leqslant$ 3.77 x 10^{-4} A cm^{-2}) exhibit a potential arrest which is negative to that observed in 0.337 M sulfate, but is approximately independent of chloride ion concentration. At higher current densities an increase in chloride concentration causes a negative shift in E_1. Arrest potentials resulting from the application of 1 x 10^{-3} A cm^{-2} vary from -0.365 V in 0.0 M potassium chloride to -0.409 V in 0.518 M potassium chloride.

Table 20

Tafel behavior during galvanostatic polarization.

Plateau	$[Cl^-]$ x 10^1	$[SO_4^{2-}]$ x 10^1	Slope (V decade^{-1})	Intercept (V)	Exchange current density (A cm^{-2})	Correlation coefficient
E_1	0.0	3.37	0.055	0.204	1.95×10^{-4}	0.97
	1.00	3.00	0.045	0.254	2.27×10^{-6}	0.84
	3.03	2.48	0.064	0.189	1.11×10^{-3}	0.97
	5.18	1.64	0.014	0.373	2.29×10^{-6}	0.80
E_{3A}	0.0	3.37	0.058	1.03	1.74×10^{-18}	0.91
	1.00	3.00	0.121	1.26	2.57×10^{-11}	0.98
	3.03	2.48	0.161	1.38	2.69×10^{-9}	0.75
E_{3B}	0.0	3.37	0.047	1.05	4.57×10^{-23}	0.97
	1.00	3.00	-	-	-	-
	3.03	2.48	0.145	1.36	4.17×10^{-10}	(1)
E_{C_2}	0.0	3.37	0.028	0.220	1.38×10^{-8}	0.98
	1.00	3.00	0.022	0.202	6.61×10^{-10}	0.97
	3.03	2.48	0.022	0.197	1.12×10^{-9}	(1)

Plateau lengths (t) associated with this arrest are irreproducible. In general it appears that t decreases with increasing current density. The charge needed to achieve the passive state, i.e., the product of current density and arrest time (indicated by a rapid change in potential to more noble values) also decreases with increasing current density.

The potential arrest found at 0.0 V, E_2, is also observed in all the systems investigated. At the chart speeds (10-20 sec in^{-1}) used to display the major portions of the potential response curve, its characteristic length and associated potential can only be determined approximately. The data suggest a positive shift in E_2 with increasing current density accompanied by a decrease in plateau length.

Potential values associated with arrests occurring at still more noble potentials as well as the stability of the maximum potential achieved are a function of current density and solution composition. In solutions which cause pitting (0.303 and 0.518 M potassium chloride), the maximum potential attained is unstable and a rapid decrease in potential to more active values occurs, despite the continued application of anodic current. Systems not susceptible to pitting attack (0.0 M and 0.100 M potassium chloride) reach and maintain a constant maximum potential. Potential arrest-current relationships are tabulated (Tables 16-19).

The arrest described at 0.8 V, E_{3A}, occurs in solutions containing 0.0, 0.100, and 0.303 M potassium chloride and is visible at the recorder speeds employed (10 to 20 sec in^{-1}) for current densities of $\leqslant 3.7 \times 10^{-4}$ A cm^{-2}. In 0.303 M potassium chloride this arrest is also seen in two of five experiments conducted at $i = 1.0 \times 10^{-3}$ A cm^{-2}. The current density-arrest potential relationship associated with this plateau follows Tafel behavior in all three systems. Tafel parameters are presented in Table 20. The reaction associated with this arrest is assumed to involve the oxidation of chromium(III) in the passive film to chromium(IV). From the slopes and intercepts of the Tafel lines, exchange current densities of 1.74×10^{-18}, 2.57×10^{-11}, and 2.69×10^{-9} A cm^{-2} are calculated for 0.0, 0.100, and 0.303 M potassium chloride, respectively. In solutions containing 0.303 M potassium chloride polarized by current densities $< 1.0 \times 10^{-3}$ A cm^{-2}, the potential of this plateau is the maximum achieved and breakdown to more active values ensues.

The next arrest observed, E_{3B}, occurs in the vicinity of 0.85 V in 0.0 M ($i \geqslant 0.99 \times 10^{-4}$ A cm^{-2}), 0.100 M ($i \geqslant 1.93 \times 10^{-4}$ A cm^{-2}), and in 0.303M ($i \geqslant 1.0 \times 10^{-3}$ A cm^{-2}) potassium chloride. The presence of a maximum in the current-potential arrest behavior is suggested in 0.100 and 0.303 M potassium chloride. The data in 0.100 M potassium chloride solutions prior to the potential maximum are insufficient for Tafel analysis. However, Tafel behavior

is exhibited in 0.0 and 0.303 M potassium chloride. Exchange current densitites of 4.57×10^{-23} and 4.17×10^{-10} A cm^{-2} are calculated for the two systems, respectively. In only two of five experiments at current densities of 1.0×10^{-3} A cm^{-2} does breakdown occur from this plateau in 0.303 M potassium chloride. In all other cases, as with non-pitting systems, further polarization to more noble potentials corresponding to oxygen evolution occurs.

The potential arrest associated with oxygen evolution, E_{O_2}, is seen in 0.0 M ($i \geqslant 1.94 \times 10^{-4}$ A cm^{-2}), 0.100 M ($i \geqslant 3.72 \times 10^{-4}$ A cm^{-2}), and 0.303 M ($i \geqslant 1.0 \times 10^{-3}$ A cm^{-2}) potassium chloride. Attainment of this plateau in 0.303 M potassium chloride is followed by pitting breakdown. Exchange current densities of 1.38×10^{-8}, 6.61×10^{-10}, and 1.12×10^{-9} A cm^{-2} are calculated for the oxygen evolution reaction for the three solutions, respectively.

Constant current polarization of specimens in 0.518 M potassium chloride initiates breakdown from potentials substantially below those observed in 0.303 M potassium chloride. Breakdown occurs from 0.447, 0.471, 0.508, 0.683, and 0.798 V during the initial imposition of 0.997×10^{-4}, 1.93×10^{-4}, 3.89×10^{-4}, 0.995×10^{-3}, and 2.02×10^{-3} A cm^{-2}, respectively. Repolarization results in successively more positive potential maxima. Values of 0.683, 0.722, and 0.763 V are observed as a result of the first, second and third application of 0.995×10^{-3} A cm^{-2}, respectively.

The steady-state potential obtained after pitting-induced potential breakdown during constant current polarization has been called the protection potential of the system under study.[42] To determine this characteristic value long-term (10 to 90 min) constant current polarization behavior was examined for samples in 0.303 and 0.518 M potassium chloride. The history of the samples used varied widely. However, the results of the recycling experiments indicate that after passivation is achieved, especially in higher chloride ion concentration solutions, the absolute value of potential arrests is only slightly affected by history while the general potential-time response remains approximately the same.

The precise definition of the course of the potential-time curves during breakdown and of the steady-state potential reached is hindered by potential oscillations varying in magnitude from ± 10 to $\pm$ 60 mV and in frequency from 4 to 6 per 100 seconds. Therefore, only the average values of the final potentials achieved for a given solution composition and current density are presented in Table 21. Also included are the maximum potentials reached prior to breakdown of the passive state. In all cases in 0.303 M potassium chloride rapid potential breakdown occurs to approximately 0.50 V. A slow negative shift in potential follows. The average final potential attained is a function of current density, ranging from 0.085 V at 1.93×10^{-4} A cm^{-2}

Table 21

Average final breakdown potentials during galvanostatic polarization.

$[Cl^-]$ x 10^1	$[SO_4^{2-}]$ x 10^1	i (A cm^{-2}) x 10^4	E_{max}(V,SCE)	t_{max}(sec)	E_{avg}(V,SCE)
3.03	2.48	1.93	0.765	5.5	0.085
		3.77	0.86 to 0.88	4 to 12	0.28 to 0.35
		10.0	0.88 to 0.89	3 to 15	0.36 to 0.39
			1.35	17	0.31
		19.74	1.37	28	0.33
0.518	1.64	0.997	0.495	3	-0.043
		1.93	0.525	2.7	0.015 to 0.02
		3.89	0.685	1	0.045 to 0.06
		9.95	0.812	0.8	0.245
		20.20	0.829	-	0.230

to 0.36 to 0.39 V at 1.0×10^{-3} A cm^{-2}. When oxygen evolution potentials are reached prior to breakdown, slightly more negative values result (0.31 and 0.33 V for 1.01×10^{-3} and 1.97×10^{-3} A cm^{-2}, respectively).

Considerably more negative average final potentials are observed in 0.518 M potassium chloride over the entire current range studied. The potential magnitude shifts in the positive direction (from -0.043 to 0.045 V) with increasing current density for the three lower currents employed. A marked positive shift to 0.245 V occurs when the applied current density is increased to 0.995×10^{-3} A cm^{-2}. A potential value of 0.230 V is observed at a current density of 2.02×10^{-3} A cm^{-2}.

Following constant current polarization, the galvanostat was removed from the circuit and the resulting open circuit potential transient was observed. Open circuit behavior is a strong function of solution composition and electrode surface history. The representative data presented in Table 22 are obtained from samples of diverse history and therefore are discussed only qualitatively. Galvanostatic parameters from the immediately preceding polarization are also included.

In solutions which do not initiate pitting breakdown during constant current polarization (0.00 and 0.100 M potassium chloride) three open circuit arrests are described.

Table 22

Open circuit decay behavior following galvanostatic polarization.

$[Cl^-]_l$ x 10^1	$[SO_4^{2-}]_l$ x 10^1	i (A cm^{-2}) x 10^4	E_{max} (V,SCE)	E_b (V,SCE)	E_1 (V,SCE)	E_2 (V,SCE)	E_3 (V,SCE)	E_F (V,SCE)	t_F (hrs)
0.0	3.37	0.98	0.85	-	0.44	0.15	-0.42	-	-
		1.9	0.88	-	0.46	0.18	-0.41	-	-
		3.7	1.20	-	0.52	0.16	-0.43	-	-
		9.95	1.37	-	0.39	0.15	-0.50	-0.11	2
		16.50	1.39	-	0.45	-0.04	-0.45	0.23	12
1.00	3.00	0.99	0.98	-	-	0.15	-0.44	-	-
		1.93	0.86	-	0.40	0.14	-0.44	-	-
		3.72	1.22	-	0.41	0.09	-0.49	-	-
		10.0	1.37	-	0.46	0.04	-0.47	-	-
		20.0	1.41	-	0.38	0.15	-0.47	-	-
3.03	2.48	1.93	0.76	0.24	-	-0.29	-0.47	-	-
		3.8	0.85	0.47	-	-0.31	-0.50	-	-
		10.0	1.30	-	0.16	-0.10	-0.47	-	-
		19.74	1.38	-	0.17	-0.27	-0.45	-	-

Table 22 continued

$[Cl^-]$ x 10^1	$[SO_4^{2-}]$ x 10^1	i (A cm^{-2}) x 10^4	E_{max} (V,SCE)	E_b (V,SCE)	E_1 (V,SCE)	E_2 (V,SCE)	E_3 (V,SCE)	E_F (V,SCE)	t_F (hrs)
5.18	1.64	0.99	0.49	0.25	-	-0.33	-0.42	-0.128	10
		1.93	0.54	0.28	-	-0.27	-0.47	-0.013	10
		3.89	0.68	0.31	-	-0.27	-0.48	-0.112	14
		9.95	0.81	0.37	-	-0.26	-0.46	-	
		20.20	0.83	-	-0.19	-0.31	-0.47	-0.105	4

Arrest potentials of 0.4 to 0.5 V, E_1, 0.12 to 0.19 V, E_2, and -0.4 to -0.5 V, E_3, are observed in 0.00 M potassium chloride. In 0.100 M potassium chloride the first two arrests occur at slightly more negative values, 0.38 to 0.40 V and 0.04 to 0.15 V, respectively. The third is found between -0.4 and -0.5 V. Although the most negative potential achieved remains constant for up to five minutes, a subsequent slow increase in potential with time occurs. Thus, after six hours at open circuit in 0.0 M potassium chloride, following constant current polarization at $i = 3.8 \times 10^{-4}$ A cm^{-2}, the electrode potential has shifted from -0.480 to -0.393 V. After twelve hours, a value of 0.228 V is recorded for the open circuit potential of a sample subjected previously to a constant current of 1.65×10^{-3} A cm^{-2}.

Systems subject to pitting attack exhibit complex open circuit behavior. In both 0.303 and 0.518 M potassium chloride, an apparent steady state potential occurs between -0.44 and -0.50 V. Following polarization at $i = 3.8 \times 10^{-4}$ A cm^{-2}, the potential remains constant in this range for four hours in 0.303 M solutions. In 0.518 M potassium chloride, however, the open circuit potential shifts positive with time from the most negative potential observed. Values of -0.128 to -0.013 V are recorded after four to ten hours at open circuit in this system. An additional arrest

is observed at -0.27 to -0.32 V in 0.518 M potassium chloride, regardless of the preceding polarization current density. This arrest is also visible in some cases in 0.303 M potassium chloride.

Other open circuit arrests are described between the average potential achieved after breakdown during constant current polarization and the arrest at -0.27 V. The variation in the potential values associated with these arrests with solution composition and the maximum potential achieved during constant current polarization as well as their relation to the arrests observed in non-pitting systems cannot be evaluated on the basis of the data available.

Following attainment of the apparent steady-state open circuit potential, the constant current was reapplied to determine the difference, if any, in the potential-time response resulting from open circuit pretreatment. Regardless of the length of time at open circuit, the most negative potential reached, or the potential arrests observed during decay, reapplication of a constant anodic current produces no observable arrests below 0.8 V. In non-pitting systems the behavior above 0.8 V is quite similar to that achieved during the initial polarization from -0.700 V. The potential arrests observed in 0.303 M potassium chloride are slightly more negative but the general pattern follows that of the initial polarization. More noble breakdown potentials are observed in 0.518 M potassium chloride.

Capacity-potential behavior

The differential capacity of the stainless steel-solution interface was determined as a function of potential during constant current polarization. Because of the manual technique employed in data correlation and the rapidity of the potential-time change, capacity behavior is not precisely defined. Although, in some cases, re-use of an electrode causes a decrease in the magnitude of the capacity associated with a given potential, the qualitative capacity-potential behavior remains unaffected. Therefore, the data accumulated for any one arrest, regardless of electrode history and polarization current density, are used to define the course of the capacity-potential (time) curve for a given solution composition. Capacity values, when given, represent initial polarization data or values not influenced strongly by electrode re-use. A capacity-time curve for a system not subject to pitting (0.0 and 0.100 M potassium chloride) is superimposed on its associated potential-time curve and is presented in Figure 28.

Steady-state capacity values determined at the end of the twenty-minute prepolarization period range from 21 to 48 μf cm^{-2} (C-700). These values are typical of capacities associated with the double layer in solutions of high ionic strength.[63]

Figure 28. Schematic representation of the capacity-time behavior of a system not subject to pitting breakdown during galvanostatic polarization.

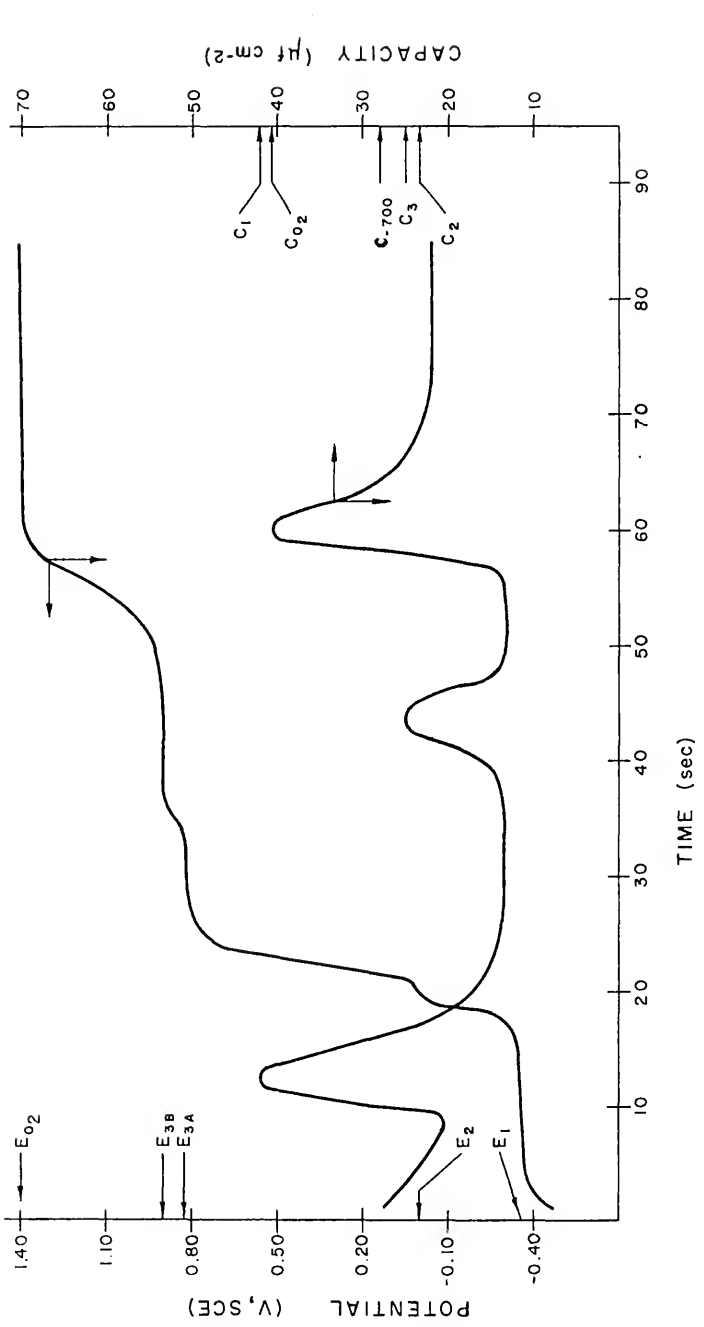
POTENTIAL (V, SCE)
1.40
1.10
0.80
0.50
0.20
-0.10
-0.40
E_{O_2}
E_{3B}
E_{3A}
E_2
E_1
10
20
30
40
50
60
70
80
90
TIME (sec)
CAPACITY ($\mu f\ cm^{-2}$)
70
60
50
40
30
20
10
C_1
C_{O_2}
C_{-700}
C_3
C_2

In all systems subjected to galvanostatic polarization (0.0 to 0.518 M potassium chloride), a capacity peak, C_1, is associated with the first potential arrest observed, E_1. Solutions containing chloride ion exhibit a slightly greater peak magnitude (38 to 58 μf cm^{-2}) than those with none (35 to 48 μf cm^{-2}).

Capacity values observed during the rapid potential transition from the active to the transpassive state range from 12 to 22 μf cm^{-2} in 0.0 and 0.1 M potassium chloride. This represents a substantial decrease from the values in the active region. Similar capacity decreases occur prior to and during potential breakdown from the transpassive region in 0.303 M potassium chloride.

The second capacity peak observed in systems containing 0.0 and 0.1 M potassium chloride is associated with the potential transition from the arrest at 0.8 V to that at 0.85 V. Peak values of 20 to 40 μf cm^{-2} are measured. The continued change in potential to oxygen evolution values is accompanied by a capacity peak only when potentials $\geq$1.3 V are attained. The maximum potentials achieved in these solutions are stable with respect to time. No pitting-induced potential breakdown occurs. Corresponding steady-state capacity values range from 15 to 26 μf cm^{-2} for final potentials $\leq$ 1.26 V and from 21 to 39 μf cm^{-2} for final potentials of $\geq$ 1.34 V.

In 0.303 M potassium chloride the potential arrests observed and the potential from which breakdown occurs coincide with arrests occurring in non-pitting systems. Capacity data, although not conclusive, suggest that the corresponding capacity-potential behavior is also similar.

In 0.303 M potassium chloride solutions a definite capacity increase is associated with potential arrests and/or maxima between 0.72 and 1.04 V. However, the relative position of the capacity peak(s) and characteristic potential(s) are not well defined. A capacity maximum occurs prior to breakdown from potentials in the oxygen evolution region (1.3 to 1.4 V). The magnitudes of the largest measured capacities are 15 to 24 and 28 to 63 μf cm^{-2}, respectively, in good agreement with those found in non-pitting systems in similar potential regions.

The rapid potential decrease to approximately 0.5 V caused by pitting in 0.303 M potassium chloride is accompanied by a capacity decrease to values of 11 to 14 μf cm^{-2} and 8 to 11 μf cm^{-2} following breakdown from the transpassive and oxygen evolution regions, respectively. An examination of long-term constant current polarization data shows that, in most cases, the capacity remains constant as the slow negative shift in potential with time is achieved. Two instances of diverse behavior are observed.

An increase in capacity to 20 μf cm^{-2} occurs at 0.12 V as the average potential (0.085 V) resulting from 1.93×10^{-4} A cm^{-2} is approached. For polarization with 1.02×10^{-3} A cm^{-2}, the capacity increases slowly from 14 to 18 μf cm^{-2} as the potential decreases from 0.461 V to the average final value, 0.391 V.

The largest potentials attained in 0.518 M potassium chloride for the three lower current densities employed (0.447 to 0.508 V) are substantially more negative than any of the potential arrests characteristic of non-pitting systems. The largest potentials reached at the two highest current densities more closely approximate non-pitting values (0.683 and 0.798 V).

The capacity-potential behavior resulting from the application of 0.997×10^{-4} and 1.93×10^{-4} A cm^{-2} exhibits a well-defined, smooth decrease in capacity from the prepassive region across the potential-time peak. Typical capacity values associated with these potential maxima range from 13 to 15 μf cm^{-2}. For 3.89×10^{-4} A cm^{-2}, the number of data points available is much smaller. The shape of the capacity-potential curve is similar to that described above but with slightly higher capacity values (16 and 18 μf cm^{-2} at potential maxima of 0.568 and 0.588 V, respectively).

Since only two data points are available at the two higher current densities, no conclusions can be drawn with respect to the presence or absence of a capacity peak associated with the potential-time maximum achieved prior to breakdown. However, capacity values determined for these higher potential maxima approach those observed in non-pitting systems. As discussed above, subsequent polarizations of an electrode result in more noble potential maxima in 0.518 M potassium chloride. Thus, capacity values of 21 to 52 μf cm^{-2} are recorded for potential maxima of 0.758 to 0.823 V.

The capacity-potential behavior following potential breakdown during long-term constant current polarization in 0.518 M potassium chloride was also observed. For the two lower current densities, an increase in capacity of 2 to 3 μ f cm^{-2} to an approximately constant value of 14 to 18 μ f cm^{-2} occurs. A similar constant capacity region is observed during polarization at 3.89×10^{-4} A cm^{-2} which for all three currents persists to approximately 0.3 V. Subsequently, the capacity increases to between 20 and 29 μf cm^{-2} within the potential range 0.27 to 0.09 V. The presence of a well-defined peak at 0.268 V in one experiment (0.518 M potassium chloride, 3.89×10^{-4} A cm^{-2}) supports the implication of this capacity increase.

During polarization by 0.995×10^{-3} A cm^{-2}, the constant capacity region (16 to 21 μf cm^{-2}) is observed to a potential of 0.25 V and is followed by an increase in value to 28 μf cm^{-2} at 0.202 and 0.129 V. No peak is defined, however. Since the average final potential attained with 2.02×10^{-3} A cm^{-2} is near 0.3 V, only the constant capacity region (14 to 22 μf cm^{-2}) is seen.

Capacity-potential behavior was also observed during open circuit decay from final state potentials induced by constant current polarization.

A decrease in capacity to a constant value after removal of constant current control is well defined in 0.0 and 0.100 M potassium chloride and is strongly suggested in 0.303 M potassium chloride. The negative boundary of this constant capacity region lies between 0.20 and 0.30 V. Capacity values range from 11 to 16 μf cm^{-2} and 7 to 14 μf cm^{-2} for systems whose preceeding current induced potential maxima occur in the transpassive and oxygen evolution regions, respectively. In 0.303 and 0.518 M potassium chloride, in most cases, final potentials achieved after pitting breakdown under the continued influence of anodic current are in or negative to this constant capacity region.

At more negative potentials, capacity values were determined only at widely spaced time intervals. However, the existence of two capacity peaks of about 30 to 40 μf cm^{-2} is suggested, occurring between 0.10 to -0.10 and

-0.20 and -0.40 V, respectively. In all cases, the potential arrest observed in the range of the former peak occurs before the capacity maximum. The second capacity peak is observed both in the presence and the absence of the potential arrest sometimes visible in the same potential range. The capacity peak precedes the potential arrest when both occur simultaneously.

CHAPTER IV

DISCUSSION

Potentiostatic Polarization

The results of the potentiostatic experiments are discussed in terms of the phenomena represented by characteristic regions of the polarization curve. The topics to be considered in detail include: the anodic dissolution-passivation mechanism(s); the hydrogen evolution reaction; the open circuit or rest potential as it relates to the rates of the active dissolution and hydrogen evolution reactions; the passive region; the pitting reaction; and transpassive dissolution.

Active dissolution and passivation

The transition from the active to the passive state observed for all systems studied here is characterized by the critical current density, the primary passivation potential, and the potential of total passivity. The presence of a current maximum in the polarization curve prior to the onset of passivation suggests a competition between the reaction leading to dissolution and the reaction leading to passivation of the metal surface. Both reactions are assumed to occur on bare metal surface sites. At the primary passivation potential the passivation reaction has succeeded to the extent that the fractional

coverage (θ) of active surface sites (kinks, ledges, etc.) has reached 0.5. Further polarization results in a continuous increase in θ until the surface becomes totally passive at E_{TP}.

The magnitude of the critical current density in any given solution should depend on the effect of the solution components on the kinetics of the two competing reactions.

Present results on stainless steel indicate an increase in the dissolution rate by both chloride and sulfate anions. In all solutions studied in the present work, it has been observed that the logarithm of the critical current density is proportional to the logarithm of the concentration function, pH + log ($[SO_4^{2-}]$ + $[Cl^-]$), where $[SO_4^{2-}]$ and $[Cl^-]$ are the analytical concentrations of the sulfate and chloride ions present, respectively (Figures 9, 19, and 25). This implies that chloride, bisulfate and sulfate ions are equivalent in their effect on the dissolution-passivation reaction and that it is the total anion concentration which determines the critical current density.

Similarly, Florianovich et al.[64] have shown a linear relationship between the logarithm of the anodic current density for iron dissolution and the logarithm of the total anion activity in acidic sulfate solutions. Since linearity is obtained only if the total sulfate activity is considered,

these authors assume that sulfate and bisulfate ions function equally. Reaction orders of +1 for both the hydroxyl and the sulfate ion are observed. Chloride ion, between 0.01 and 1.9 M, has also been demonstrated to have a positive reaction order for iron dissolution.[65]

Little work has been done to evaluate the effect of solution composition on the rate of the reaction leading to passivation, although sulfate ion has been shown to depolarize the passivation reaction for iron.[66] Present results indicate that, at constant pH, the primary passivation potential is independent of solution composition in the range studied (Tables 1 and 7). This behavior implies that both the dissolution and passivation reactions are depolarized equally in a given solution. The positive shift in primary passivation potential observed when the pH is decreased suggests that hydroxyl ion, while participating in both reaction, accelerates the dissolution reaction more so than the passivation reaction.

A capacity peak is associated with the active to passive transition in these studies and occurs, in most cases, 0 to 40 mV negative to the primary passivation potential. In view of the arguments given above it is likely that this peak indicates the specific adsorption of the anions participating in the dissolution and passivation reactions (hydroxyl, sulfate, bisulfate and

chloride ions). The adsorption of these anions on iron in acid solutions has been demonstrated by Hackerman et al.[67, 47, 48, 50] The evaluation of the effect of solution composition on capacity peak magnitude is hindered by the presence of absorbed hydrogen and hydrogen bubbles. In systems exhibiting no evidence of interference (see below), values of 62 to 73 μf cm^{-2} are observed in all solutions.

The majority of the relationships observed between the potential of total passivity and the solution in which it is determined are linear with respect to the solution composition rather than the logarithm of solution composition. This suggests that the potential of total passivity is dependent on kinetic, rather than thermodynamic, factors. It is unlikely that the positive shift in the potential of total passivity with increasing total anion concentration can be directly attributed to an increase in film solubility in the concentration range studied. If this were the case, the primary passivation potential (θ = 0.5) would also undergo a positive shift and a monotonic increase in the passive current density would occur. Neither effect is observed (Tables 1 and 7).

It is possible, however, that expulsion of specifically adsorbed anions from the inner double layer, caused by a change in the zero point of charge of the metal surface upon passivation, may increase the local aggressiveness of the solution sufficiently to decrease passive film stability.

The number of specifically adsorbed anions on a metal surface increases with the concentration of adsorbable anions in the solution.[46] A positive shift in the potential of total passivity with adsorbable anion concentration would therefore be expected.

A decrease in the rate at which the applied potential is changed would then be expected to cause a negative shift in E_{Tp} since additional time would be provided at each potential for adjustment of the double layer structure to that representative of the bulk solution, but this effect was not studied.

The hydrogen evolution reaction

The net cathodic current density measured at -0.700 V is the algebraic sum of the internal anodic and cathodic currents flowing at this potential. The maximum anodic current density observed during polarization (i_{crit}) is approximately two orders of magnitude less than the cathodic current observed at -0.700 V ($\sim 10^{-3}$ A cm^{-2}) and occurs in the vicinity of -0.40 V. Since the anodic current density is expected to decrease exponentially with potential as the potential is made more negative, it can be assumed that the magnitude of the residual internal anodic current at -0.700 V is negligible with respect to the cathodic current. Any change in the net cathodic current density with solution composition is therefore attributed to a variation in the kinetics of the hydrogen evolution reaction, only.

Chloride ion has been shown to depolarize the hydrogen evolution reaction on stainless steel.[68, 69] A similar effect has been observed on chromium in 0.5 M sulfuric acid where the addition of hydrochloric acid decreases the reduction reaction overvoltage.[70] The negative shift in the potential of the Outer Helmholtz Plane produced by the presence of specifically adsorbed chloride ion is believed to accelerate reduction of the hydronium ion by decreasing the activation energy for the reaction. The effect of sulfate on the kinetics of the hydronium ion reduction reaction on ferrous metals has not been studied, although sulfate ion has been shown to be specifically adsorbed on an active iron surface.[47]

Since the zero point of charge of an active stainless steel surface is assumed to be approximately -0.69 V, specifically adsorbed chloride ions are expected to be present in the inner double layer at -0.700 V. However, the increase in cathodic current density at -0.700 V with increasing chloride ion concentration expected on the basis of literature results is not observed in the present studies. In primary solutions at pH 2.4 and at constant ionic strength with chloride ion concentrations between 0.0 and 0.508 M (sulfate ion concentrations from 0.334 to 0.163 M), the cathodic current density is approximately constant. The variations observed within this concentration range (Table 1) are most likely a result of differences in the true electrode

area of the electrodes employed. A variation in the true electrode area by up to a factor of 1.5 would account for the changes observed. Parallel changes occurring in the corresponding differential capacity values (Table 11) support this conclusion.

It therefore appears that sulfate ion counteracts the depolarizing effect of chloride ion if it is present in sufficient quantities. The large increase in cathodic current density occurring when the sulfate ion concentration is decreased from 0.163 to 0.016 M supports this contention (Table 1).

Data accumulated in systems of varying chloride ion concentration and ionic strength at constant pH (2.4) differ considerably from those at constant ionic strength discussed above. The cathodic current density at -0.700 V for a given chloride ion concentration is two to three times lower than that observed in solutions containing sulfate ion and a decrease in current density with increasing chloride ion concentration is observed. That these phenomena are not artifacts is supported by the good agreement between results obtained two months apart for 0.102 and 0.123 M potassium chloride (Table 7).

The lower current densities observed in 0.102 and 0.123 M potassium chloride may be caused, in part, by differences in roughness factor, i.e., the ratio of the actual surface area to the apparent geometric area from

one electrode to another. If the differential capacities measured at -0.700 V in 0.1 M potassium chloride solutions in the presence (63 μf cm^{-2}) and absence (21 to 31 μf cm^{-2}) of sulfate ion are compared, ratios of two to three are also observed. Since both current density and differential capacity are calculated on the basis of geometric area, the parallel variations in these two parameters support the idea of an area effect.

The behavior of the 1.0 M potassium chloride system is reproducible but cannot be explained in terms of the data accumulated here. The presence of 0.016 M sulfate would be expected to exert little influence but the values obtained in the presence and absence of this species are widely divergent (5.31 x 10^{-3} versus 7.06 x 10^{-4} A cm^{-2}, respectively).

Insufficient data are available from present experiments to determine the mechanism by which hydrogen is evolved at the stainless steel surface in acid solutions. Tafel slopes of 0.087 to 0.133 V decade^{-1},[71, 72, 58] exchange current densities of 2 to 33 x 10^{-6} A cm^{-2},[58, 72] and a reaction order of 0.85 for hydronium ion[71] have been reported in the literature. The electrochemical discharge step,

$$H^+ + e \rightarrow H_{ads} \qquad \text{(Volmer reaction)} \quad (6)$$

where H_{ads} is an adsorbed hydrogen atom, has been shown to be

rate-determining in basic solutions.[73] This step is also rate-determining for the hydrogen evolution reaction on iron in acid solutions.[74, 75]

Correlation of the capacity-potential and current density-potential data observed here suggests that the hydrogen evolution reaction is also associated with the random cathodic loop seen during anodic polarization. Wilde[69] has studied the effect of cathodic pretreatment on the capacity-potential behavior of AISI 304 in 0.5 M sulfuric acid. Since austenitic stainless steels are known to absorb hydrogen, he attributes the increase in the magnitude of the capacity peak in the active-passive transition range with increasing pretreatment time to an adsorption pseudocapacitance.

In the majority of cases in the present results in which the loop occurs or low anodic net currents are observed in the potential range of the loop, significantly higher capacity values and broader capacity peaks are measured (Tables 3 and 10). It appears likely, therefore, that these high capacity values are caused by the presence of absorbed hydrogen atoms in the stainless steel.

The reversible potential of the hydrogen evolution reaction is a function of the pH at the electrode-solution interface,

$$E = -0.06\ pH - 0.245 \qquad (7)$$

where E is the reversible potential in V versus SCE and

0.245 V is the potential of the saturated calomel electrode on the hydrogen scale. As the potential is shifted positive past the reversible potential, oxidation of the absorbed hydrogen atoms from the metal will occur, causing an increase in the capacity value measured. The accumulation of the resulting hydronium ion at the interface will cause a decrease in pH and a produce a positive shift in the reversible potential of the reaction. If the interfacial pH becomes low enough, hydrogen evolution will again become energetically feasible. The interfacial pH necessary to allow hydronium ion reduction in the potential range of the cathodic loop (-0.30 to 0.0 V) is calculated from equation 7 as 0.91 to - 4.10. If it is assumed that all of the hydrogen produced at -0.700 V ($\sim$2.4 coul) is absorbed by the stainless steel and then emitted into an approximately 100 Å double layer, an interfacial pH of -4.1 is calculated. Since only a fraction of the hydrogen produced is expected to be absorbed, this is obviously an approximation.

With the present data it is not possible to make the distinction between one broad capacity peak or two separate, narrower peaks in the active-passive transition region. Spurious results are caused, in part, by the presence of hydrogen bubbles on the horizontal surface of the electrode. 76

The influence of chloride ion on the degree of hydrogen absorption by stainless steel is open to question. Present data suggest that in 0.3 and 0.5 M potassium chloride (pH 2.4, ionic strength = 1) as well as in 0.102, 0.123, and 1.0 M potassium chloride (pH 2.4, variable ionic strength) absorption is considerably diminished when compared to lower chloride ion concentrations in the presence of sulfate. Wilde's data,[69] on the other hand, show an enhancement in the degree of absorption in the presence of chloride ion with respect to that observed in dilute sulfuric acid.

The appearance of a cathodic loop in the polarization curves of chromium and chromium alloys following passivation in deaerated acid solutions has been noted by many investigators.[77, 78, 16, 29] Attempts to study the kinetic parameters associated with this loop for nickel-chromium[79] and cobalt-chromium[80] alloys have been unsuccessful. However, Wilde and Hodge[81] have examined the hydrogen evolution reaction on active and passive chromium in dilute sulfuric acid in detail. The substantial decrease in exchange current density on the passive surface (5.3×10^{-9} A cm^{-2}) from that on the active surface (3.5×10^{-7} A cm^{-2}) is attributed to the presence of a chromium-deficient semiconducting oxide on the metal surface. The Tafel slope corresponding to hydrogen evolution on the passive metal is given as 0.067 V $decade^{-1}$.

The exchange current density reported in the literature for hydrogen evolution on active stainless steels is approximately 10^{-5} A cm^{-2} (see above). If, similar to chromium, the exchange current density on the passive steel surface is assumed to be two orders of magnitude less than that on the active surface (i.e., $\sim 10^{-7}$ A cm^{-2}) and a Tafel slope of 0.067 V $decade^{-1}$ is valid, the current density at a given overvoltage in the cathodic loop can be calculated. Applying the high-field modification of the Butler-Volmer equation and assuming an overvoltage of -0.2 V, a value of 2.0×10^{-6} A cm^{-2} is obtained. This agrees very well with the value, 1.36×10^{-6} A cm^{-2}, measured in 0.334 M sodium sulfate at pH 2.4.

Rest potential

It appears from the present results that the rates of both the hydrogen evolution reaction (i_{-700}) and the dissolution reaction (i_a) depend on chloride as well as on sulfate ion concentration. At the rest potential these two reaction rates must be equal. Therefore, it is difficult to evaluate changes in the rest potential with solution composition when both sulfate and chloride ion concentrations are varied simultaneously (primary solutions). Rest potential values observed under these conditions range from -0.453 to -0.510 V.

The negative shift in rest potential with increasing chloride ion concentration seen in the absence of sulfate

ion interference (secondary solutions) is similar to that reported for AISI 304[82] and AISI 304L[83] in solutions of constant sulfate concentration. Chin and Nobe,[65] using constant ionic strength perchlorate solutions to eliminate possible sulfate interference, report a negative shift in rest potential of 0.020 V per decade increase in chloride ion concentration.

On the other hand, numerous investigators have found the rest potential to be independent of chloride ion concentration. Thus, for AISI 304,[36] iron,[43] and an iron-25 nickel alloy[84] in sulfuric acid solutions as well as for iron in sodium chloride at pH 2.58[85] and iron-chromium alloys in saline solutions varying in pH from 4.5 to 11,[86] no change in rest potential as a function of chloride ion concentration has been observed.

The data obtained in the present work suggest 1.) that the rest potentials observed in the secondary solution experiments fall within the range of values found for the primary solutions; 2.) that the rest potential values in 0.1 M potassium chloride with and without sulfate additions (-0.470 and -0.480 V, respectively) are approximately the same; and 3.) that the addition of only 0.016 M sulfate ion to 1.0 M potassium chloride is unlikely to produce any change in the rest potential, although a 40 mV positive shift is observed. From these observations it is concluded that for AISI 304 in the solutions employed,

chloride ion exerts no influence on the measured rest potential. This implies that both the cathodic and anodic reactions are depolarized by chloride ion to a similar extent.

The above data are not entirely conclusive, however, and two facts must be noted. The typical variation in rest potential values for any given solution is only 5 to 10 mV (Tables 2 and 8). Also, in both cases in which rest potentials of $\leqslant$ -0.50 V are observed, correspondingly low cathodic current densities are recorded at -0.700 V, suggesting polarization of the cathodic reaction in these systems.

Passive region

The current flowing across a passive metal-solution interface may have three components: an electron current, flowing through the passive film, e.g., if a redox couple is present; an ionic current, caused by the passage of ions through the film resulting in film growth; and an equivalent ionic current, arising from dissolution of the passive film.

The low current densities observed in these studies in the passive region in systems not subject to pitting breakdown are independent of potential. In the absence of an electron current, this implies that the rate of film growth is independent of potential since, for short times ($<$ 1 hour), the ionic current of film dissolution has been shown to be

negligible with respect to the film growth current.[87] An increase in potential in the passive region must therefore induce a proportional increase in film thickness, resulting in the maintenance of a constant field across the film.

For an 18-8 stainless steel in 0.5 M sulfuric acid, Schwenk and Rahmel[88] have shown that the logarithm of the rate of passive film growth is inversely proportional to the thickness of the film, i.e., growth occurs in accordance with the inverse logarithmic law,

$$i = A \exp (BV/d) \qquad (8)$$

where i is the current density, V is the potential drop across the film, d is the film thickness, and A and B are constants. This behavior satisfies the constant current density-constant field relation and can be explained in terms of the Mott-Cabrera[89] theory of high field film growth. This theory, originally derived for valve metals such as tantalum, has been extended to include the films formed on passive metals.[90] Growth occurs by the high field ($\sim 10^6$ V cm^{-1}) conduction of metal cations through the film. The current-potential behavior is therefore exponential rather than ohmic.

If the presence of a constant current in the passive region implies a proportionality between potential and passive layer thickness and if the interfacial capacitor can be represented as a parallel plate condenser with the passive

layer as its dielectric, then a plot of reciprocal capacity (1/C) with respect to potential (E) should be linear. The contribution of the film-solution capacity to the total interfacial capacity is assumed to be small (see below). This theory does not apply to the entire potential range in which the passive current density remains constant or in the potential region preceding the break in capacity at E_b. However, in the potential range bounded by E_b and the potential at which the capacity minimum occurs, excellent correlation between the two functions is exhibited (Table 15).

The capacity of a parallel plate condenser is given by

$$C = \epsilon\rho / 0.113d \qquad (9)$$

where C is the capacitance in $\mu f\ cm^{-2}$, ϵ is the dielectric constant, ρ, the surface roughness factor and d, the distance between the capacitor plates in $\mathring{A}$. The constant, 0.113, has the units $cm^2\ \mu f^{-1}\ \mathring{A}^{-1}$. The film thickness may therefore be calculated from the measured value of capacity at a given potential in the potential range in which the condition of linearity between 1/C and E is satisfied. Since the measured capacities are not steady state values, only an approximation of the film thickness corresponding to a given potential is obtained. Evaluation of the passive layer thickness is complicated by the lack of knowledge concerning the exact nature of the passive film and its dielectric constant.

Engell and Ilschner,[91] using a value of 10 and roughness factor of 4, have calculated the thickness of the passive layer formed on iron in 0.5 M sulfuric acid at potentials of 0.614 and 1.13 V. They obtain thicknesses of 10 and 20 Å, respectively, after subtracting 2 Å from the calculated value to account for the effect of the film-solution capacity on the total measured capacity. The use of 2 Å is valid since, in concentrated solutions, the Outer Helmholtz Plane is expected to be located within a few angstroms of the passive metal surface. The field strength corresponding to film thicknesses of 10 and 20 Å at potentials of 0.614 and 1.13 V is calculated as 5.14×10^{6} V cm^{-1}.

A similar analysis can be applied to the capacity-potential behavior observed in the present experiments. A sample calculation is presented for data obtained on AISI 304 in 0.334 M sodium sulfate at pH 2.4. Using the roughness factor of 1.2 reported for an iron surface mechanically polished through 600 grit emery[92] and the dielectric constant, 15.6, determined for films formed on AISI 304 in 0.5 M sulfuric acid,[93] film thicknesses of 5.9 and 10.7 Å at 0.31 and 0.60 V, respectively, are obtained. The passive current density evaluated at 0.30 V is 1.26×10^{-6} A cm^{-2}. The field required to maintain this rate of film formation is therefore, $(0.60 - 0.31)/(10.7 - 5.9)$, 6.8×10^{8} V $Å^{-1}$, or 6.8×10^{6} V cm^{-1}.

The capacity values associated with 18-8 stainless steel in the passive region prior to E_b ($\sim 20\ \mu f\ cm^{-2}$) agree well with those observed for platinum in the passive region.[94] Similar agreement, coupled with the lack of hysteresis in the capacity-potential behavior for an 18-8 stainless steel, have lead Popat and Hackerman[95] to assume that, like platinum, stainless steel has no bulk oxide on its surface in the passive region.

The break in the capacity-potential relationship occurring at 0.3 V implies a change in the nature of the passive film resulting in a decrease in the conductivity or dielectric constant of the film. The ionic current resulting in film growth, i_p, remains constant during the capacity change and passive films on stainless steel have been shown to be good electron conductors.[96] Consequently, it is more likely that a decrease in dielectric constant occurs.

Studies of the passive state of AISI 304 in 0.5 M sulfuric acid show an increase in the protective nature of the passive film at 0.4 V.[97] This has been attributed to a change in film structure through the loss of bound water. Values of the dielectric constant of bulk iron (III) oxide have been shown to increase significantly with an increase in iron (II) content.[98] Either the elimination of a lower valence ion or of bound water from the passive film could, therefore, account for the decrease in capacity at 0.3V observed here.

It appears, therefore, that the nature of the passive film on stainless steel in the solutions studied here is similar to that observed on platinum in the passive state up to a potential of 0.3 V. The passivity of platinum is attributed to an adsorbed "oxygen" species. At 0.3 V a change occurs in the structure of the film on stainless steel. Although this change may correspond to an increase in the degree of crystallinity of the passive film, it is unlikely that a film of only 5 to 10 Å in thickness would possess the properties of a bulk oxide.

The passive current density observed in 0.334 M sodium sulfate (1.26×10^{-6} A cm^{-2}) is significantly higher than that observed in solutions containing chloride ion. A similar observation has been made by Moshtev,[99] who attributes the phenomenon on iron to the incorporation of sulfate anion into the passive film. The resulting increase in film defect density brings about an increase in the ionic conductivity of the film. The slight increase in passive current density with increasing chloride ion concentration observed here (Table 1) implies an increase in the solubility of the film. An increase in passive current density from 0.3×10^{-3} to 1.3×10^{-3} A cm^{-2} is also observed by Lebet and Piotrowski[100] for an 18-9 steel when M sodium chloride is added to 0.5 M sulfuric acid. (The relatively high current densities reported by these investigators are most likely the result of the high (0.330 V sec^{-1}) scan rate employed.)

Pitting

The increase in anodic current density caused by the onset of pitting dissolution occurs at a well-defined potential, E_{pit}, which is a function of the metal composition, its history, and the composition of the solution in which polarization is carried out (see Introduction).

The active shift in pitting potential with increasing chloride ion concentration observed in the present experiments is well supported by literature data.[101, 28, 27] Values of $\partial E_{pit}/\partial \log a_{Cl^-}$, where a_{Cl^-} is the activity of the chloride ion, of -0.07 and -0.09 V decade^{-1} have been found by Leckie and Uhlig[28] and by Leckie[27] for AISI 304 in acid solutions. Various anions, e.g., the hydroxyl, perchlorate, sulfate and nitrate anions, have been shown to have an inhibiting effect on the activating action of chloride ion.[102, 33, 103] A critical activity of the inhibiting anion above which no pitting can occur for a given chloride ion activity has been proposed by Leckie and Uhlig.[28] For sulfate ion the relationship is given by

$$\log a_{Cl^-} = 0.85 \log a_{SO_4^{2-}} - 0.05. \qquad (10)$$

Application of this equation to the present results accurately predicts the observed behavior. For 1.17×10^{-2} and 0.3 M potassium chloride, the calculated critical sulfate concentrations are 7.6×10^{-2} and 0.295 M, respectively. Since the sulfate content of the 0.3 M potassium chloride solution is only 0.248 M, pitting breakdown is expected

and is seen to occur. The inhibiting effect of sulfate ion in the present systems is demonstrated by the susceptibility of the steel to pitting breakdown in 0.1 M potassium chloride when no sulfate ion is present. No pitting is observed in 0.100 M potassium chloride with 0.300 M sulfate.

Present results indicate a slight positive shift ($\sim$30 mV) in the pitting potential when the pH is decreased from 2.35 to 1.52 in 0.3 M potassium chloride. Since hydroxyl ion has been shown to act as a pitting inhibitor for pH$>$ 7,[28] the effect of a decrease in pH in the acid range, if any, should be a negative shift in pitting potential. Literature data suggests,[29, 28, 27] however, that the pitting potential is independent of solution pH in the acid range (pH$<$ 7). The positive shift in pitting potential observed is, therefore, attributed to the inherent irreproducibility of the pitting potential as it is determined here.

The presence of an induction time is evidenced in the present studies by the current-time behavior observed at potentials positive to the pitting potential. A positive shift in potential results in an initially high current density attributed to charging of the double layer. When the potential is stepped to potentials positive to the pitting potential, an initially steady decrease in current density with time is observed signifying the continuation of the passivation process. The increase in film thickness caused by the ionic current flow results in a decrease in

the magnitude of the field across the film. The current density therefore decreases until the steady state film thickness corresponding to the applied potential is reached. The fluctuations in current which follow this current decrease at a given potential have been attributed to the activation and subsequent repassivation of pits on the metal surface.[36]

Recent studies have associated the observed current oscillations with the increase and decrease in the resistance of the solution within pits caused by the successive formation and release of hydrogen bubbles.[104, 105] The formation of a bubble in a pit causes a negative shift in the potential of the pit base by increasing the ohmic (iR) potential drop across the pit solution. Since the potential at the pit base has been shown to be in the region of active dissolution, a decrease in anodic current density results. Release of the bubble reverses the effect.

The most widely accepted theory suggests that passivity of the metal surface is destroyed by the local replacement of an adsorbed "oxygen" species by chloride ions at areas of high metal activity.[106] Rapid metal dissolution ensues. An increase in chloride ion concentration and electrode potential favors adsorption of chloride ion and stabilizes the pitting reaction.

The addition of sulfate ion inhibits the pitting reaction.

The occurrence of sulfate-chloride ion competitive adsorption on a passive metal surface has been demonstrated by Maksimchuk and Rozenfel'd.[107] The amount of chloride ion adsorbed on a passive porous chromium surface decreases with sulfate concentration and is completely eliminated above a critical sulfate concentration ($[SO_4^{2-}] / [Cl^-] > 5$). The relative adsorption characteristics of sulfate ion and chloride ion have been predicted from considerations based on Freundlich isotherms.[28, 103] The observed induction time for pitting breakdown has been attributed to the time-consuming reaction of competitive adsorption. Golovina et al.[108] have shown that the induction time is related to the relative rates of the passivation and pitting reaction at a given potential. On the other hand, cyclic voltammetric behavior of an 18 - 10 stainless steel in solutions of sulfate and chloride ions shows no evidence of adsorption of chloride on the passive surface.[109]

For iron, the zero point of charge of the passive surface has been shown to occur at 0.10 V in 0.01 M sodium hydroxide.[52] This value is considerably more positive than that of the assumed bare active metal in 5×10^{-4} M sulfuric acid ($\sim$-0.61 V). The zero point of charge of active iron is controversial because of the participation of adsorbed hydroxyl ions in the active dissolution reaction.[110] If passivation results in a similar positive shift in the zero

point of charge for the stainless steel surface, then no specific adsorption of chloride or sulfate ions would be expected until potentials are slightly negative to the zero point of charge. In solutions containing only chloride ion, the negative shift in pitting potential would then be attributed to the known variation in zero charge potential in the presence of a specifically adsorbed species. How positive the pitting potential is shifted with respect to the zero point of charge by the addition of sulfate ion would be determined by the relative preferential adsorption of the two species since a critical surface concentration of chloride ions is necessary to induce pitting.

If pitting breakdown does indeed occur through the specific adsorption of chloride ion to a critical surface concentration, the effect should be reflected in the behavior of the differential capacity-potential curve. If the interface can be represented in terms of equipotential planes parallel to the metal surface then it is unlikely that only local changes in double layer composition occur.

However, no capacity-potential peak is observed between the potential of total passivity and the pitting potential or in the capacity-time relationship at potentials exhibiting an induction period prior to breakdown. This does not necessarily imply the absence of specific adsorption. The capacity of the electrical double layer must be considered to be in series with that of the passive film. From the

expression relating total capacity to the individual values of capacities in series,

$$1/C = 1/C_1 + 1/C_2, \qquad (11)$$

it can be seen that the presence of a relatively small passive film capacity would obscure changes in the capacity of the film-solution interface caused by specific adsorption. If the passive film capacity (C_1) is assumed to be 15 μf cm^{-2}, then a change in the film-solution capacity from 30 to 60 μf cm^{-2} as a result of specific adsorption would only increase the total measured differential capacitance of the interface from 10 to 12 μf cm^{-2}.

A similar domination of the interfacial capacity by that of the passive film has been reported by Posey and Sympson.[111] The rate of copper(II) reduction on a passive stainless steel electrode has been shown to increase in the presence of chloride ion as a result of the specific adsorption of the anion. However, no change occurs in the capacity-potential relationship in the corresponding potential region.

Analysis of the capacity-potential curves presented here shows that the same behavior persists both in the presence and absence of pitting breakdown. The break in capacity at E_b occurs at 0.3 V whether the pitting potential is positive or negative to this value. This behavior supports the concept that the capacity of the passive film dominates the interfacial capacity. Since changes in the passive film caused by pitting breakdown are only

local, they will not be reflected in the measured capacity values which are an average property of the interface.

In conclusion, it can therefore be stated that differential capacity measurements cannot differentiate between the presence or absence of the specific adsorption of chloride ion prior to the onset of pitting corrosion. The domination of the interfacial capacitance by that of the passive film acting in series with the film-solution capacity obscures any changes which may occur in the latter. Since pitting induces only local changes in the passive film, these changes will not be reflected in the measured capacity which is a property of the average condition of the film.

Transpassive dissolution

Transpassivity is common to passive alloys one or more of whose components exhibit a second stable oxidation state. For alloys containing chromium, the current increase in the transpassive region is attributed to the oxidation of chromium (III) in the passivating film to chromium (VI) which dissolves as the chromate[112] or hydrogen chromate anion.[79, 113] The standard potentials for the oxidation of various forms of chromic oxide to either of these species range from 0.872 to 1.141 V.[114]

Dissolution in the transpassive region exhibits Tafel behavior over 1 to 1.5 decades of current. A Tafel slope of 0.114 V decade^{-1} is observed for 0.0 M and 1.17 x 10^{-2} M potassium chloride. This value is considerably higher than

those reported in the literature for stainless steels in acid solutions (0.055 to 0.090 V decade^{-1}).[115, 116, 117] Values determined for pure chromium range from 0.038 to 0.048 V decade^{-1}.[5, 80]

The increase in slope to 0.150 V decade^{-1} in 9.97 x 10^{-2} M potassium chloride implies a change in dissolution mechanism. This is unexpected in light of the results of Heumann and Panesar[112] for chromium and iron-chromium alloys in which neither chloride ion nor sulfate ion participates in the dissolution reaction. Although the Tafel slope for transpassive dissolution of nickel in sulfuric acid solutions has been shown to be 0.150 to 0.172 V decade^{-1},[79, 118] the transpassive current-potential relationship for chromium dissolution from both nickel-chromium binary alloys[79] and iron-chromium alloys containing nickel[116] is independent of nickel content. Therefore, the Tafel slope of 0.150 V decade^{-1} observed in the present work cannot be attributed to an effect of nickel on the transpassive dissolution of stainless steel.

The onset of secondary passivity following the region of Tafel behavior is evidenced by a current maximum. Neither the current maximum (1 x 10^{-4} A cm^{-2}) nor its associated potential (0.95 V) is affected by solution composition (in non-pitting systems) at constant pH. The current then decreases to a minimum followed by an increase which is the result of oxygen evolution. The degree of

stability of the secondary passive state is represented by the difference in magnitude of the current density value of the maximum and subsequent minimum, Δ i. Present results indicate that stability decreases slightly on the addition of chloride ion (1.17×10^{-2} M) to a solution originally containing sulfate only at pH 2.4. Current differences, Δ i, of 14×10^{-6} to 17×10^{-6} and 21×10^{-6} A cm^{-2}, respectively, are observed. These results agree well with those of Szklarska-Smialowska and Janik-Czachor,[38] who, for an iron-13 chromium alloy, find a decrease in Δ i on adding 0.05 M sodium chloride to 0.035 M sodium sulfate but see no change in the parameters of secondary passivation.

The presence of a differential capacity peak at potentials in the vicinity of the secondary passivation potential observed in the present work suggests the involvement of an adsorption step in the passivation mechanism. A capacity maximum in the region of secondary passivity has also been observed by Prazak and Cihal[119] for an 18 - 9 stainless steel in 0.5 M sulfuric acid. The cause of secondary passivity has been attributed to the adsorption of an "oxygen" species which is facilitated by the presence of carbon in the alloy. Carbon is thought to increase the affinity of the alloy for adsorbed oxygen.[120, 121]

Transpassive dissolution initiates between 0.57 and 0.64 V in the systems studied here. These values are substantially negative to the standard potentials for chromium oxide oxidation defined above. This is explained, in part, by the negative shift of the reversible potential for the transpassive dissolution reaction with increasing pH. Variations of -0.058 V pH^{-1} and -0.065 V pH^{-1} have been observed for a stainless steel in nitric acid[117] and for iron chromium alloys in sulfuric acid,[112] respectively. If the cold work generated by mechanical polishing during electrode preparation causes an increase in the diffusion of chromium to the alloy surface as suggested by Rhodin,[13] then the negative shift in E_{tr} with increasing chromium concentration reported for stainless steels in 6 M sulfuric acid could also contribute.[116, 16]

The negative shift observed in E_{tr} with increasing chloride ion concentration (Table 1) has also been observed by Shock et al.[122] for AISI 304 in 67 percent sulfuric acid. No effect of chloride ion concentration on E_{tr} for AISI 304 in 5 M sulfuric acid is observed by Acello and Greene,[82] however.

In summary, in systems not subject to pitting corrosion, transpassive dissolution occurs, starting at 0.57 to 0.64 V. Dissolution in this region is attributed to the oxidation of chromium(III) in the passive film to chromium(VI). Tafel behavior is observed. A slope of 0.114 V $decade^{-1}$ occurs in 0.0 and 1.17 x 10^{-2} M potassium chloride. The

change in slope to 0.150 V decade^{-1} when the chloride concentration is increased to 9.97 x 10^{-2} V decade^{-1} implies a change in the mechanism by which transpassive dissolution proceeds. The subsequent maximum in the current density-potential relationship indicates the onset of secondary passivity. Both the current density at the maximum and its corresponding potential are independent of solution composition. The capacity peak observed in this region is attributed to the adsorption of the passivating species.

Galvanostatic Polarization

The potential-time behavior of stainless steel samples subjected to galvanostatic polarization in the solutions studied has been shown to depend both on current density and solution composition. Systems which are not susceptible to pitting corrosion reach and maintain a positive steady state potential under influence of an anodic current. In systems subject to pitting breakdown, the maximum potential attained is unstable and a shift in potential to more active values is observed. Similar results have been reported by several investigators.[123, 42, 41, 38, 40]

From the values of the potential arrests and maxima as well as from the presence of an induction time prior to pitting breakdown, it appears that the initial action of the anodic current is the same in all cases. Schmid[41] has suggested that this initial action involves the

conversion of adsorbed water dipoles to an adsorbed "oxygen" species.

This hypothesis is supported by the presence of the initial potential arrest, E_1, leading to passivation of the alloy surface in all the solutions studied here. In 0.0 through 0.303 M potassium chloride, a Tafel slope of 0.06 V decade^{-1} is associated with the reaction occurring at E_1.

Very little work has been done to elucidate the dissolution mechanism of stainless steels in acid solution. According to Mueller,[124] most of the dissolution current observed on stainless steels containing nickel should represent the oxidation of iron. Chromium and nickel should passivate as soon as they are exposed to the solution by removal of iron from the lattice. If steady-state polarization is approximated, only one passivation peak will be observed as soon as the fraction of the surface consisting of passivated chromium and nickel exceeds 0.5. It is possible, therefore, that the effect of solution composition on the kinetics and mechanism of stainless steel dissolution may be similar to that on pure iron.

For iron in acidic solutions of weakly adsorbable anions (e.g., sulfate and perchlorate ions), dissolution is believed to proceed through the adsorption of water dipoles which dissociate to form specifically adsorbed hydroxyl ions. Two mechanisms have been proposed to account for the kinetic parameters observed: the

Bockris-Kelly[125, 126] mechanism and the Heusler[127] mechanism.

The reaction sequence representing the Bockris-Kelly mechanism is

$$Fe + H_2O = Fe(H_2O)_{ads} \quad (12)$$

$$Fe(H_2O)_{ads} = Fe(OH^-)_{ads} + H^+ \quad (13)$$

$$Fe(OH^-)_{ads} = Fe(OH)_{ads} + e \quad (14)$$

$$Fe(OH)_{ads} \rightarrow FeOH^+ + e \quad (15)$$

$$FeOH^+ + H^+ = Fe^{2+} + H_2O \quad (16)$$

where reaction 15is the rate-determining step. A Tafel slope of 0.040 V decade^{-1} and a reaction order with respect to hydronium ion of -1 are characteristic of this mechanism.

Dissolution by the Heusler mechanism proceeds through the steps,

$$Fe + H_2O = Fe(H_2O)_{ads} \quad (17)$$

$$Fe(H_2O)_{ads} = Fe(OH^-)_{ads} + H^+ \quad (18)$$

$$Fe(OH^-)_{ads} = Fe(OH)_{ads} + e \quad (19)$$

$$Fe(OH)_{ads} + Fe = Fe(FeOH)_{ads} \quad (20)$$

$$Fe(FeOH)_{ads} + OH^- \rightarrow FeOH^+ + Fe(OH)_{ads} + 2e \quad (21)$$

$$FeOH^+ + H^+ = Fe^{2+} + H_2O. \quad (22)$$

Reaction 21 is the rate-determining step and involves the surface catalyst, $(FeOH)_{ads}$. The value of the kinetic parameters characterizing this reaction sequence depends on the manner in which they are measured. Steady-state polarization results in a Tafel slope of 0.030 V decade and

a hydronium ion reaction order of -2. Non-steady-state measurements yield values of 0.060 V decade and -1, respectively.

In both cases, an increase in pH accelerates the dissolution reaction. Recent work[128] has suggested that the Bockris-Kelly mechanism predominates at low energy surface sites while the Heusler mechanism is favored by a high imperfection density and grain boundary to grain area ratio.

In solutions containing a specifically adsorbable ion, e.g., chloride ion, participation of the ion in the dissolution mechanism has been indicated.[129, 130] The influence of chloride and hydroxyl ions on dissolution depends on the relative concentrations of the two species. McCafferty and Hackerman[131] have shown that, in solutions of high chloride content (6M), hydronium ion, in excess of 2.4 M, accelerates rather than inhibits the dissolution reaction. Similar results have been reported by Darwish, et al.[132]

In solutions of low pH ($\leqslant$ 1.52 to 2) and moderate chloride ion concentrations ($\geqslant 10^{-2}$ M), Lorenz[133] has shown that chloride ion has an inhibiting effect on iron dissolution. A change in reaction mechanism characterized by a change in Tafel slope to 0.060 V decade^{-1} and a reaction order of -1 for both hydronium and chloride ions is

observed. However, below 10^{-2} M potassium chloride at low pH (< 1.52 to 2)[133] as well as in 1 M potassium chloride at pH 2,[130] iron dissolution again proceeds according to the Bockris-Kelly or Heusler mechanisms.

The mechanism by which dissolution of stainless steel occurs in the chloride-sulfate containing solutions employed here cannot be determined precisely from available data. However, because of the increase in critical current density with increasing total anion concentration observed during potentiostatic polarization, it is assumed that, in the pH range studied (1.52 to 6.22), chloride ion does not inhibit the dissolution process. The Tafel slope of 0.060 V decade^{-1} observed in 0.0 through 0.303 M potassium chloride is determined galvanostatically, i.e., using a non-steady-state technique. It therefore seems likely that the dissolution reaction associated with the potential arrest at E_1 proceeds according to the Heusler mechanism. The high number of surface imperfections ($\sim 10^{12}$ cm^{-2}) expected on the mechanically polished (cold worked) surfaces used here[134] supports this conclusion. Based on the results of impedance measurements, a similar conclusion has been reached by Schwenk and Buhler.[135] Verification of this hypothesis awaits determination of the reaction orders of the species involved in the dissolution reaction.

The change in Tafel slope from 0.060 to 0.014 V decade^{-1} observed on increasing the chloride concentration from 0.303 to 0.518 M indicates that a change in dissolution mechanism has occurred. The significant depolarization of the reaction implied by this Tafel slope (0.014 V decade^{-1}) results in the high value of the critical current density seen in 0.5 M potassium chloride during potentiostatic polarization (Table 1).

The charge necessary to bring about passivation in any given solution determined from the product of the applied current density and the length of the arrest at E_1 appears to decrease with increasing current density. This is probably related to the corresponding positive shift in E_1 which occurs. The more positive the potential in the active dissolution region, the higher the internal anodic current will be. Since it is the total anodic charge passed which determines plateau length, a decrease in t with increasing applied current density will therefore occur as the potential of the arrest becomes more positive.

Potential arrests observed at more noble potentials ($\geqslant$ 0.8 V) agree well with characteristic potential regions observed during potentiostatic polarization. The plateau occurring at 0.8 V is attributed to the transpassive dissolution of chromium from the passive film. The Tafel slope observed in 0.337 M sulfate (0.058 V decade^{-1}) is in

much better accord with literature values (see above) than that determined potentiostatically (0.114 V decade^{-1}). This may be attributed, in part, to the different measuring techniques employed. In potentiostatic polarization, the time spent at each potential permits the surface to approach the steady-state conditions corresponding to that potential. This results in the film's being thicker at 0.8 V during potentiostatic polarization than at the same potential during galvanostatic polarization. The presence of a thicker film will inhibit the transpassive dissolution reaction. A higher overvoltage is therefore necessary to produce a given current density, as shown by the change in the Tafel slope to 0.114 V decade^{-1}.

A change in dissolution mechanism in 0.1 M potassium chloride is reflected both in the galvanostatic and the potentiostatic results as shown by an increase in Tafel slope from 0.058 and 0.114 V decade^{-1} to 0.121 and 0.150 V decade^{-1}, respectively. A value of 0.161 V decade^{-1} is determined galvanostatically in 0.303 M potassium chloride. The increase in exchange current density from 1.74×10^{-18} to 2.69×10^{-9} A cm^{-2} over the chloride concentration range 0.0 to 0.303 M suggests that the reaction is depolarized by chloride ion.

During the change in potential from the plateau at 0.8 V to that at 0.85 V, a peak in the capacity-potential relationship occurs. The presence of a potential maximum

at $\sim$0.90 V in the current-potential arrest relationship associated with the plateau at 0.85 V also indicates its relation to the secondary passivation process. The value of the current density maximum associated with secondary passivity in potentiostatic experiments is 1×10^{-4} A cm^{-2}. The current density at which the potential maximum is produced during galvanostatic polarization, 1×10^{-3} A cm^{-2}, is higher. This emphasizes the importance of the age of the film on its protective properties.[37]

The Tafel slopes, calculated from the current values prior to the potential maximum, range from 0.047 V $decade^{-1}$ in 0.337 M sulfate to 0.145 V $decade^{-1}$ in 0.3 M potassium chloride. This again suggests a change in mechanism in the presence of chloride ion. Schmid[41] has also reported a Tafel slope of 0.147 V $decade^{-1}$ in this potential region. An increase in exchange current density from 4.57×10^{-23} to 4.17×10^{-10} A cm^{-2} with increasing chloride concentration is also observed for this arrest.

The oxygen evolution reaction occurring in 0.0 through 0.303 M potassium chloride appears to be unaffected by solution composition at constant pH in the range studied.

In 0.100 M potassium chloride solutions, no pitting breakdown occurs, while samples subjected to constant current polarization in 0.303 M potassium chloride solutions undergo pitting corrosion. However, comparison

of the more noble potential arrests observed in these two systems supports the conclusion that the initial surface states produced by the applied anodic current are similar and that it is a perturbation of these initial surface states which results in the onset of pitting.

In both systems transpassive dissolution (Tafel slopes of 0.121 and 0.161 V decade^{-1}, respectively), secondary passivity, and oxygen evolution (Tafel slope of 0.022 V decade^{-1} in both cases) are observed (Tables 17 and 18). In 0.3 M potassium chloride, however, the chloride concentration is high enough to produce, by competitive adsorption, the critical surface concentration needed to induce pitting breakdown. Noble potentials in the transpassive dissolution or oxygen evolution regions are then no longer necessary to maintain the imposed current density, and a decrease in potential to values associated with the pitting reaction occurs.

In 0.5 M potassium chloride solutions pitting breakdown occurs from potentials considerably below those observed in 0.3 M potassium chloride (0.447 to 0.798 V versus 0.765 to 1.390 V, respectively). It appears that the increase in chloride ion concentration, coupled with the decrease in sulfate concentration, allows the critical surface concentration of chloride needed to cause pitting to be reached at a smaller positive charge on the metal and with a shorter induction time.

Analysis of the capacity-potential behavior observed in both 0.303 and 0.518 M potassium chloride solutions shows that the only capacity peaks occurring are those associated with the primary and secondary passivation reactions (and, in some cases, the oxygen evolution reaction). No capacity peak appears to be associated with the time-consuming alteration of the surface occurring prior to pitting breakdown. This behavior, coupled with the capacity values observed during breakdown from potentials below 0.8 V (8 to 15 μf cm^{-2}), support the idea that the capacity of the interface is dominated by that of the passive film, as discussed above.

The steady-state potential achieved after pitting-induced potential breakdown has been described as the protection potential of the system.[42] Above this potential, previously nucleated pits can grow. In the presence of inhibiting ions in concentrations insufficient to prevent pitting, the determination of the value of the steady-state potential is hampered by oscillations in the potential with time. The phenomena leading to current oscillations are described by Rozenfel'd and Maksimchuk.[136] To maintain current flow through the solution, chloride ion migrates into the pits. The resulting depolarization of the dissolution reaction in the pit causes a shift in the potential within the pit to active values. Because of local cell

action, this induces a negative shift in the potential of the entire surface. This causes partial desorption of chloride ions. Under the continued influence of the applied current, a positive shift in potential then occurs, causing re-adsorption of the chloride ion. The resulting cyclic behavior is reflected in potential oscillations.

The potential at the base of a pit has been shown to be in the region of active dissolution of the metal under study.[105, 104] The positive shift in the average potential attained after pitting breakdown with increasing current density at a given chloride ion concentration is representative of the behavior expected if the potential within the pit is in the active dissolution region of the pit metal-solution interface. The composition of the anolyte in the pit has been shown to be significantly higher in chloride ion and hydronium ion because of the influence of chloride ion migration and metal ion hydrolysis, respectively.[137] Because of the depolarizing effect of the chloride ion on active metal dissolution, the average potential observed in 0.518 M potassium chloride is considerably more active than that in 0.303 M (Table 21).

The pit density on a metal surface has been shown to be a function of potential.[40] The slight negative shift in the average final potential when oxygen evolution potentials are reached prior to breakdown may therefore be attributed to an increase in the number of pits formed

on the surface. This results in a decrease in the current density associated with each pit.

Very few data are reported in the literature on the open circuit decay behavior of stainless steels in acid solutions. During forced decay (constant current reduction) of the passive film on iron-chromium alloys in 0.100 M sodium sulfate at pH 2.2, Aronowitz and Hackerman[11] find three potential arrests occurring at approximately 0.48, 0.05 and -0.1 V, respectively. Because no interrelation in plateau lengths is found, it is assumed that the arrests do not involve stepwise reduction of a single passivating species but are a result of the reduction of three independent surface entities.

The first arrest (0.48 V) is shown to result from reduction of a species produced during transpassive dissolution. For alloys with $<$ 12 percent chromium, reduction of the surface material associated with the second arrest results in activation of the metal surface. When the chromium content of the alloy is increased to $>$ 12 percent, the surface species reduced during the third arrest, corresponding to a charge of 0.7 mcoul cm^{-2}, is sufficient to maintain the alloy in the passive state.

The arrests observed in the present experiments during open circuit decay in non-pitting systems show similar potential values. The one between 0.4 and 0.5 V occurs

only when transpassive dissolution occurs before constant current control is removed. This supports its association with a substance produced in the transpassive dissolution region.

The two lower arrests observed in the present results occur at more negative potentials than those seen during constant current reduction. This is, in part, a result of the increased stability observed in the passive films formed on nickel-containing stainless steels. Capacity peaks of 20 to 40 μ f cm^{-2} seen in conjunction with these two lower arrests suggest the participation of a desorption reaction related to the activation of the alloy surface.

The most negative potential observed during open circuit decay is not a steady state value. A positive shift in potential occurs over extended periods of time (Table 22). This positive shift is probably a result of the equilibration of the double layer and bulk solution which is expected to contain oxidizing species (Fe^{3+}, $Cr_2O_7^{2-}$, O_2) produced during the polarization process.

CHAPTER V

SUMMARY

The mechanism by which chloride ion acts to initiate pitting breakdown of a passive metal surface is unknown. If specific adsorption of chloride ion to a critical surface concentration is a necessary precursor to pitting, then its occurrence should cause a change in the differential capacity of the passive film-solution interface.

To examine this possibility, the differential capacity of an AISI 304 stainless steel-solution interface was determined during potentiostatic and galvanostatic polarization in solutions of potassium chloride at pH 2.4. Sodium sulfate was added to maintain an ionic strength of one. The current density-potential and potential-time behavior resulting from constant potential and constant current polarization, respectively, were also observed.

During potentiostatic polarization, the transition from the active to the passive state is obtained for all solutions studied (0.0 through 1.0 M potassium chloride). The rest potential ($\sim$ -0.48 V versus SCE) and the primary passivation potential ($\sim$ -0.42 V versus SCE) are independent of solution composition. The critical current density increases linearly with the concentration function, pH + log ($[SO_4^{2-}]$ + $[Cl^-]$),

where $[SO_4^{2-}]$ and $[Cl^-]$ are the total analytical concentration of the sulfate and chloride species present. This behavior implies that sulfate and chloride ions are equivalent in their influence on the dissolution-passivation mechanism(s). The invariance of the primary passivation potential at constant pH suggests that the reaction leading to dissolution and the reaction leading to passivation are equally depolarized at any given solution composition. The capacity peak occurring slightly negative to the primary passivation potential is attributed to the specific adsorption of the anionic species involved in the reaction (hydroxyl, sulfate, bisulfate and chloride ions).

The potential at which the electrode becomes totally passive is a linear function of solution composition, rather than of the logarithm of solution composition. It appears, therefore, that its value is determined by kinetic rather than thermodynamic factors.

In systems not subject to pitting (<0.3 M potassium chloride), transpassive dissolution occurs, initiating between 0.57 and 0.64 V. Dissolution in this region is attributed to the oxidation of chromium (III) in the passive film to chromium (VI). Tafel behavior is observed. A slope of 0.114 V decade^{-1} occurs in 0.0 and 1.17×10^{-2} M potassium chloride. The change in slope to 0.150 V decade^{-1} when the chloride concentration is increased to 9.9×10^{-2} M implies a change in the mechanism by which transpassive dissolution proceeds.

The subsequent maximum in the current density-potential relationship indicates the onset of secondary passivity. Both the current density at the maximum (1×10^{-4} A cm^{-2}) and its corresponding potential (0.95 V) are independent of solution composition. The capacity peak observed in this region is attributed to the adsorption of the passivating species.

In solutions of $\geqslant$ 0.3 M potassium chloride, the passive state is not stable and pitting corrosion occurs at potentials normally in the passive region. Sulfate ion is found to inhibit the activating effect of chloride ion. The pitting potential, therefore, depends on the relative amounts of chloride and sulfate ions in the solution, shifting toward more active values as the chloride ion concentration is increased.

No capacity peak is observed prior to pitting breakdown. However, this does not imply the absence of a specific adsorption event. Rather, it is found that the capacity, between the potential of total passivity and the capacity minimum at 0.60 V, is approximately independent of the stability of the passive state. This independence results from the domination of the interfacial capacitance by that of the passive film, obscuring any changes in the film-solution capacity which may arise.

In both pitting and non-pitting systems, the capacity changes suddenly at 0.3 V from a value of $\sim 18\ \mu f\ cm^{-2}$ to $\sim 15\ \mu f\ cm^{-2}$. This change is attributed to a decrease in

the dielectric constant of the film caused either by the elimination of bound water or of low valence ions (e.g., Fe(II)) from the film. Between 0.3 and 0.6 V, a linear relationship is observed between the reciprocal of the differential capacity and the potential. Film growth, therefore seems to follow an inverse logarithmic law. The passive film formed in 0.334 M sodium sulfate at 0.31 and 0.6 V is found to have thicknesses of 5.9 and 10.7 Å, respectively.

The potential-time behavior of samples subjected to galvanostatic polarization depends on both current density and solution composition. Arrests are observed at -0.4, 0.0, 0.8, 0.85, and 1.12 V. Systems not susceptible to pitting (< 0.3 M potassium chloride) reach and maintain a steady-state potential between 0.8 and 1.4 V for the current densities employed (1×10^{-4} to 2×10^{-3} A cm^{-2}). In systems subject to pitting, the maximum potential attained is unstable and a shift in potential to more active values occurs. The final average potential observed following breakdown is shown to be in the potential range of active dissolution for the metal in contact with the solutions in the pit.

In 0.303 M potassium chloride, intermediate arrests produced by a given current density as well as the maximum potential achieved prior to breakdown correspond to potential arrests in non-pitting systems. In 0.518 M potassium chloride, pitting breakdown occurs from a potential maximum which is considerably below that observed in 0.303 M but the behavior at more negative potentials in the two solutions is similar.

It is assumed therefore, that the initial effect of the anodic current on the metal surface at a given potential is the same in all cases and that pitting succeeds through a perturbation of these initial surface states by chloride ions.

Tafel behavior is associated with the arrests at -0.4, 0.8, 0.85 and 1.12 V. Active dissolution at -0.40 V exhibits a Tafel slope of 0.06 V decade^{-1} in 0.0 through 0.303 M potassium chloride. A mechanism change occurs in 0.518 M potassium chloride where a slope of 0.014 V decade^{-1} is observed. In all cases, a capacity peak is associated with this arrest. Since the critical current density is shown to increase with chloride concentration and galvanostatic polarization is a non-steady-state technique, dissolution is assumed to proceed through the Heusler mechanism.

The arrest at 0.8 V results from transpassive dissolution. The discrepancy between the Tafel slope observed in 0.337 M sodium sulfate during potentiostatic polarization (0.114 V

decade^{-1}) and that observed during galvanostatic polarization (0.058 V decade^{-1}) is attributed to the thicker film expected at this potential under potentiostatic conditions. Tafel slopes of 0.121 and 0.161 V decade^{-1} are observed in 0.100 and 0.303 M potassium chloride, respectively, confirming the presence of a different reaction sequence at higher chloride ion concentrations. Arrests at 0.85 and 1.12 V correspond to secondary passivity and oxygen evolution, respectively.

Capacity peaks are associated with the onset of secondary passivity and in some cases with oxygen evolution. However, no capacity peak is associated with pitting breakdown per se.

LITERATURE CITED

1. M. Faraday, Phil. Mag., 9, 57, 122, 153 (1836).
2. K. Vetter, Z. Elektrochem., 62, 642 (1958).
3. T. P. Hoar, Corrosion Sci., 7, 341 (1967).
4. U. R. Evans, J. Chem. Soc., 1024 (1927).
5. Ya. M. Kolotyrkin, Z. Elektrochem., 62, 664 (1968).
6. B. Kabanov, R. Burstein, and A. Frumkin, Disc. Faraday Soc., 1, 259 (1947).
7. H. G. Feller and H. H. Uhlig, J. Electrochem. Soc., 107, 864 (1960).
8. H. H. Uhlig, J. Electrochem. Soc., 97, 215c (1950).
9. B. N. Kabanov and D. I. Leikis, Zh. Fiz. Khim., 20, 995 (1946).
10. N. Hackerman, Z. Electrochem., 62, 632 (1958).
11. G. Aronowitz and N. Hackerman, J. Electrochem. Soc., 110, 633 (1963).
12. R. P. Frankenthal, J. Electrochem. Soc., 114, 542 (1967).
13. T. N. Rhodin, Jr., Corrosion, 12, 123 (1956).
14. C. L. McBee and J. Kruger, Electrochim. Acta, 17, 1337 (1972).
15. H. H. Uhlig, Corrosion, 19, 231t (1963).
16. K. Osozawa and H. J. Engell, Corrosion Sci., 6, 389 (1966).
17. Ya. M. Kolotyrkin, Corrosion, 19, 261t (1963).
18. Z. Szklarska-Smialowska, Corrosion, 27, 223 (1971).
19. H. Böhni and H. H. Uhlig, Corrosion Sci., 9, 353 (1969).
20. S. A. Glazkova, L. I. Freiman, G. L. Shvarts, and G. S. Raskin, Zashch. Metal., 8, 660 (1972).

21. A. P. Bond, J. Electrochem.. Soc., 120, 603 (1973).

22. A. P. Bond and E. A. Lizlovs, J. Electrochem.. Soc., 115, 1130 (1968).

23. V. Cihal and M. Prazak, J. Iron Steel Inst., 193, 360 (1959).

24. M. Fujii and M. Kumada, Nippon Kinzoku Gakkaishi, 34, 1001 (1970).

25. A. Randak and F. W. Trautes, Werkst. Korros., 21, 97 (1970).

26. N. T. Tomashov and O. N. Markova, Zashch. Metal,, 6, 21 (1970).

27. H. P. Leckie, J. Electrochem.. Soc., 117, 1152 (1970).

28. H. P. Leckie and H. H. Uhlig, J. Electrochem. Soc., 113, 1262 (1966).

29. V. Hospadaruk and J. V. Petrocelli, J. Electrochem.. Soc., 113, 878 (1966).

30. B. Rondot, M. Da Cunha Belo and J. Montuollo, C. R. Acad. Sci., Ser. C., 274, 1028 (1972).

31. G. S. Eklund, J. Electrochem.. Soc., 121, 467 (1974).

32. M. Smialowski, Z. Szklarska-Smialowska, M Rychcik, and A. Szummer, Corrosion Sci., 9, 123 (1969).

33. L. L. Rozenfel'd and V. P. Maksimchuk, Zh. Fiz. Khim., 35, 2561 (1961).

34. H. Uhlig and J. Gilman, Corrosion, 20, 289t (1964).

35. M. Pourbaix, L. Klimzack-Mathieiu, Ch. Mertons, J. Meunier, Cl. Vanleugenhaghe, L. DeMunck, J. Laureys, L. Neelmans, and M. Warzce, Corrosion Sci., 3, 329 (1963).

36. R. P. Jackson and D. Van Rooyen, Corrosion, 27, 203 (1971).

37. N. Stolica, Corrosion Sci., 9, 205 (1969).

38. Z. Szklarska-Smialowska and M. Janik-Czachor, Corrosion Sci., 7, 65 (1967).

39. N. Stolica, Corrosion Sci., 9, 455 (1969).

40. W. Schwenk, Corrosion, 20, 129 (1964).

41. G. M. Schmid and N. Hackerman, J. Electrochem. Soc., 108, 741 (1961).

42. Z. Szklarska-Smialowska and M. Janik-Czachor, Corrosion Sci., 11, 901 (1971).

43. K. Nobe and R. F. Tobias, Corrosion, 20, 263t (1964).

44. N. Sato, Electrochim. Acta, 16, 1683 (1971).

45. T. P. Hoar and W. R. Jacob, Nature, 216, 1299 (1967).

46. J. O'M. Bockris and A. K. N. Reddy, "Modern Electrochemistry," Vol. 1, pp. 749-769, Plenum Press, New York (1970).

47. T. Murakawa, T. Kato, S. Nagaura, and N. Hackerman, Corrosion Sci., 7, 657 (1967).

48. H. Vaidyananthan and N. Hackerman, Electrochim. Acta, 16, 2193 (1971).

49. T. Murakawa, T. Kato, S. Nagaura, and N. Hackerman, Corrosion Sci., 8, 341 (1968).

50. T. Murakawa and N. Hackerman, Corrosion Sci., 4, 387 (1964).

51. B. S. Krasikov and V. V. Sysoeva, Proc. Acad. Sci. USSR, Phys. Chem. Sect., 114, 363 (1957).

52. R. S. Perkins and T. N. Andersen, "Modern Aspects of Electrochemistry," Vol. 5, J. O'M. Bockris and B. E. Conway, Editors, pp. 203-290, Plenum Press, New York (1969).

53. R. de Levie, Electrochim. Acta, 10, 113 (1965).

54. J. S. Riney, G. M. Schmid, and N. Hackerman, Rev. Sci. Instr., 32, 588 (1961).

55. R. P. Frankenthal and H. W. Pickering, J. Electrochem. Soc., 112, 514 (1965).

56. S. Harrar, Anal. Chem., 34, 1036 (1963).

57. G. M. Schmid and N. Hackerman, J. Electrochem. Soc., 115, 1033 (1968).

58. B. E. Wilde, Corrosion Sci., 7, 315 (1967).

59. P. F. King and H. H. Uhlig, J. Phys. Chem., 63, 2026 (1959).

60. H. J. Rocha and G. Lennartz, Arch. Eisenhuttenw., 26, 117 (1955).

61. R. N. Adams, "Electrochemistry at Solid Electrodes," pp. 183-184, Marcel Dekker, Inc., New York (1969).

62. P. Delahay, "New Instrumental Methods in Electrochemistry," pp. 208-209, Interscience, New York (1954).

63. P. Delahay, "Double Layer and Electrode Kinetics," pp. 33-80, Interscience, New York (1965).

64. G. M. Florianovich, L. A. Sokolova, and Ya. M. Kolotyrkin, Electrochim. Acta, 12, 879 (1967).

65. R. J. Chin and K. Nobe, J. Electrochem. Soc., 119, 1457 (1972).

66. G. Kreysa, U. Ebersbach, and K. Schwabe, Electrochim. Acta, 16, 1489 (1971).

67. N. Hackerman and S. J. Stephens, J. Phys. Chem., 58, 904 (1954).

68. M. Pourbaix and F. Vander'velden, Corrosion Sci., 5, 81 (1965).

69. C. D. Kim and B. E. Wilde, Corrosion, 28, 26 (1972).

70. Ho Ngok Ba and Nguyen Dyk Vi, Soviet Electrochem., 4, 894 (1968).

71. L. Peraldo Bicelli and C. Romagnani, Chim. Ind. (Milan), 53, 1128 (1971).

72. L. Troselius, Corrosion Sci., 11, 473 (1971).

73. R. N. O'Brien and P. Seto, J. Electrochem Soc., 117, 32 (1970).

74. M. A. V. Devanathan and Z. Stachurski, J. Electrochem. Soc., 111, 619 (1964).

75. C. D. Kim and B. E. Wilde, J. Electrochem. Soc., 118, 202 (1971).

76. E. McCafferty and N. Hackerman, J. Electrochem. Soc., 119, 146 (1972).

77. F. G. Hodge and B. E. Wilde, Corrosion, 26, 146 (1970).

78. H. W. Pickering and R. P. Frankenthal, J. Electrochem. Soc., 112, 761 (1965).

79. J. R. Myers, F. H. Beck and M. G. Fontana, Corrosion 21, 277 (1965).

80. G. T. Seaman, J. R. Myers, and R. K. Saxer, Electrochim. Acta, 12, 855 (1967).

81. B. E. Wilde and F. G. Hodge, Electrochim. Acta, 14, 619 (1969).

82. S. J. Acello and N. D. Greene, Corrosion 18, 286 (1962).

83. N. D. Greene and G. Judd, Corrosion, 21, 15 (1965).

84. D. O. Condit, Corrosion, 28, 95 (1972).

85. S. E. Trauenberg and R. T. Foley, J. Electrochem. Soc., 118, 1066 (1971).

86. E. D. Verink and M. Pourbaix, Corrosion, 27, 495 (1971).

87. G. M. Bulman and A. C. C. Tseung, Corrosion Sci., 12, 415 (1972).

88. W. Schwenk and A. Rahmel, Electrochim. Acta, 5, 180 (1961).

89. N. Cabrera and N. F. Mott, Repts. Prog. Phys., 12, 163 (1948-9).

90. J. L. Ord. and J. H. Bartlett, J. Electrochem. Soc., 112, 160 (1965).

91. H. J. Engell and B. Ilschner, Z. Elektrochem., 59, 716 (1955).

92. S. Thibault, J. M. Godot, J. Pagetti, and J. Talbot, Proc. Int. Cong. Metal. Corrosion, 4th, 1969, 594 (1972).

93. Go. Okamoto and T. Shibata, Corrosion Sci., 10, 371 (1970).

94. H. A. Laitenen and C. G. Enke, J. Electrochem. Soc., 107, 773 (1960).

95. P. Popat and N. Hackerman, J. Phys. Chem., 65, 1201 (1961).

96. M. Stern, J. Electrochem. Soc., 104, 559 (1957).

97. Go. Okamoto and T. Shibata, Proc. Int. Congr. Metal. Corrosion, 4th, 1969, 620 (1972).

98. O. Jantzen, Z. Angew. Physik, 18, 560 (1965).

99. R. V. Moshtev, Ber. Bunsenges. Phys. Chem., 72, 452 (1968).

100. R. Lebet and A. Piotrowski, Corrosion, 22, 257 (1966).

101. Z. Szklarska-Smialowska and M. Janik-Czachor, Proc. Int. Congr. Metal. Corrosion, 4th, 1969, 651 (1972).

102. I. L. Rozenfel'd and V. P. Maksimchuk, Z. Physik. Chem. (Leipzig), 215, 25 (1960).

103. M. Frazak, V. Spanily and J. Tousek, Corros. Week Manifestation Eur. Fed. Corros., 41st, 1968, 776 (1970).

104. H. W. Pickering and R. P. Frankenthal, J. Electrochem. Soc., 119, 1297 (1972).

105. A. A. Seys, M. J. Brabers, and A. A. VanHawte, Corrosion, 30, 47 (1974).

106. Ya. M. Kolotyrkin, J. Electrochem. Soc., 108, 209 (1961).

107. V. P. Maksimchuk and I. L. Rozenfel'd, Dokl. Akad. Nauk. SSSR, 131, 354 (1960).

108. G. V. Golovina, G. M. Florianovich, and Ya. M. Kolotyrkin, Soviet Electrochem., 1, 8 (1965).

109. P. Forchhammer and H. J. Engell, Corrosion Sci., 11, 49 (1971).

110. W. J. Lorenz and H. Fischer, Electrochim. Acta, 11, 1597 (1966).

111. F. A. Posey and R. F. Sympson, J. Electrochem.. Soc., 109, 716 (1962).

112. Th. Heumann and H. S. Panesar, J. Electrochem. Soc., 110, 628 (1963).

113. R. Olivier, Thesis, Leiden (1955).

114. M. Pourbaix, "Atlas of Electrochemical Equilibria in Aqueous Solutions," pp. 256-261, Pergamon Press, New York (1966).

115. B. E. Wilde and J. S. Armijo, Corrosion, 24, 393 (1968).

116. N. A. Bozin and M. M. Kurtepov, Zh. Fiz. Khim., 85, 152 (1961).

117. I. K. Burtseva, G. F. Plotnikova, and A. I. Krasil'shchikov, Zh. Fiz. Khim., 38, 1956 (1964).

118. M. Zamin and M. B. Ives, J. Electrochem. Soc., 121, 1141 (1974).

119. M. Prazak, V. Prazak, and V. L. Cihal, Z. Electrochem., 62, 739 (1958).

120. J. deBecdelievre, A. M. deBecdelievre, and C. Courty, C. R. Acad. Sci., Ser. C, 259, 1333 (1964).

121. I. Epelboin, Bull, Soc. Chim. France, 475 (1964).

122. D. A. Shock, J. D. Sudbury, and O. L. Riggs, Jr., Proc. Int. Congr. Metal. Corrosion, 1st, 1961, 336 (1961).

123. M. Janik-Czachor and Z. Szklarska-Smialowska, Corrosion Sci., 8, 215 (1968).

124. W. A. Mueller, Corrosion, 18, 73t (1962).

125. J. O'M. Bockris, D. Drazic, and A. R. Despic, Electrochim. Acta, 4, 325 (1961).

126. E. J. Kelly, J. Electrochem. Soc., 112, 124 (1965).

127. K. E. Heusler, Z. Elektrochem., 62, 582 (1958).

128. F. Hilbert, Y. Miyoshi, G. Eichkorn, and W. J. Lorenz, J. Electrochem. Soc., 118, 1919 (1971).

129. A. J. Arvia and J. J. Podesta, Corrosión Sci., 8, 203 (1968).

130. L. Felloni, Corrosion Sci., 8, 133 (1968).

131. E. McCafferty and N. Hackerman, J. Electrochem. Soc., 119, 999 (1972).

132. N. A. Darwish, F. Hilbert, W. J. Lorenz, and H. Rosswag, Electrochim. Acta, 18, 421 (1973).

133. W. J. Lorenz, Corrosion Sci., 5, 121 (1965).

134. M. Schorr and J. Yahalom, Corrosion Sci., 12, 867 (1972).

135. W. Schwenk and H. E. Buhler, Corrosion Sci., 3, 261 (1963).

136. I. L. Rozenfel'd and V. P. Maksimchuk, Zh. Fiz. Khim., 35, 1832 (1961).

137. T. Suzuki, M. Yamabe, and Y. Kitamura, Corrosion, 29, 18 (1973).

BIOGRAPHY

M. Elain Curley was born in Dorchester, Massachusetts, on June 3, 1944. She attended Saint Gregory's Grammar and High Schools, graduating in June of 1962. In June, 1966 she received her Bachelor of Arts in Chemistry Degree from Regis College, Weston, Massachusetts.

She entered graduate study at the University of Florida in September, 1966. While there, she was the holder of Teaching and Research Assistanceships and the recipient of two Graduate School Fellowships and the Dupont Teaching Award. She married John A. Fiorino in February, 1972. She re-enrolled at the University of Florida in March, 1975, to complete the requirements for her graduate degree.

I certify that I have read this study and that in my opinion it conforms to acceptable standards of scholarly presentation and is fully adequate, in scope and quality, as a dissertation for the degree of Doctor of Philosophy.

Gerhard M. Schmid, Chairman
Associate Professor of Chemistry

I certify that I have read this study and that in my opinion it conforms to acceptable standards of scholarly presentation and is fully adequate, in scope and quality, as a dissertation for the degree of Doctor of Philosophy.

Ellis D. Verink, Jr.
Professor of Materials Science and Engineering

I certify that I have read this study and that in my opinion it conforms to acceptable standards of scholarly presentation and is fully adequate, in scope and quality, as a dissertation for the degree of Doctor of Philosophy.

James D. Winefordner
Professor of Chemistry

I certify that I have read this study and that in my opinion it conforms to acceptable standards of scholarly presentation and is fully adequate, in scope and quality, as a dissertation for the degree of Doctor of Philosophy.

Wallace S. Brey
Professor of Chemistry

I certify that I have read this study and that in my opinion it conforms to acceptable standards of scholarly presentation and is fully adequate, in scope and quality, as a dissertation for the degree of Doctor of Philosophy.

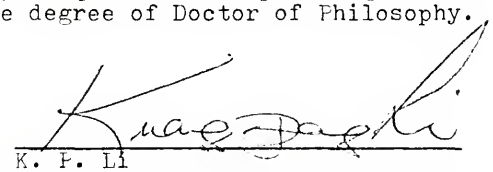

K. P. Li
Assistant Professor of Chemistry

This dissertation was submitted to the Graduate Faculty of the Department of Chemistry in the College of Arts and Sciences and to the Graduate Council, and was accepted as partial fulfillment of the requirements for the degree of Doctor of Philosophy.

June, 1975

Dean, Graduate School